An Ifnar1 allele impairs the colonization of gut bacteria and promotes tuberculosis

Lingming Chen
Department of Microbiology, Zhongshan School of Medicine, Key Laboratory for Tropical Diseases Control of the Ministry of Education, Sun Yat-sen University, Guangzhou 510080, China.

Guoliang Zhang
National Clinical Research Center for Infection Diseases, Guangdong Key Laboratory for Emerging Infectious Diseases, Shenzhen Third People's Hospital, Southern University of Science and Technology,

Guobao Li
National Clinical Research Center for Infection Diseases, Guangdong Key Laboratory for Emerging Infectious Diseases, Shenzhen Third People's Hospital, Southern University of Science and Technology,

Wei Wang
Department of Clinical Laboratory, Foshan Fourth People's Hospital, Foshan 528000, China.

Zhen-Huang Ge
Sun Yat-sen University

Yi Yang
Department of Microbiology, Zhongshan School of Medicine, Key Laboratory for Tropical Diseases Control of the Ministry of Education, Sun Yat-sen University, Guangzhou 510080, China.

Xing He
National Clinical Research Center for Infection Diseases, Guangdong Key Laboratory for Emerging Infectious Diseases, Shenzhen Third People's Hospital, Southern University of Science and Technology,

Zhi Liu
National Clinical Research Center for Infection Diseases, Guangdong Key Laboratory for Emerging Infectious Diseases, Shenzhen Third People's Hospital, Southern University of Science and Technology,

Zhiyi Zhang
Department of Microbiology, Zhongshan School of Medicine, Key Laboratory for Tropical Diseases Control of the Ministry of Education, Sun Yat-sen University, Guangzhou 510080, China.

Qiongdan Mai
Department of Microbiology, Zhongshan School of Medicine, Key Laboratory for Tropical Diseases Control of the Ministry of Education, Sun Yat-sen University, Guangzhou 510080, China.

Yiwei Chen
Department of Microbiology, Zhongshan School of Medicine, Key Laboratory for Tropical Diseases Control of the Ministry of Education, Sun Yat-sen University, Guangzhou 510080, China.

Zixu Chen

Department of Microbiology, Zhongshan School of Medicine, Key Laboratory for Tropical Diseases Control of the Ministry of Education, Sun Yat-sen University, Guangzhou 510080, China.

Jiang Pi

Department of Microbiology and Immunology, Center for Primate Biomedical Research, University of Illinois College of Medicine, Chicago, IL 60612, USA

Shuai Yang

Key Laboratory of Gene Function and Regulation of the Ministry of Education, State Key Laboratory of Biocontrol, School of Life Sciences, Sun Yat-sen University, Guangzhou, 510006, Guangdong, China

Jun Cui

Key Laboratory of Gene Function and Regulation of the Ministry of Education, State Key Laboratory of Biocontrol, School of Life Sciences, Sun Yat-sen University, Guangzhou, 510006, Guangdong, China

Haipeng Liu

Shanghai Pulmonary Hospital, Tongji University School of Medicine

Ling Shen

Department of Microbiology and Immunology, Center for Primate Biomedical Research, University of Illinois College of Medicine, Chicago, IL 60612, USA

Lingchan Zeng

Clinical Research Center, Department of Medical Records Management, Guanghua School of Stomatology, Hospital of Stomatology, Sun Yat-sen University, Guangzhou, Guangdong, China.

Lin Zhou

Guangdong Center for Tuberculosis Control, National Clinical Research Center for Tuberculosis, Guangzhou 510430, China

Xinchun Chen

Department of Pathogen Biology, Shenzhen University School of Medicine, Shenzhen, Guangdong 518060, China

Baoxue Ge

Shanghai Pulmonary Hospital https://orcid.org/0000-0002-4086-8299

Zheng W. Chen

Department of Microbiology and Immunology, Center for Primate Biomedical Research, University of Illinois College of Medicine, Chicago, IL 60612, USA

Gucheng Zeng (zenggch@mail.sysu.edu.cn)

Department of Microbiology, Zhongshan School of Medicine, Key Laboratory for Tropical Diseases Control of the Ministry of Education, Sun Yat-sen University, Guangzhou 510080, China

---

Article

Keywords: tuberculosis, host genetics, gut bacteria, disease susceptibility

Posted Date: September 2nd, 2021

DOI: https://doi.org/10.21203/rs.3.rs-847439/v1

Version of Record: A version of this preprint was published at Nature Metabolism on March 14th, 2022.
See the published version at https://doi.org/10.1038/s42255-022-00547-3.

An *Ifnar1* allele impairs the colonization of gut bacteria and promotes tuberculosis

Lingming Chen[1, #], Guoliang Zhang[2, #], Guobao Li[2, #], Wei Wang[3, #], Zhenhuang Ge[4, #], Yi Yang[1], Xing He[2], Zhi Liu[2], Zhiyi Zhang[1], Qiongdan Mai[1], Yiwei Chen[1], Zixu Chen[1], Jiang Pi[5], Shuai Yang[6], Jun Cui[6], Haipeng Liu[7], Ling Shen[5], Lingchan Zeng[8], Lin Zhou[9], Xinchun Chen[10], Baoxue Ge[7], Zheng W. Chen[5], Gucheng Zeng[1*]

1. Department of Microbiology, Zhongshan School of Medicine, Key Laboratory for Tropical Diseases Control of the Ministry of Education, Sun Yat-sen University, Guangzhou 510080, China.
2. National Clinical Research Center for Infection Diseases, Guangdong Key Laboratory for Emerging Infectious Diseases, Shenzhen Third People's Hospital, Southern University of Science and Technology, Shenzhen 518112, China.
3. Department of Clinical Laboratory, Foshan Fourth People's Hospital, Foshan 528000, China.
4. School of Chemistry, Sun Yat-sen University, Guangzhou 510275, China.
5. Department of Microbiology and Immunology, Center for Primate Biomedical Research, University of Illinois College of Medicine, Chicago, IL 60612, USA.
6. Key Laboratory of Gene Function and Regulation of the Ministry of Education, State Key Laboratory of Biocontrol, School of Life Sciences, Sun Yat-sen University, Guangzhou, 510006, Guangdong, China.
7. Shanghai Key Lab of Tuberculosis, Shanghai Pulmonary Hospital, School of

Medicine, Tongji University, Shanghai, China.

8. Clinical Research Center, Department of Medical Records Management, Guanghua School of Stomatology, Hospital of Stomatology, Sun Yat-sen University, Guangzhou, Guangdong, China.

9. Guangdong Center for Tuberculosis Control, National Clinical Research Center for Tuberculosis, Guangzhou 510430, China.

10. Department of Pathogen Biology, Shenzhen University School of Medicine, Shenzhen, Guangdong 518060, China.

# These authors contributed equally to this work.

* Corresponding author

Address: Department of Microbiology, Zhongshan School of Medicine,

Sun Yat-sen University, Guangzhou 510080, China

E-mail: zenggch@mail.sysu.edu.cn

Phone: +86-13610059833

Abstract

Both host genetics and gut microbiome have important effects on human health, yet how host genetics regulates gut bacteria and further determines disease susceptibility remains unclear. Here, we find that gut microbiome pattern of active tuberculosis (TB) patients is characterized by a reduction of core species found across healthy controls, particularly *Akkermansia muciniphila* (*A. muciniphila*). Oral treatments of *A. muciniphila* or palmitoleic acid, an *A. muciniphila*-derived metabolite, strongly inhibit TB infection through epigenetically inhibiting TNF-α. We use three independent cohorts comprising 6512 individuals and identify that single-nucleotide polymorphism rs2257167 "G" allele of type I interferon (IFN-I) receptor 1 (*Ifnar1*) contributes to stronger IFN-I signaling, impaired colonization and abundance of *A. muciniphila*, reduced production of palmitoleic acid, higher TNF-α, and much severer TB disease in humans and transgenic mice. Thus, host genetics are critical in modulating structure and functions of gut microbiome and gut microbial metabolites, which further determines disease susceptibility.

1. Main

Gut microbial dysbiosis is linked to the development of intra- and extra-intestinal diseases [1,2]. The structures and functions of human gut microbiome are now believed mainly to be shaped by environmental factors [3] and diet [4-7]. However, both innate and adaptive immune components are becoming increasingly critical in regulating the colonization, composition, and abundance of gut microbiota [8-10]. Thus, the alteration of structure and function of gut microbiome should be the result of bi-directional interactions between host factors and its microbial composition and abundance [8-10], and it is unlikely that host genetics only play a redundant or less important role in determining the structure and function of gut microbiota [11-15].

Tuberculosis (TB), a severe infectious disease with extremely high morbidity and mortality, is caused by an airborne bacterial pathogen, *Mycobacterium tuberculosis* (*M. tuberculosis*) [16]. Susceptibility to *M. tuberculosis* infection is affected by multiple intrinsic and extrinsic factors driving host-pathogen interactions. Accumulating evidence has shown that changes in the gut microbiota's structure and activity encode a broad array of functions associated with lung diseases [2,17,18], which is now commonly referred to as the "gut-lung axis" [19-21]. While immune deficiencies or disorders represent key rationales leading to severe and recurrent TB infections, the excessive inflammatory response may be a cause of exacerbated TB during *M. tuberculosis* infection [22-26]. Therefore, regulating immune homeostasis of the "gut-lung axis" may serve as a key approach for successful TB control. Although it was shown that gut microbiota aberration might correlate with TB pathogenesis [27-29], it is

still unclear whether and how host genetics influence the structure and function of gut microbiome to maintain immune homeostasis of "gut-lung axis" and therefore determine the variable TB pathogenicity and susceptibility in *M. tuberculosis*-infected individuals.

In this study, we focused on investigating the relationship among inter-individual variations in host genetic factors, gut microbial abundance, and inflammatory responses in influencing susceptibility and severity of TB infection. We identified a single-nucleotide polymorphism (SNP) in the type I interferon (IFN-I) receptor (*Ifnar1*) gene from 3,125 active TB patients (TB) and 3,387 healthy controls (HC) in three independent cohorts. Importantly, we found that *Ifnar1* rs2257167 G allele could enhance IFN-I signaling, impair the intestinal colonization of *A. muciniphila*, reduce the production of an *A. muciniphila*-derived metabolite, palmitoleic acid, increase production of pro-inflammatory TNF-α, and promote TB infection in both humans and transgenic mouse models, and oral administrations of *A. muciniphila* or palmitoleic acid could reduce TB infections in *M. tuberculosis*-infected mouse models. This work reveals that compositional structures and functions of gut microbiome and gut microbial metabolites are partially determined by host genetic factors, which could have translational potentials for new prevention strategies and therapeutics in TB and potentially other diseases.

2. Results

2.1 Active TB infection is associated with reductions in diversity and abundance

within gut bacteria, particularly *A. muciniphila*.

As an initial step to investigate the relationship among host genetic factors, gut microbiota, and disease susceptibility, we performed 16S rDNA sequencing on fecal samples to assess the features of the gut bacteria in healthy controls (HC) and active TB patients (TB). Since the composition and abundance of gut microbiota might be affected by environmental factors and dietary habits [3,4], faeces were collected in two independent cohorts (**Supplementary Table 1**). There were significant differences of gut bacteria communities in the fecal contents of HC and TB (**Fig. 1a; Extended Data Fig.1a**).

Notably, compared to HC, TB patients showed a broad reduction in diversity and abundance of gut bacteria species (**Fig. 1b; Extended Data Fig. 2a)**. Particularly, Verrucomicrobia was the only phylum with reduced levels in both two cohorts (**Extended Data Fig. 1b, 2b)**, and *A. muciniphila*, a representative species member of Verrucomicrobia phylum [30], was repeatedly observed in two different cohorts to show reduced species richness (**Extended Data Fig. 1c，2c**). Also, the analysis of top 10 species highly enriched in HC or TB showed that *A. muciniphila* was the only bacterial species with reduced abundance in TB patients in both two cohorts (**Fig. 1c-d; Extended Data Fig. 2d**). Importantly, *A. muciniphila* was a critical bacterial species played a significant role in contributing to the abundance of the entire gut microbiome in both HC and TB (**Extended Data Fig. 1d, 2e).**

Since compositional shifts in the microbiota, such as reduced microbial diversity and abundance, may confer negative effects on microbiota's functionality, random

117 forest analysis [31] was performed to further investigate the contribution of the top 10
118 most-reduced species in TB patients, and found that *A. muciniphila* displayed the
119 confirmed importance Z-score (**Fig. 1e; Extended Data Fig. 2f**). In addition, such
120 abundance reduction of *A. muciniphila* in TB patients was consistent with the altered
121 abundance of *A. muciniphila* observed in another study [32].

122 To further verify the random forest analysis, LEfSe analysis was carried out.
123 Several bacteria including *B. vulgatus*, *Bacteroides uniformis*, *Erysipelatoclostridium*
124 *ramosun*, *A. muciniphila*, *Bacteroides caccae,* and *Parabacteroides merdae* were
125 found to have strong influences on compositional shifts of HC or TB (**Extended Data**
126 **Fig. 1e, 2g**). Additionally, *A. muciniphila* was the most significantly upregulated
127 bacterial species in HC, and *B. vulgatus* showed the largest proportion among these
128 six bacteria (**Extended Data Fig. 1f, 2h-i)**. Therefore, these results collectively
129 suggested that reduced abundance of *A. muciniphila* or *B. vulgatus* was highly
130 associated with the development of active TB.

131 **2.2 *A. muciniphila* confers anti-TB protection *via* inhibiting production of pro-**
132 **inflammatory TNF-α.**

133 We then examined whether loss or reduction of the abundance of *A. muciniphila* or
134 *B. vulgatus* might be correlated with abnormal inflammation statuses in active TB. Six
135 major Th1/Th2 cytokines (TNF-α/IFN-γ/IL-10/IL-2/IL-4/IL-6) were selected for
136 analyses based on their well-established importance in mediating TB susceptibility
137 and severity [33-38]. *Ex vivo* production of TNF-α/IFN-γ was higher in TB than those of
138 HC, and such increased production of TNF-α/IFN-γ/IL-10 was at least partially *M.*

139 *tuberculosis*-specific as *ex vivo* re-stimulation using lysates of *M. tuberculosis* further
140 enhanced their productions (**Fig. 1f-g**). Interestingly, the abundance of *A. muciniphila*
141 was negatively correlated with TNF-α production (**Fig. 1h)**. However, there was an
142 erratic association between *A. muciniphila* abundance and IFN-γ (**Fig. 1i**) or IL-10
143 response (**Fig. 1j),** and also no significant correlation between *B. vulgatus* abundance
144 and TNF-α/IFN-γ/IL-10 production (**Extended Data Fig. 3)**. Collectively, these
145 results indicated that a higher TNF-α response was linked to the decreased abundance
146 of *A. muciniphila* but not *B. vulgatus* in *M. tuberculosis* infection, highlighting that *A.*
147 *muciniphila* might function to regulate TB susceptibility or severity *via* regulating
148 TNF-α response.

149 We then investigated potential *in vivo* effect of *A. muciniphila* and *B. vulgatus*
150 during *M. tuberculosis* infection. An aerosol *M. tuberculosis* infection model [39] was
151 developed, and antibiotics-treated mice exhibited much severer pathological
152 impairment and much higher bacillus burdens in lungs (**Extended Data Fig. 4a-e**),
153 confirming that gut microbiota was necessary for mediating anti-TB protection.
154 Moreover, *M. tuberculosis*-infected mice were orally treated with *A. muciniphila* or *B.*
155 *vulgatus*, and it was mice gavaged with *A. muciniphila* but not *B. vulgatus* showed
156 much less hemorrhage and pathological impairment in lungs (**Fig. 2a-f**) and exhibited
157 lower pulmonary bacillus burdens (**Fig. 2g-h**). Additionally, it showed that *M.*
158 *tuberculosis*-infected mice with *A. muciniphila* but not *B. vulgatus* treatments
159 exhibited significantly lower levels of TNF-α, but not IFN-γ/IL-2/IL-4/IL-6/IL-10
160 (**Fig. 2i; Extended Data Fig. 6a**). However, such anti-TB protection effects of *A.*

muciniphila in *M. tuberculosis*-infected mice were partially compromised with TNF-α signaling blockade (**Extended Data Fig. 5a-e)**. Thus, these data collectively suggested that *A.muciniphila* could confer anti-TB protection *via* modulating TNF-α signaling, and such protection effects required intact host TNF-α signaling.

2.3 Impaired colonization of *A. muciniphila* reduces production of its metabolite, palmitoleic acid, and dietary palmitoleic acid inhibits TNF-α production and confers strong protection against TB infection.

We then investigated what bacterial components of *A. muciniphila* mediated anti-TB effects. Metabolite signatures of bacterial cell components and culture supernatants of *A. muciniphila* were subjected to GC-TOF-MS and random forest analyses. It showed that *A. muciniphila*-derived 2-Hydroxybutanoic acid, 3-Hydroxybutyric acid, and palmitoleic acid were potential dominant metabolites involved in mediating anti-TB immunity **(Fig. 3a-b)**. However, only palmitoleic acid but not 2-Hydroxybutanoic acid and 3-Hydroxybutyric acid could significantly reduce TNF-α production (**Fig. 3c; Extended Data Fig. 6c)**. Consistently, KEGG analysis revealed that *A. muciniphila* was less likely to express long-chain-fatty-acid-CoA ligase than *B. vulgatus* (**Extended Data Fig. 7a-e)** and the expression of essential *FAT* gene were significantly increased in feces of mice with *A. muciniphila* treatment (**Extended Data Fig. 7f)**, which might in together allow more production and accumulation of palmitoleic acid in *A. muciniphila*.

Furthermore, oral administrations of *A. muciniphila*, but not *B. vulgatus*,

182 significantly increased palmitoleic acid concentrations in plasma of mice (**Fig. 3d**).
183 Oral administrations of live but not inactivated *A. muciniphila* significantly increased
184 palmitoleic acid concentrations in both plasma and feces of mice (**Fig. 3e, f**).
185 Moreover, KEGG analysis showed that other gut bacteria, which displayed
186 significantly differential abundance between HC and TB, could not produce or
187 accumulate palmitoleic acid as like *A. muciniphila* (**Extended Data Fig. 7g-j**). These
188 data collectively indicated that intestine-colonized *A. muciniphila* was a most
189 important contributor to higher palmitoleic acid levels.

190 Importantly, the relative concentration of palmitoleic acid were significantly higher
191 in both feces and plasma from HC than those from TB (**Fig. 3g-h**), indicating that
192 decreased palmitoleic acid concentration was correlated with active TB in humans.
193 Indeed, *M. tuberculosis*-infected mice with dietary treatments of palmitoleic acid but
194 not butyrate showed much less pulmonary unresolved hemorrhage and pathological
195 impairment (**Fig. 4a-d**) and exhibited lower pulmonary bacillus burdens (**Fig. 4e-f**).
196 Consistently, there was no significant difference in butyrate concentrations in feces
197 between HC and TB (**Fig. 3g**), suggesting that palmitoleic acid might play a more
198 important role than butyrate in mediating TB protection or susceptibility. Additionally,
199 *M. tuberculosis*-infected mice with dietary palmitoleic acid showed significantly
200 lower expression of TNF-α but not IFN-γ/IL-2/IL-4/IL-6/IL-10 in serum compared to
201 butyrate or water treatment (**Fig. 4g; Extended Data Fig. 6b**). These results indicate
202 that such a palmitoleic acid-mediated inhibition effect against pro-inflammatory TNF-
203 α is a key mechanism for *A. muciniphila*-conferred anti-TB protective immunity.

2.4 Intestinal colonization patterns of *A. muciniphila* are influenced by IFN-I signaling.

IFN-I signaling plays critical roles in determining TB pathogenicity, intestinal epithelium development and homeostasis of gut microbial ecosystem [40-45]. Thus, we hypothesized that IFN-I signaling affected the abundance of *A. muciniphila* and in turn resulted in varied TB susceptibility and severity. We fed wild-type and *Ifnar1*$^{-/-}$ mice with feces from HC and TB, respectively (**Extended Data Fig. 8a**), and found that *Ifnar1*$^{-/-}$ mice harbored approximately 2-6 times more abundance of anaerobic bacteria in jejunum or cecum compared to wild-type mice (**Extended Data Fig. 8b)**. Interestingly, regardless of whether feces came from HC or from TB, *A. muciniphila* exhibited much higher levels of colonization and abundance in jejunum, ileum, and cecum of *Ifnar1*$^{-/-}$ mice compared to wild-type controls (**Extended Data Fig. 8c)**. Together, these results suggested that deletion or reduction of IFN-I signaling favored intestinal colonization and abundance of *A. muciniphila*.

2.5 *Ifnar1* rs2257167 G allele dictates stronger IFN-I signaling and increases the risk of developing active TB in humans.

We further postulated that there might be host genetic variants present in *Ifnar1* gene that altered the strength of IFN-I signaling and resulted in inter-individual variations in the abundance and immune regulation function of *A. muciniphila* and *A. muciniphila*-derived metabolites during *M. tuberculosis* infection. Targeted sequencing was performed to analyze the human *Ifnar1* gene in a discovery cohort in

225 Guangzhou, China (**Supplementary Table 2**). Nine SNPs in the intron and only one
226 SNP rs2257167 (which would result in a valine-to-leucine substitution at codon 168
227 in human IFNAR1 (termed as hIFNAR1-V168L) (**Extended Data Fig. 10**)) in the
228 exon, were identified (**Supplementary Table 3**). Since *Ifnar1* rs2257167 GG and GC
229 as well as rs1041868 GG and GA genotypes showed the most significant trend toward
230 higher risk of developing active TB in the Guangzhou cohort (**Supplementary Table**
231 **3**), two larger independent cohorts, including Shenzhen (HC = 1445, TB = 1533) [46]
232 and Foshan cohort (HC = 1679, TB = 1328) in China were recruited to further
233 investigate whether rs2257167 G or rs1041868 G was indeed a risk allele of
234 developing active TB or much severer TB (**Supplementary Table 2**). Indeed, further
235 sequencing analysis [47] validated that individuals carrying rs2257167 G allele
236 exhibited significantly increased risk of developing active TB in both Shenzhen and
237 Foshan cohorts (**Supplementary Table 4**).

238 Notably, we also discovered that individuals carrying rs2257167 genotypes GG and
239 GC displayed higher expression levels of phospho (p)-STAT1, *IFN-β* and *ISG15* than
240 those carrying genotype CC (**Fig. 5a; Extended Data Fig. 11a-c**), suggesting that the
241 G allele enhanced IFN-I signaling. To confirm it, we developed two transgenic mouse
242 lines, denoted as IFNAR1-V168V (harboring G allele) and IFNAR1-V168L
243 (harboring C allele), respectively (**Extended Data Fig. 12a**). There was no significant
244 difference in gene copies or expression levels of h*Ifnar1* between IFNAR1-V168V
245 and IFNAR1-V168L mice (**Extended Data Fig. 12b-c**). However, the expression of
246 p-STAT1, *IFN-β* and *ISG15* in BMDM were higher in IFNAR1-V168V mice than in

IFNAR1-V168L mice (**Fig. 5b; Extended Data Fig. 11d-e)**. Furthermore, the levels of p-STAT1 in intestinal epitheliums as well as IFN-β protein in serum were higher in IFNAR1-V168V mice than in IFNAR1-V168L mice, but these differences weren't observed in the lungs during *M. tuberculosis* infection (**Extended Data Fig. 11f-g**). Additionally, IFNAR1-V168V mice showed higher expression of *IFN-β* and *ISG1* in BMDM and intestinal epitheliums, but not in the lungs, compared to IFNAR1-V168L mice (**Extended Data Fig. 11h-l)**. Collectively, these results suggested that the *Ifnar1* rs2257167 G allele enhanced IFN-I signaling in both humans and mouse models.

2.6 *Ifnar1* rs2257167 G allele decreases the intestinal abundance of *A. muciniphila*, reduces productions of *A. muciniphila*-derived palmitoleic acid, and promotes TB infection.

To explore whether *Ifnar1* rs2257167 G allele affected the intestinal colonization and abundance of *A. muciniphila* as well as production of *A. muciniphila*-derived palmitoleic acid, IFNAR1-V168L and IFNAR1-V168V mice with antibiotics pretreatment were orally given with the same amounts of *A. muciniphila* (**Fig. 5c**). IFNAR1-V168V mice indeed harbored less *A. muciniphila* in intestinal epitheliums, compared to their IFNAR1-V168L counterparts (**Fig. 5d-g; Extended Data Fig. 13**). Importantly, IFNAR1-V168V mice contained lower concentration levels of palmitoleic acid in plasma than IFNAR1-V168L mice did after *A. muciniphila* treatment (**Fig. 5h**). These findings collectively revealed that *Ifnar1* rs2257167 G allele dictating stronger IFN-I signaling could impede the intestinal abundance of *A.*

muciniphila and reduce palmitoleic acid levels.

Meanwhile, there were significantly lower *A. muciniphila* abundance and palmitoleic acid concentration in both fecal samples and plasma in *M. tuberculosis*-infected IFNAR1-V168V mice, compared to IFNAR1-V168L mice (**Fig. 5i-j)**. IFNAR1-V168V mice exhibited larger-scale pathological impairment and more infiltration of inflammatory cells (**Fig. 5k-m**), higher pulmonary bacillus burdens (**Fig. 5n-o**) and TNF-α production than IFNAR1-V168L mice during *M. tuberculosis* infection (**Fig. 5p; Extended Data Fig. 6d**). We also analyzed whether increased *A. muciniphila* abundance could reverse the *Ifnar1* rs2257167 G allele-induced TB severity. Interestingly, *A. muciniphila* treatment showed consistent protective effects against *M. tuberculosis* infection (**Fig. 6a-d; Extended Data Fig. 14a**) and significantly lower levels of TNF-α in IFNAR1-V168V mice (**Fig. 6e; Extended Data Fig. 14b**). Dietary palmitoleic acid alleviated pulmonary TB pathology, reduced bacillus burdens and TNF-α production in *M. tuberculosis*-infected IFNAR1-V168V mice (**Fig. 6f-j; Extended Data Fig. 14c**). These results suggested that oral administrations of *A. muciniphila* or palmitoleic acid could reverse *Ifnar1* rs2257167 G allele-induced TB severity and confer anti-TB protection in a genotype-specific manner.

2.7 *Ifnar1* rs2257167 G allele is associated with less *A. muciniphila* abundance, higher TNF-α production, severer TB pathology, and poorer prognosis in patients with active TB.

We then investigated whether *Ifnar1* rs2257167 G allele could affect *A. muciniphila* abundance in active human TB. TB patients carrying genotypes GC and GG possessed a significantly lower abundance of *A. muciniphila* than patients carrying genotype CC (**Fig. 7a-b**). Importantly, the relative concentration of palmitoleic acid were significantly lower in both feces and plasma from TB patients carrying *Ifnar1* rs2257167 GC and GG than carriers of genotypes CC (**Fig. 7c-d)**. Additionally, compared to TB patients carrying *Ifnar1* rs2257167 CC, carriers of genotypes GC and GG showed much higher (approximately 5-6 folds) *ex vivo* expression levels of *M. tuberculosis*-specific TNF-α (**Fig. 7e-f; Extended Data Fig. 15**). Furthermore, high-resolution computed tomography (HRCT) images were assessed [24,48,49] to analyze the association of *Ifnar1* SNP rs2257167 with clinical features of active TB. TB patients carrying the *Ifnar1* rs2257167 G allele showed significantly higher HRCT scores (suggesting much severer disease) (**Fig. 7g**) and less favorable disease outcomes following a WHO-recommended 2HRZE/4HR treatment regimen (**Fig. 7h**) than patients carrying genotype CC. Collectively, these data indicated that *Ifnar1* rs2257167 G allele was associated with reduced abundance of *A. muciniphila* and hyper-reactive TNF-α, which led to an increased risk of developing active TB and much severer TB disease in humans.

2.8 *A. muciniphila* uses palmitoleic acid to reduce H3K4 tri-methylation (Me3) at *tnfα* promoter and inhibits *M. tuberculosis*-specific TNF-α production.

We previously found that histone modification states at *tnfα* loci determined TNF-α

production by T cells [50]. Therefore, we examined whether *A. muciniphila* and *A. muciniphila*-derived palmitoleic acid had any effect on *M. tuberculosis*-specific TNF-α expression by mediating histone modification of *tnfα* promoter. Immunoblot and ChIP-qPCR analysis showed *A. muciniphila* indeed induced less enrichment of mono-methylation (Me1) of H3K9 and tri-methylation (Me3) of H3K4 at *tnfa* promoter regions (**Extended Data Fig. 16a-f, 17a-b)**. Consistently, palmitoleic acid also significantly decreased *M. tuberculosis*-specific TNF-α production in culture supernatants of mouse T cells, reduced *in vivo* expression of intracellular TNF-α in $CD4^+$/$CD8^+$T cells (**Extended Data Fig. 16g-h, 17c-d)**, and epigenetically reduced enrichment of H3K4Me3 at the *tnfa* promoter during *M. tuberculosis* infection (**Extended Data Fig. 16i, 17e-f)**. Since both H3K9Me1 and H3K4Me3 are histone modifications capable of promoting gene transcription [51], these findings collectively indicated that *A. muciniphila* utilized its effector metabolite, palmitoleic acid, to induce less euchromatin at *tnfα* promoter and inhibit *M. tuberculosis*-specific TNF-α expression.

Discussions

The exact contributions and underlying mechanisms of host genetics, environmental factors, and diet to the structure and function of gut microbiota are still unclear despite recent research advances [3-7,11,13,15]. The precise mechanisms of TB pathogenesis also remain elusive as TB continues to pose as a leading global public health threat [16]. While this study and other groups have shown that the disruption of

the microbiota contributes to increased susceptibility to TB [29,52], fecal transplantation[29] or oral administration of gut bacteria such as *Lactobacillus plantarum* [53] has shown the possibility to restore anti-TB immunity or prevent extra-pulmonary dissemination of pulmonary TB. However, how human genetics modulate compositional shifts of gut microbiome and gut microbial metabolites and elicit varying degrees of TB pathogenicity and severity in different individuals is still unclear.

This work has demonstrated that host genetic factors modulated IFN-I signaling for better colonization and composition of protective gut bacteria, increased levels of gut microbial metabolites, and a more successful control of *M. tuberculosis* infection and TB pathology. Even though long-term or short-term previous medications might also directly or indirectly contribute to altered gut microbiota structures and host immune homeostasis, this work implicated that host genetics might exert a significant impact on colonization and abundance of gut microbiota, which further affect the intestinal or systemic levels of gut microbial metabolites, in some biological settings. Thus, further studies may be useful to uncover how medications including antibiotics treatments may impact gut microbiota and how gut microbiota may facilitate anti-TB treatments in a genotype-specific manner.

While IFN-I signaling is correlated with highly heterogeneous outcomes of TB in different models, with either a protective or pathogenic role [41-43,54-58], the exact mechanisms of how IFNAR1 (i.e. IFN-I) signaling modulates the intestinal colonization of *A. muciniphila* require further studies. Since the gut IFN-I signaling is

353 the primary innate defense mechanism to directly or indirectly facilitate the control of
354 gut pathogens [44], IFN-I signaling driven by a protective *ifnar1* allele may help
355 establish a favorable gene network or ecosystem for colonization of selected gut
356 bacteria, which may lead to increased growth, colonization, and abundance of *A.*
357 *muciniphila*. Moreover, since gut bacteria might utilize soluble IgA antibody for
358 colonization in the intestinal mucosa [10], the gut IFN-I signaling could affect other
359 immune mediators like IgA antibody and further influence the intestinal colonization
360 of *A. muciniphila*.

361 TNF-α is essential to activate innate immunity program for killing intracellular *M.*
362 *tuberculosis* and is required for TB control [59,60]. Indeed, anti-TNF-α therapies have
363 been shown to be associated with an increased risk of developing active TB [59,61].
364 However, hyper-reactive TNF-α inflammation may also be detrimental [22,24] and the
365 delicate modulation of moderate TNF-α inflammation levels was therefore one of the
366 central ideas for avoiding development of active TB disease. While highly excessive
367 or inappropriate TNF-α production was induced by host genetics-dictated lower
368 abundance of *A. muciniphila* in the intestinal compartment in severe TB diseases,
369 colonization dominance of *A. muciniphila* might help prevent aberration of microbial
370 ecosystem and avoid impairment of homeostasis of immune networks.

371 In addition, this work demonstrated that host genetics can determine the structure
372 and function of gut bacteria and impact the concentration levels and immune
373 regulatory functions of gut bacteria-produced effector metabolites. We have shown
374 that *A. muciniphila* utilized its effector metabolite, palmitoleic acid, to regulate

systemic *M. tuberculosis*-specific TNF-α expression. It would also be interesting to explore whether and what metabolites derived from gut bacteria may migrate into the pulmonary compartment and regulate local inflammation (e.g. local TNF-α/IL-1β response in or adjacent lung granuloma [24]) during *M. tuberculosis* infection. It is worth to explore whether manipulating other host genetic factors and/or other gut bacteria or metabolic pathways capable of producing palmitoleic acid could also confer similar or better anti-TB protection effects. Notably, although butyrate appeared to inhibit TNF-α expression in some disease models or biological settings [62-64], we did not observe significant inhibition effect on TNF-α expression and anti-TB protective effects of butyrate in this work.

In summary, this study not only demonstrates the previously unrecognized significance of host genetics-gut microbiota interaction axis in regulating varying TB susceptibility and severity but also provides a new paradigm for deciphering the role of gut microbiota in human health and diseases as well as for developing genotypes-dictated precision therapeutics of TB, particularly MDR-TB, targeting gut microbiota and its metabolites.

Methods

Study subjects. This project aims to identify genetic, microbial, and microbial metabolites responsible for the initiation and severity of tuberculosis (TB). This study uses two independent Chinese Han population cohort for 16S rDNA sequencing analysis: the Shenzhen cohort consists of 28 healthy controls (HC) (age range 23.46 – 54.65 years) and 26 TB patients (age range 23.80 – 47.96 years); the Foshan cohort consists 17 HC (age range 23.36 – 43.84 years) and 19 TB patients (age range 21.85 – 48.78 years). On entry to the study, subjects are screened using a standardized questionnaire by general practitioner and the demographic information was recorded. Subjects were excluded if they had received probiotics treatment three months before their recruitment into the study. Detailed information on the distributions of age, sex, height, weight, and BMI for each cohort samples are provided in **Supplementary Table 1** and **Extended Data Fig. 9a**.

For SNP analysis, this work uses three independent Chinese Han population cohort: Guangzhou cohort as a discovery cohort and Shenzhen cohort and Foshan cohort as replication cohorts. The Guangzhou cohort consists 263 HC (age range 20.78 – 45.18 years) and 264 TB patients (age range 19.91 – 55.51 years). The replication cohorts comprise 2978 individuals from Shenzhen cohort (1445 HC, age range 17.00 – 56.75 years; 1533 TB patients, age range 21.38 – 52.69 years) and 3007 individuals from Foshan cohort (1679 HC, age range 19.90 – 46.70 years; 1328 TB patients, age range 21.21 – 49.08 years). These individuals are not related, neither from a same village or a same family. Detailed information on the distributions of age, sex, height, weight,

and BMI for all cohort samples are provided in **Supplementary Table 2** and **Extended Data Fig. 9b**.

All the patients were prospectively recruited on the basis of TB symptomatic features. The diagnosis of TB was based on clinical signs and symptoms, chest radiography, acid-fast bacilli (AFB) identification (sputum smear, *M. tuberculosis* culture or nucleic acid amplification techniques (NAAT) assay), and response to anti-TB treatment. TB patients with cancers, diabetes, hypertension, or HIV infection were excluded. HC were defined as individuals with normal chest radiograph findings, negative IFN-γ release assay (IGRA), no clinical history of TB, other infectious diseases, and major conditions like cancers, diabetes, and hypertension. The study is designed to recruit the HC in the same regions at the same time. No participant in the cohorts dropped out during the study. All participants were given written informed consent according to protocols approved by the Internal Review and the Ethics Boards of Zhongshan School of Medicine of Sun Yat-sen University.

Isolation of peripheral blood mononuclear cells (PBMCs). PBMCs were isolated from freshly collected heparin lithium blood by Ficoll-Paque Plus density gradient centrifugation. Briefly, Ficoll-Paque Plus was loaded into the blood and centrifuged at 1500 rpm for 20 minutes at 20°C. The isolated monocytes were washed with pH 7.4 PBS (GIBCO), and finally resuspended in 10% fetal bovine serum (FBS) / RPMI-1640 (GIBCO) medium and cultured for further research.

Cytometric Bead Array (CBA) analysis. Culture supernatants of PBMCs derived

435 from HC and TB, or serum isolated from the *M. tuberculosis*-infected mice were
436 subject for analysis of the following cytokines: IL-2, IL-4, IL-6, IL-10, TNF-α, IFN-γ,
437 or IL-17A using the BD Cytometric Bead Array (CBA) Th1/Th2 Cytokine Kit or
438 Th1/Th2/Th17 Cytokine Kit (purchased from BD) as previously described [50]. Data
439 were collected on the Beckman CytoFLEX S (Beckman) and analyzed as previously
440 described [50].

441 **Intracellular cytokine staining (ICS)**. These experiments were performed as
442 previously described [50]. Cells were first stained with cell-surface markers, and then
443 permeabilized for 30 minutes (cytofix/cytoperm, BD) and stained 45 minutes for
444 intracellular molecules such as TNF-α, before being fixated with 2% formalin/PBS.
445 Cells were then analyzed using polychromatic flow cytometry. Isotype matched IgG
446 staining or blank staining served as negative controls to ensure the specificity of ICS
447 experiments. Data were collected on the Beckman CytoFLEX S (Beckman) and
448 analyzed with Kaluza 1.2 software (Beckman).

449 **Antibodies.** Rabbit-signal transducer and activator of transcription 1 (STAT1) (sc-
450 346), rabbit-phosphorylated- (p-) STAT1 (#9167,CST), rabbit anti H3K9Me1
451 (ab9045, Abcam), mouse anti-H3K27Me3 (ab6002, Abcam), rabbit anti-H3K4Me3
452 (ab8580, Abcam), rabbit anti-H3 (ab1791, Abcam), rabbit anti-β actin (ab6276,
453 Abcam), rabbit anti-H3K27Me2 (ab24684, Abcam), mouse anti-H3k9Me2 (ab1220,
454 Abcam), rabbit anti-H3K9Me3 (ab8898, Abcam), CD4-APC-CY7 (GK1. 5,
455 BioLegend), CD8-V450 (53-6.7, BioLegend), TNF-α (MP6-XT22, BioLegend), anti-

TNF-α MAb (BE0244, Bio X Cell), isotype control IgG (BE0091, Bio X Cell).

DNA extraction, 16S rDNA gene amplification, and pyrosequencing (human fecal samples). Fresh fecal samples were collected from TB and HC. DNA was isolated with the DNA Stools Kit (QIAGEN) by following the manufacturer's instructions. Garose gel electrophoresis detection was performed for the purity and concentrations of DNA in fecal samples from the Shenzhen cohort. The corresponding primers were used to amplify DNA: 341F and 806R for V3+V4 regions, 515F and 907R for V4+V5 regions, 515F and 806R for V4 regions. Amplified DNA fragments were PE250 paired-end sequenced by Illumina NovaSeq. For DNA of fecal samples derived from the Foshan cohort, the corresponding primers were used to amplify DNA: 341F-805R for V3+V4 regions, 338F-533R for the V3 Regions, and 967F-1046R for the V6 regions. The index sequences were added and enriched after the extraction was complete. The Qubit 2.0, Agilent 2100, and Bio-RAD CFX 96 were used to quantify the concentrations and purity of the library to ensure DNA quality. Afterward, the library was sequenced on an Illumina HiSeq2500 using the 250 paired-end protocol.

Antibiotics treatment. A mixture of ampicillin (1 mg/ml), streptomycin (5 mg/ml), and colistin (1mg/ml) (Sigma-Aldrich) was added to sterile drinking water for mice. Solutions and bottles were changed 3 times per week. Antibiotic activity was confirmed by cultivating fecal pellets resuspended in BHI + 15% glycerol at 0.1 g/ml and cultured on blood agar plates for 48 hours at 37°C in aerobic and anaerobic

conditions weekly.

Gut colonization with commensal species. *A. muciniphila* (ATCC BAA-835) and *B.vulgatus* (ATCC-8482) were purchased from the ATCC and grown on COS (Columbia Agar with 5% Sheep Blood) plates in an anaerobic atmosphere at 37ºC for at least 72 hours and 48 hours, respectively. Bacteria were harvested from the agar plates and suspended in sterile saline with 10% glycerol to obtain suspensions of 10^9 colony-forming unit (CFU)/ml at an optical density of 600 nm. Gut colonization of antibiotics pre-treated mice was performed by oral gavage with 200 µl suspension containing 2×10^8 bacteria for 3 times per week.

Dietary treatment of metabolites. Palmitoleic acid (Sigma) or butyrate (Sigma) was added to drinking water containing NaOH at a final concentration of 36 mM [65]. Water with same concentration of NaOH was used as control. 100 mg palmitoleic acid was dissolved in 0.1 M NaOH aqueous solution.

Mice and infection. Specific-pathogen free C57BL/6 mice were purchased from Sun Yat-sen University Laboratory Animal Center. Transgenic mice were constructed using microinjection technology for DNA fragments consisting of the human *Ifnar1* gene "G" allele or "C" allele to randomly integrate into the mouse's intestinal epitheliums genome in the C57BL/6 background (Extended Data Fig. 12a). For *M. tuberculosis* infection, each mouse was infected through aerosols with approximately 150 CFU *M. tuberculosis* (H37Rv) for five weeks at Biosafety Level-3 (BSL-3) Laboratory of Sun Yat-sen University (SYSU).

Bacterial and histopathological analysis of *M. tuberculosis*-infected mice. To determine *M. tuberculosis* burden, lungs of mice were homogenized carefully for *M. tuberculosis* CFU counting analysis as we previously described [50]. For tissue histopathological analysis, lung tissues of mice were fixed in 10% zinc formalin and embedded in paraffin. Five μm-thick sections were stained with hematoxylin and eosin (H&E) and images were obtained using Digital Slide Scanning System AxioScan Z1. Images of acid-fast staining were obtained under a microscope (Olympus BX51). An overall histology score was assigned to the lungs of mice based on the degree of granulomatous inflammation as follows: 0 = no lesion, 1 = minimal lesion (1–10% area of tissue in the section involved), 2 = mild lesion (11–30% area involved), 3 = moderate lesion (30–50% area involved), 4 = marked lesion (50–80% area involved), and 5 = severe lesion (> 80% area involved).

Transwell assays. To mimic the effects of epithelium-colonized gut bacteria on cytokine production, a transwell assay was performed using 24-well transwell plates with 0.4 μm-pore inserts (Corning). 2×10^5 intestinal epitheliums in RPMI 1640 medium (Gibco) with 10% FBS with 1×10^5 CFU *A. muciniphila* or medium were seeded into the upper chamber, while 2×10^5 CD3+ T lymphocytes isolated from the spleens of autologous mouse in RPMI 1640 (Gibco) with 10% FBS were added to the lower chamber. T cell isolation was performed as previously described [50]. After 12 hours of incubation, the productions of cytokines in the lower chamber were detected by CBA analysis.

High-resolution computed tomography (HRCT) examination and radiological scoring. HRCT was performed at 10 mm-section interval (120 kV, 50–450 mAs, 1 mm slice thickness, 1.5 second scanning time) with a window level between 2550 and 40 Hounsfield Units (HU) and window width between 300 and 1600 HU using the Toshiba Aquilion 64 CT Scanner (Toshiba, Tokyo, Japan). HRCT scans were analyzed by two independent chest radiologists and conclusions on the findings were reached by consensus. Radio-pathological changes were quantified using a scoring system developed by Ors *et al.* The arbitrary scores were based on the percentage of lung parenchyma abnormality as we and others previously described [48,49].

DNA extraction and SNP genotyping. Fresh blood samples were collected from TB and HC. Genomic DNA was isolated using the DNA Blood Kit (QIAGEN) following the manufacturer's instructions. In the TB discovery study, we used targeted sequencing of the 11 exons in human *Ifnar1* gene and found a SNP rs2257167 in the fourth exon in HC and TB. For validation cohorts, SNP rs2257167 was genotyped in HC and TB using TaqMan assays (ABI, Carlsbad, CA).

Western Blots and chemical reagents. Cells were isolated from indicated individuals or mice and were treated differently based on specific experimental settings. Cells were co-cultured with Sendai virus in some experiments. Total proteins were extracted from cells using RIPA lysis buffer and quantified using BCA Protein Assay Kit (Thermo Fisher Scientific). Extracted proteins mixed with loading buffer were electrophoresed through 10% SDS-PAGE and then transferred to PVDF

membranes (Bio-Rad), which were then blocked in 5% fat-free milk for one hour. The membranes were incubated with primary antibodies at 4°C overnight, and further incubated with a secondary antibody (Thermo Fisher) for 1 hour at room temperature. Signals were detected using Immobilon™ Western Chemiluminescent HRP Substrate (Millipore). Images were captured by the BIO-RAD ChemiDoc Touch machine and analyzed by ImageJ 1.43 software.

Chromatin Immunoprecipitation (ChIP) and ChIP-qPCR. CD3+ T cells were isolated from spleens of mice and treated with *M. tuberculosis* and *A. muciniphila* lysates or metabolites. 1×10^6 cells were collected for each round of ChIP. ChIP was performed using ChIP Assay Kit (Millipore) according to the manufacturer's manual. The antibodies used included rabbit anti-H3K9Me1 (ab9045, Abcam), mouse anti-H3K27Me3 (ab6002, Abcam), rabbit anti-H3K4Me3 (ab8580, Abcam), rabbit anti-H3 (ab1791, Abcam), rabbit anti-H3K27Me2 (ab24684, Abcam), mouse anti-H3k9Me2 (ab1220, Abcam), and rabbit anti-H3K9Me3 (ab8898, Abcam). Real-time qPCR was performed with 2 μl of the immunoprecipitated DNA.

Detection of anaerobic bacteria and *A. muciniphila*. The jejunum, cecum, ileum, and fecal samples of each mouse were homogenized in PBS, respectively. Ten-fold serial dilutions were made using PBS and plated on COS plates (Columbia Agar with 5% Sheep Blood), and incubated at 37°C in anaerobic conditions for 48 hours or at least 72 hours based on experiment settings. Genomic DNA was isolated from tissues or fecal samples using the QIAamp DNA Tissue or Stools Mini Kit (Qiagen)

following the manufacturer's instructions. Targeted qPCR systems were applied using either TaqMan or SYBR Green technology. The primers and probes were used as previously described [66].

Liquid culture of *A. muciniphil*, *B.vulgatus* and *L. salivarius*. Cultures of *A. muciniphila* (ATCC BAA-835) were grown in brain heart infusion (BHI) for at least 72 hours at 37°C in anaerobic conditions. Cultures of *B.vulgatus* (ATCC-8482), which were purchased from the ATCC, were grown in BHI for at least 48 hours at 37°C in anaerobic conditions. Cultures of *L. salivarius* (BNCC 138618) were grown in Man Rogosa Sharpe (MRS) for at least 48 hours at 37°C in anaerobic conditions.

Liquid culture of *A. johnsonii*. Cultures of *A. johnsonii* (BNCC 341940) were grown in Zobell Marine Broth 2216 (2216E) for at least 48 hours at 30°C in aerobic conditions.

Bacterial cell ingredients, bacterial culture supernatant, and plasma metabolites extraction. 100 μl samples were added into 2 ml EP tubes. 0.35 ml extraction liquid (VMethanol) containing 20 μl of L-2-Chlorophenylalanine (1 mg/ml stock in dH2O) was added to each sample as an internal standard. Samples were vortexed for 30 seconds and then centrifuged for 15 minutes at 4℃, 12000 rpm. Supernatants (0.4 ml) were transferred into a fresh 2 ml GC/MS glass vial and then spend-vacuumed to dry. 40 μl Methoxy amination hydrochloride (20 mg/ml in pyridine) was added to each sample and incubated for 30 minutes at 80℃. Then, 60 μl of the BSTFA regent (1% TMCS, v/v) was added to the sample aliquots and incubated for 1.5 hours at 70℃. All

582 samples were analyzed by a gas chromatograph system coupled with a Pegasus HT
583 time-of-flight mass spectrometer (GC-TOF-MS).

584 **Fecal metabolite extraction.** 100 ± 1 mg samples were added into 2 ml EP tubes.
585 0.48 ml of extraction liquid (VMethanol: VChloroform = 3:1) containing 20 μl of L-
586 2-Chlorophenylalanine (1 mg/ml stock in dH2O) was added to each sample as internal
587 standard followed by vortex mixing for 30 seconds. Samples were homogenized in
588 ball mill for 4 minutes at 45 Hz, then treated with ultrasound for 5 minutes (incubated
589 in ice water) for 5 times and centrifuged for 15 minutes at 4℃, 12000 rpm. The
590 supernatant (0.4 ml) was transferred into a fresh 2 ml GC/MS glass vial and then
591 spend-vacuumed to dry. 40 μl Methoxy amination hydrochloride (20 mg/ml in
592 pyridine) was added to each sample and incubated for 30 minutes at 80℃. Then, 60 μl
593 of the BSTFA regent *(*1% TMCS, v/v*)* was added to the sample aliquots and
594 incubated for 1.5 hours at 70℃. All samples were analyzed by a gas chromatograph
595 system coupled with a Pegasus HT time-of-flight mass spectrometer (GC-TOF-MS).

596 **GC-TOF-MS Analysis.** All GC-TOF-MS analyses were performed using an Agilent
597 7890 gas chromatograph system coupled with a Pegasus HT time-of-flight mass
598 spectrometer. The system utilized a DB-5MS capillary column coated with 5%
599 diphenyl cross-linked with 95% dimethylpolysiloxane (30 m × 250 μm inner diameter,
600 0.25 μm film thickness; J & W Scientific, Folsom, CA, USA). A 1 μl aliquot of the
601 analyte was injected in splitless mode. Helium was used as the carrier gas; the front
602 inlet purge flow was set at 3 ml/min, and the gas flow rate through the column was 1

603 ml/min. The initial temperature was kept at 50°C for 1 minute, then raised to 310°C at
604 a rate of 10°C/min, and kept at 310°C for 8 minutes. The injection, transfer line, and
605 ion source temperatures were 280°C, 280°C, and 250°C, respectively. The energy was
606 -70 eV in electron impact mode. The mass spectrometry data were acquired in full-
607 scan mode with the m/z range of 50-500 at a rate of 20 spectra per second after a
608 solvent delay of 6.27 min.

609 **Analysis of GC-TOF-MS.** Data were collected using the Chroma TOF 4.3X software
610 (LECO Corporation) and the LECO-Fiehn Rtx5 database were used for raw peaks
611 exacting, data baselines filtering and calibration of the baseline, peak alignment,
612 deconvolution analysis, peak identification, and integration of the peak area [67]. Both
613 mass spectrum match and retention index match were considered in metabolites
614 identification.

615 **RNA Extraction and Real-Time PCR.** Total RNA was extracted from tissues or
616 PBMCs using Trizol reagent (Takara, Japan) and total RNA concentration was
617 determined by a Nanodrop spectrometer. First-strand cDNA was synthesized using
618 the PrimeScript One Step Strand cDNA Synthesis Kit (Takara, Japan) following the
619 manufacturer's instructions; qPCR was performed in technical triplicates using SYBR
620 Green to determine the expression of *IFN-β* and *ISG15*. GADPH was used as an
621 endogenous control to normalize gene expression (Supplementary Table 5). Relative
622 mRNA expression levels were presented as means ± SEM. Statistical differences were
623 analyzed by Student's *t*-test.

***A. muciniphila* colonization study using transmission electron microscopy (TEM).** The jejunum, cecum, and ileum from mono-colonized mice were trimmed into 2-3 mm cube size and immediately fixed with an ice-cold solution of 3% glutaraldehyde in 0.1 M sodium cacodylate buffer at 4°C overnight. Samples were then post-fixed in 2% osmium tetroxide buffered solution and were embedded in epoxy resin. Subsequently, samples were processed as previously described [10]. Micrographs were produced using a FEI Tecnai G2 Spirit BioTwin 634 transmission electron microscope.

Fluorescent *in situ* hybridization (FISH) and immunofluorescence of *A. muciniphila* in cecum. Paraformaldehyde-fixed, paraffin-embedded colon tissue sections (5 μm) were deparaffinized. A specific fluorescein-labeled oligonucleotide probe [66] targeting one region of the 16S rDNA gene of *A. muciniphila* was used to detect bacterial colonization. Monitoring of nonspecific hybridizations was done using the probe Non-EUB [68] as a negative control. These probes were hybridized to the tissue overnight at 50°C. Then, slides mounted with ProLong® Gold with DAPI (Invitrogen) were sealed with coverslips, left to dry at 4°C in the dark overnight, and imaged using a confocal microscope (LSM 880 with Airyscan).

Statistical analysis. Statistical analysis was performed using GraphPad Prism software. For SNPs and TB susceptibility studies, (1) the Hardy-Weinberg Equilibrium analysis for *Ifnar1* SNP distribution was used in TB patients and HC; (2)The Pearson $\chi 2$ test was used to compare the genotypic and allelic frequencies of

645 SNPs between patients and controls; (3) Unconditional logistic regression adjusted by
646 gender and age was used to calculate the odd ratios (OR), 95% confidence intervals
647 (CIs), and corresponding *p* values using four alternative models (multiplicative,
648 additive, dominant and recessive). For statistical analysis of other experiments,
649 Normal distributions of data was determined with D'Agostino-Pearson omnibus test,
650 statistical significance was determined using one-way ANOVA with Newman-Keuls
651 or Tukey·s multiple comparison test, Student's two-tailed unpaired *t*-test, or Mann-
652 Whitney U test. $P < 0.05$ was considered as statistically significant. *$P < 0.05$, **$P <$
653 0.01, ***$P < 0.001$, and ****$P < 0.0001$. NS, no statistical significance. Odds ratio
654 and *P*-value for SNP analysis were determined by SPSS.

655

Data and code availability

Data of 16S rDNA sequencing are available at https://dataview.ncbi.nlm.nih.gov/. The accession number of 16S rDNA sequencing data is PRJNA609532. Fig. 1, Extended Data Fig. 1, and Extended Data Fig. 2 have associated raw data. All other data are available from the corresponding author upon reasonable request.

Acknowledgments

This work was supported by NSFC Grants 82072250 (To G.C.Z.), and 81873958 (To G.L.Z); National Key R&D Plan Grant 2016YFE0106900 (To G.C.Z.); The National Science and Technology Major Project 2017ZX10201301 and 2017ZX106019, and 2017ZX10103004 (To G.L.Z.); Guangdong Science and Technology Project Grant 2018A050506032 (To G.C.Z.); Shenzhen Scientific and Technological Foundation JCYJ20180228162511084 (To G.L.Z.); and Sanming Project of Medicine in Shenzhen SZSM201911009 (To G.L.Z.).

Author Contributions

L.M.C., Z.H.G., Y.Y., Z.Y.Z., Y.W.C., Q.D.M., Y.W., S.Y., G.H.Z., J.P., L.C.Z. and G.B.L. performed the experiments and analyzed the data. G.L.Z., G.B.L., Z.L., W.W., X.H., and L.Z. collected clinical samples and conducted analysis. S.Y. and J.C. helped with signaling analysis experiments. X.H. and G.L.Z. performed SNP and clinical analysis works, and X.H., Z.L., J.C., L.S., L.C.Z., H.P.L., X.C.C., and B.X.G. assisted data analysis and manuscript preparations. L.M.C., G.C.Z., Z.W.C., X.C.C., and B.X.G. drafted, discussed, and revised the manuscript. G.C.Z. conceived this study.

Declaration of Competing Interests None

References

1. Schirmer, M., *et al.* Dynamics of metatranscription in the inflammatory bowel disease gut microbiome. *Nat Microbiol* **3**, 337-346 (2018).
2. Fujimura, K.E. & Lynch, S.V. Microbiota in allergy and asthma and the emerging relationship with the gut microbiome. *Cell Host Microbe* **17**, 592-602 (2015).
3. Rothschild, D., *et al.* Environment dominates over host genetics in shaping human gut microbiota. *Nature* **555**, 210-215 (2018).
4. David, L.A., *et al.* Diet rapidly and reproducibly alters the human gut microbiome. *Nature* **505**, 559-563 (2014).
5. Wu, G.D., *et al.* Linking long-term dietary patterns with gut microbial enterotypes. *Science* **334**, 105-108 (2011).
6. Muegge, B.D., *et al.* Diet drives convergence in gut microbiome functions across mammalian phylogeny and within humans. *Science* **332**, 970-974 (2011).
7. Ley, R.E., Turnbaugh, P.J., Klein, S. & Gordon, J.I. Microbial ecology: human gut microbes associated with obesity. *Nature* **444**, 1022-1023 (2006).
8. Kawamoto, S., *et al.* The inhibitory receptor PD-1 regulates IgA selection and bacterial composition in the gut. *Science* **336**, 485-489 (2012).
9. Hapfelmeier, S., *et al.* Reversible microbial colonization of germ-free mice reveals the dynamics of IgA immune responses. *Science* **328**, 1705-1709 (2010).
10. Donaldson, G.P., *et al.* Gut microbiota utilize immunoglobulin A for mucosal colonization. *Science* **360**, 795-800 (2018).
11. Bonder, M.J., *et al.* The effect of host genetics on the gut microbiome. *Nat Genet* **48**, 1407-1412 (2016).
12. Igartua, C., *et al.* Host genetic variation in mucosal immunity pathways influences the upper airway microbiome. *Microbiome* **5**, 16 (2017).
13. Goodrich, J.K., *et al.* Human genetics shape the gut microbiome. *Cell* **159**, 789-799 (2014).
14. Lim, M.Y., *et al.* The effect of heritability and host genetics on the gut microbiota and metabolic syndrome. *Gut* **66**, 1031-1038 (2017).
15. Wang, J., *et al.* Genome-wide association analysis identifies variation in vitamin D receptor and other host factors influencing the gut microbiota. *Nat Genet* **48**, 1396-1406 (2016).
16. WHO. Global tuberculosis report. *Geneva: World Health Organization* (2019).
17. Bradley, C.P., *et al.* Segmented Filamentous Bacteria Provoke Lung Autoimmunity by Inducing Gut-Lung Axis Th17 Cells Expressing Dual TCRs. *Cell Host Microbe* **22**, 697-704 e694 (2017).
18. Gauguet, S., *et al.* Intestinal Microbiota of Mice Influences Resistance to Staphylococcus aureus Pneumonia. *Infect Immun* **83**, 4003-4014 (2015).
19. Schuijt, T.J., *et al.* The gut microbiota plays a protective role in the host defence against pneumococcal pneumonia. *Gut* **65**, 575-583 (2016).
20. Budden, K.F., *et al.* Emerging pathogenic links between microbiota and the gut-lung axis. *Nat Rev Microbiol* **15**, 55-63 (2017).
21. Wypych, T.P., Wickramasinghe, L.C. & Marsland, B.J. The influence of the microbiome on respiratory health. *Nat Immunol* **20**, 1279-1290 (2019).

22. Roca, F.J. & Ramakrishnan, L. TNF dually mediates resistance and susceptibility to mycobacteria via mitochondrial reactive oxygen species. *Cell* **153**, 521-534 (2013).
23. Stallings, C.L. Host response: Inflammation promotes TB growth. *Nat Microbiol* **2**, 17102 (2017).
24. Mishra, B.B*., et al.* Nitric oxide prevents a pathogen-permissive granulocytic inflammation during tuberculosis. *Nat Microbiol* **2**, 17072 (2017).
25. Zumla, A*., et al.* Host-directed therapies for infectious diseases: current status, recent progress, and future prospects. *Lancet Infect Dis* **16**, e47-63 (2016).
26. Orme, I.M., Robinson, R.T. & Cooper, A.M. The balance between protective and pathogenic immune responses in the TB-infected lung. *Nat Immunol* **16**, 57-63 (2015).
27. Botero, L.E*., et al.* Respiratory tract clinical sample selection for microbiota analysis in patients with pulmonary tuberculosis. *Microbiome* **2**, 29 (2014).
28. Namasivayam, S*., et al.* Longitudinal profiling reveals a persistent intestinal dysbiosis triggered by conventional anti-tuberculosis therapy. *Microbiome* **5**, 71 (2017).
29. Khan, N*., et al.* Alteration in the Gut Microbiota Provokes Susceptibility to Tuberculosis. *Front Immunol* **7**, 529 (2016).
30. Derrien, M., Vaughan, E.E., Plugge, C.M. & de Vos, W.M. Akkermansia muciniphila gen. nov., sp. nov., a human intestinal mucin-degrading bacterium. *Int J Syst Evol Microbiol* **54**, 1469-1476 (2004).
31. Miron B. Kursa, W.R.R. Feature Selection with the Boruta Package. *Journal of Statistical Software* **36(11)**, p. 1-13 (2010).
32. Hu, Y*., et al.* The Gut Microbiome Signatures Discriminate Healthy From Pulmonary Tuberculosis Patients. *Front Cell Infect Microbiol* **9**, 90 (2019).
33. Behar, S.M. & Sassetti, C.M. Immunology: Fixing the odds against tuberculosis. *Nature* **511**, 39-40 (2014).
34. Ernst, J.D. The immunological life cycle of tuberculosis. *Nat Rev Immunol* **12**, 581-591 (2012).
35. Flynn, J.L. & Chan, J. Immunology of tuberculosis. *Annu Rev Immunol* **19**, 93-129 (2001).
36. Kaufmann, S.H.E., Dorhoi, A., Hotchkiss, R.S. & Bartenschlager, R. Host-directed therapies for bacterial and viral infections. *Nat Rev Drug Discov* **17**, 35-56 (2018).
37. O'Garra, A*., et al.* The immune response in tuberculosis. *Annu Rev Immunol* **31**, 475-527 (2013).
38. Zeng, G., Zhang, G. & Chen, X. Th1 cytokines, true functional signatures for protective immunity against TB? *Cell Mol Immunol* **15**, 206-215 (2018).
39. Wang, L*., et al.* Oxidization of TGFbeta-activated kinase by MPT53 is required for immunity to Mycobacterium tuberculosis. *Nat Microbiol* **4**, 1378-1388 (2019).
40. Qiu, L*., et al.* Severe tuberculosis induces unbalanced up-regulation of gene networks and overexpression of IL-22, MIP-1alpha, CCL27, IP-10, CCR4, CCR5, CXCR3, PD1, PDL2, IL-3, IFN-beta, TIM1, and TLR2 but low antigen-specific cellular responses. *J Infect Dis* **198**, 1514-1519 (2008).
41. Teles, R.M*., et al.* Type I interferon suppresses type II interferon-triggered human anti-mycobacterial responses. *Science* **339**, 1448-1453 (2013).
42. Berry, M.P*., et al.* An interferon-inducible neutrophil-driven blood transcriptional signature in human tuberculosis. *Nature* **466**, 973-977 (2010).
43. Mayer-Barber, K.D*., et al.* Host-directed therapy of tuberculosis based on interleukin-1 and

type I interferon crosstalk. *Nature* **511**, 99-103 (2014).
44. Tschurtschenthaler, M.*, et al.* Type I interferon signalling in the intestinal epithelium affects Paneth cells, microbial ecology and epithelial regeneration. *Gut* **63**, 1921-1931 (2014).
45. Sun, L.*, et al.* Type I interferons link viral infection to enhanced epithelial turnover and repair. *Cell Host Microbe* **17**, 85-97 (2015).
46. Zhang, G.*, et al.* A proline deletion in IFNAR1 impairs IFN-signaling and underlies increased resistance to tuberculosis in humans. *Nat Commun* **9**, 85 (2018).
47. Zhang, G.*, et al.* A functional single-nucleotide polymorphism in the promoter of the gene encoding interleukin 6 is associated with susceptibility to tuberculosis. *J Infect Dis* **205**, 1697-1704 (2012).
48. Zhang, G.*, et al.* Allele-specific induction of IL-1beta expression by C/EBPbeta and PU.1 contributes to increased tuberculosis susceptibility. *PLoS Pathog* **10**, e1004426 (2014).
49. Ors, F.*, et al.* High-resolution CT findings in patients with pulmonary tuberculosis: correlation with the degree of smear positivity. *J Thorac Imaging* **22**, 154-159 (2007).
50. Wang, Y.*, et al.* Long noncoding RNA derived from CD244 signaling epigenetically controls CD8+ T-cell immune responses in tuberculosis infection. *Proc Natl Acad Sci U S A* **112**, E3883-3892 (2015).
51. Wang, J.*, et al.* Sequence features and chromatin structure around the genomic regions bound by 119 human transcription factors. *Genome Res* **22**, 1798-1812 (2012).
52. Khan, N.*, et al.* Intestinal dysbiosis compromises alveolar macrophage immunity to Mycobacterium tuberculosis. *Mucosal Immunol* **12**, 772-783 (2019).
53. Negi, S., Pahari, S., Bashir, H. & Agrewala, J.N. Gut Microbiota Regulates Mincle Mediated Activation of Lung Dendritic Cells to Protect Against Mycobacterium tuberculosis. *Front Immunol* **10**, 1142 (2019).
54. Giosue, S.*, et al.* Effects of aerosolized interferon-alpha in patients with pulmonary tuberculosis. *Am J Respir Crit Care Med* **158**, 1156-1162 (1998).
55. Boxx, G.M. & Cheng, G. The Roles of Type I Interferon in Bacterial Infection. *Cell Host Microbe* **19**, 760-769 (2016).
56. McNab, F., Mayer-Barber, K., Sher, A., Wack, A. & O'Garra, A. Type I interferons in infectious disease. *Nat Rev Immunol* **15**, 87-103 (2015).
57. Moreira-Teixeira, L., Mayer-Barber, K., Sher, A. & O'Garra, A. Type I interferons in tuberculosis: Foe and occasionally friend. *J Exp Med* **215**, 1273-1285 (2018).
58. Ji, D.X.*, et al.* Type I interferon-driven susceptibility to Mycobacterium tuberculosis is mediated by IL-1Ra. *Nat Microbiol* **4**, 2128-2135 (2019).
59. Flynn, J.L.*, et al.* Tumor necrosis factor-alpha is required in the protective immune response against Mycobacterium tuberculosis in mice. *Immunity* **2**, 561-572 (1995).
60. Miller, E.A. & Ernst, J.D. Anti-TNF immunotherapy and tuberculosis reactivation: another mechanism revealed. *J Clin Invest* **119**, 1079-1082 (2009).
61. Keane, J.*, et al.* Tuberculosis associated with infliximab, a tumor necrosis factor alpha-neutralizing agent. *N Engl J Med* **345**, 1098-1104 (2001).
62. Aden, K.*, et al.* Metabolic Functions of Gut Microbes Associate With Efficacy of Tumor Necrosis Factor Antagonists in Patients With Inflammatory Bowel Diseases. *Gastroenterology* **157**, 1279-1292 e1211 (2019).
63. Scott, N.A.*, et al.* Antibiotics induce sustained dysregulation of intestinal T cell immunity by

perturbing macrophage homeostasis. *Sci Transl Med* **10**(2018).
64. Lachmandas, E.*, et al.* Diabetes Mellitus and Increased Tuberculosis Susceptibility: The Role of Short-Chain Fatty Acids. *J Diabetes Res* **2016**, 6014631 (2016).
65. Arpaia, N.*, et al.* Metabolites produced by commensal bacteria promote peripheral regulatory T-cell generation. *Nature* **504**, 451-455 (2013).
66. Collado, M.C., Derrien, M., Isolauri, E., de Vos, W.M. & Salminen, S. Intestinal integrity and Akkermansia muciniphila, a mucin-degrading member of the intestinal microbiota present in infants, adults, and the elderly. *Appl Environ Microbiol* **73**, 7767-7770 (2007).
67. Kind, T.*, et al.* FiehnLib: mass spectral and retention index libraries for metabolomics based on quadrupole and time-of-flight gas chromatography/mass spectrometry. *Anal Chem* **81**, 10038-10048 (2009).
68. Amann, R.I.*, et al.* Combination of 16S rRNA-targeted oligonucleotide probes with flow cytometry for analyzing mixed microbial populations. *Appl Environ Microbiol* **56**, 1919-1925 (1990).

Fig. 1

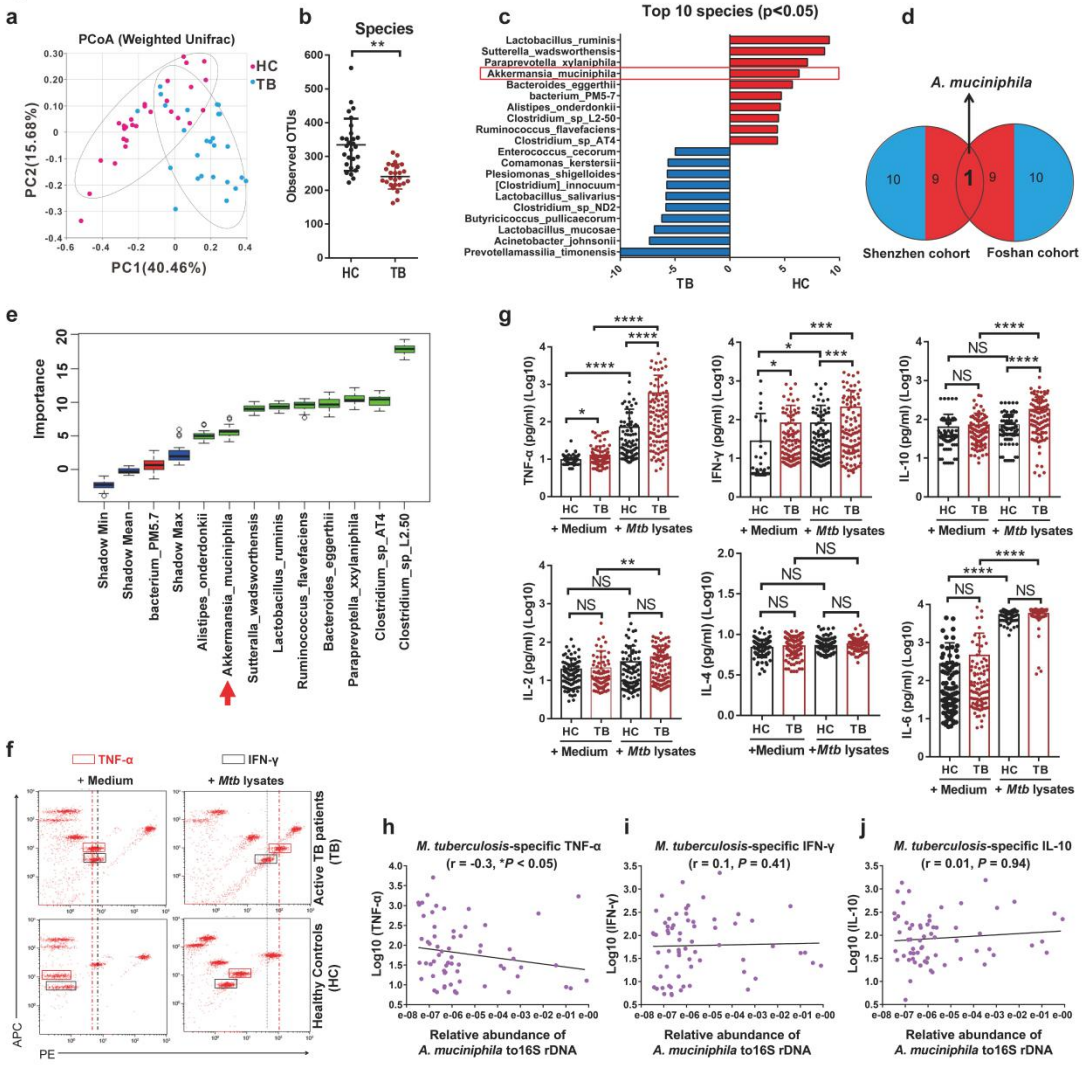

Fig. 1. Reduction of *A. muciniphila* abundance is associated with active TB infection and higher *M. tuberculosis*-specific TNF-α production in humans.

(a) Principal Co-ordinates Analysis (PCoA) plot (based on weighted UniFrac distances) (HC = 28, TB = 26, Shenzhen cohort).

(b) Numbers of observed operational taxonomic units (OTUs) of species in fecal microbiota of indicated individuals (HC = 28, TB = 26, Shenzhen cohort).

(c) The top 10 bacterial species with enriched relative abundance in HC were adjusted $P < 0.05$ and log2 (HC/TB) > 0, species with enriched relative abundance in TB were adjusted $P < 0.05$ and log2 (HC/TB) < 0 (HC, n = 28; TB, n = 26). The red

box indicates *A. muciniphila*.

(d) Venn diagram analysis of top 10 species enriched in HC or TB from Shenzhen and Foshan cohorts.

(e) Predictive power of top 10 species enriched in HC (i.e. the top 10 most reduced species in TB) assessed by random forest analysis. Blue boxplots acted as benchmarks. Green boxplots represent confirmed species and red boxplots represent rejected species. Red arrowhead marks *A. muciniphila*.

(f) CBA analysis of culture supernatants of PBMCs derived from TB patients and HC in the Shenzhen cohort. Red- and black-boxed areas mark fluorescent clusters of TNF-α and IFN-γ, respectively, and dashed lines mark the shift of fluorescent clusters of TNF-α and IFN-γ, respectively.

(g) Pooled bar data show expressions of TNF-α/IFN-γ/IL-2/IL-4/IL-6/IL-10 in cultured supernatants of PBMCs derived from TB (n = 96) and HC (n = 96) of Shenzhen cohort.

(h-j) Spearman correlation analysis shows the association between *ex vivo* concentration of TNF-α/IFN-γ/IL-10 and the relative abundance of *A. muciniphila* in fecal samples of TB (n = 63).

Error bars indicate SD. $P < 0.05$ (*); $P < 0.01$ (**); $P < 0.001$ (***); $P < 0.0001$ (****); NS (no statistical significance). *P* values were calculated by Mann-Whitney *U* test [(b) and (c)], one-way ANOVA with Newman-Keuls multiple comparison test (g), and Spearman correlation (h-j).

Fig. 2

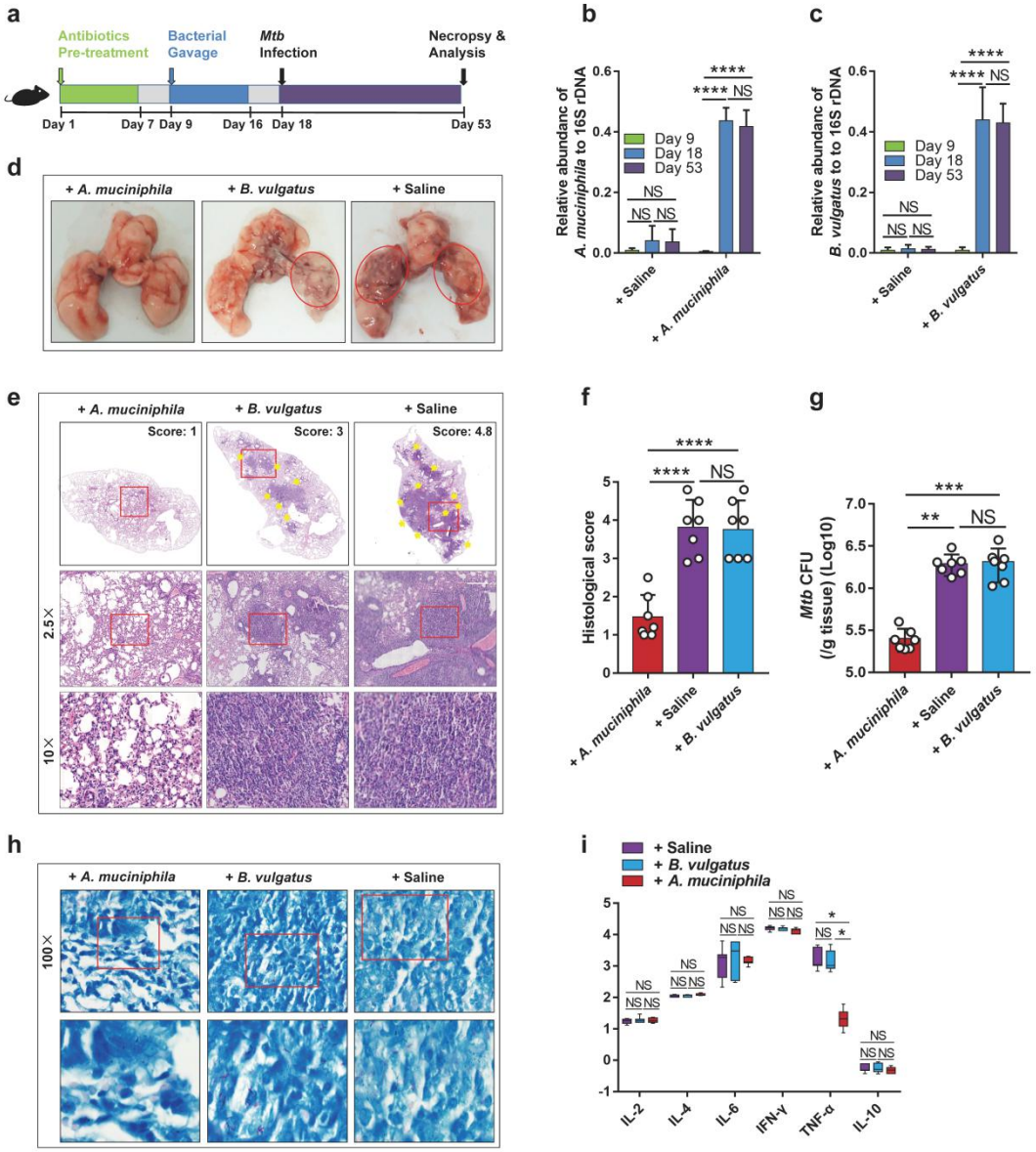

Fig. 2. *A. muciniphila* confers anti-TB protection and reduces TNF-α expression.

(a) Experimental diagram for determining the role of *A. muciniphila* or *B. vulgatus* during *M. tuberculosis* infection.

(b-c) Analysis of *A. muciniphila* (b) or *B. vulgatus* (c) abundance in stool samples from mice at day 9, 18 and 53 using qPCR analysis.

(d) Three representative lungs of *M. tuberculosis*-infected mice treated with *A. muciniphila*, *B. vulgatus* or saline. Red circles mark the severe, unresolved

hemorrhage, massive disruption or caseous necrosis on the lungs of *M. tuberculosis*-infected mice.

(e-f) Hematoxylin and eosin (H&E) staining of three representative lungs (e) and histological score (f) of *M. tuberculosis*-infected mice treated with *A. muciniphila*, *B. vulgatus* and saline at 5 weeks post infection. Top: original magnification; Middle: 2.5× of original magnification; Bottom: 10× of original magnification. The red-boxed areas at the top are enlarged below. Yellow arrowheads mark lesions and infiltration of inflammatory cells.

(g) Quantitative analysis of bacillus CFU in lung homogenates of *M. tuberculosis*-infected mice treated with *A. muciniphila*, *B. vulgatus* and saline at 5 weeks post infection.

(h) *M. tuberculosis* was visualized in lung sections using acid-fast staining at 5 weeks post infection. Top: 100× of original magnification. The red-boxed areas at the top are enlarged below.

(i) Pooled bar graphic data show the expression of TNF-α/IFN-γ/IL-2/IL-4/IL-6/IL-10 in serum derived from *M. tuberculosis*-infected mice with *A. muciniphila*, *B. vulgatus* and saline treatment.

N = 7 mice per group. Error bars indicate SD. $P < 0.01$ (**); $P < 0.001$ (***); $P < 0.0001$ (****); NS (no statistical significance). *P* values were calculated by one-way ANOVA with Tukey's multiple comparison test [(b), (c), (f), (g) and (i)]. At least two biological repeats were performed.

Fig. 3

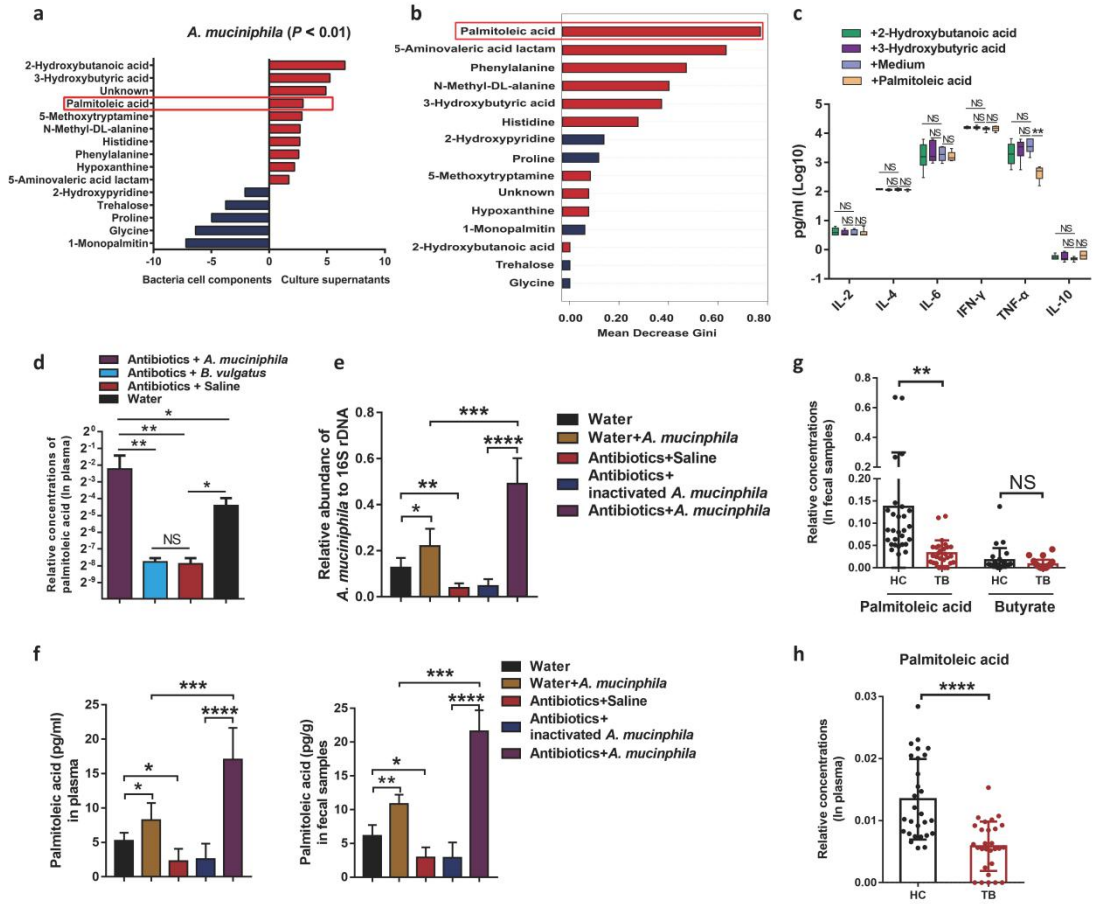

888

889 **Fig. 3. *A. muciniphila* produces high levels of palmitoleic acid, an effector**

890 **metabolite with TNF-α inhibition effects, and healthy controls (HC) show higher**

891 **palmitoleic acid levels in both feces and plasma than active TB patients (TB).**

892 **(a)** Palmitoleic acid marked in red box was the ingredient with higher concentrations

893 in culture supernatants of *A. muciniphila*, compared to *A. muciniphila* bacterial

894 cell ingredients. *A. muciniphila* was cultured for 72 hours, and then bacteria

895 lysates and culture supernatants were, respectively, subjected to GC-TOF-MS-

896 based metabolic analysis. More ingredients enriched in *A. muciniphila* culture

897 supernatants with an adjusted $P < 0.01$ and log2 (culture supernatants / bacterial

898 cell ingredients) > 0; More ingredients enriched in *A. muciniphila* bacterial cell

899 ingredients with an adjusted $P < 0.01$ and log2 (cultured supernatants / bacterial

cell ingredients) < 0. *A. muciniphila* culture supernatants were normalized to Brain Heart Infusion (BHI). Data are representative of three experiments with three independent biological replicates.

(b) The selected metabolites showing the significant concentration differences between bacterial cell ingredients and culture supernatants of *A. muciniphila,* as determined in (A), showed the most significant influences on Gini of random forest classification in culture supernatants between *A. muciniphila* and *B. vulgatus*. Palmitoleic acid marked in red box shows the strongest influence on Gini of random forest classification in culture supernatants of *A. muciniphila* and *B. vulgatus*. *A. muciniphila* was cultured for 72 hours and *B. vulgatus* was cultured for 48 hours, and their productions of metabolites in culture supernatants were detected by GC-TOF-MS analysis. Data are representative of three experiments with three independent biological replicates.

(c) Pooled bar graphic data showed the *in vitro* expression of TNF-α/IFN-γ/IL-2/IL-4/IL-6/IL-10 in culture supernatants of CD3+ T cells. T cells were co-cultured with *M. tuberculosis* lysates (10 μg/ml) only or with 2-Hydroxybutanoic acid, 3-Hydroxybutyric acid, or palmitoleic acid for 3 days. N = 6 mice per group.

(d) Palmitoleic acid concentrations in plasma derived from mice with oral administration of *A. muciniphila* were higher than those in plasma of mice treated with *B. vulgatus* or saline or mice with drinking water only. Mice for bacteria transplantation and saline were pretreated with antibiotics for one week and plasma samples were collected at the third day after oral gavage of bacteria.

Plasma of mice treated with *A. muciniphila*, *B. vulgates*, saline and water only were subjected to GC-TOF-MS-based metabolic analysis. N = 6 mice per group.

(e) The qPCR-based quantitative analyses of *A. muciniphila* abundance in stool samples from mice with drinking water only, mice with drinking water plus oral administration of *A. muciniphila* and antibiotics-treated mice with oral administration of inactive *A. muciniphila* or *A. muciniphila* at the third day after bacteria gavage.

(f) The quantitative analyses of palmitoleic acid concentrations in plasma and fecal samples derived from mice with drinking water only, mice with drinking water plus oral administration of *A. muciniphila* and antibiotics-pretreated mice with oral administration of inactive *A. muciniphila* or live *A. muciniphila* at the third day after bacteria gavage.

(g) Palmitoleic acid showed much higher relative concentrations in fecal samples in HC than TB. There was no significant difference of butyrate in fecal samples between HC and TB. Fecal samples of HC and TB were subjected to GC-TOF-MS-based metabolic analysis. (HC = 28, TB = 26, Shenzhen cohort).

(h) Relative concentrations of palmitoleic acid in plasma of HC were higher than those in plasma of TB. Plasma of HC and TB were subjected to GC-TOF-MS-based metabolic analysis. (HC = 28, TB = 26, Shenzhen cohort). Note that butyrate was non-detectable in plasma in both HC and TB.

N = 6 mice per group. Error bars indicate SD. $P < 0.05$ (*); $P < 0.01$ (**); $P < 0.001$ (***); $P < 0.0001$ (****). *P* values were calculated by Mann-Whitney test (A), one-

944 way ANOVA with Tukey's multiple comparison test [(c), (d), (e) and (f)] and
945 Student's two-tailed unpaired *t*-test [(g) and (h)]. At least two biological repeats were
946 performed.
947

Fig. 4

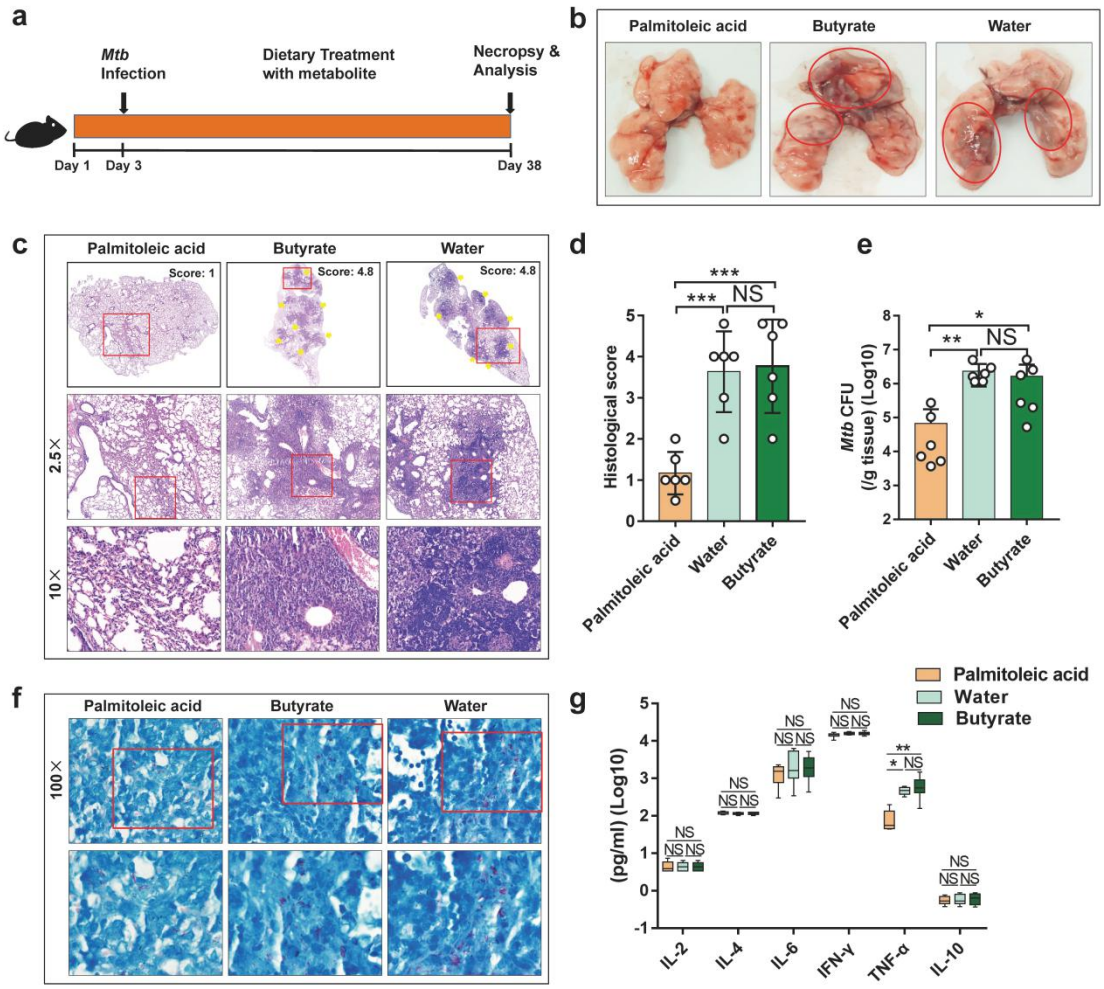

948

949 **Fig. 4. Dietary an *A. muciniphila*-derived metabolite, palmitoleic acid, reduces**

950 **TB pathology, bacillus burdens and TNF-α production in mice.**

951 **(a)** Experimental diagram for determining the role of palmitoleic acid or butyrate

952 during *M. tuberculosis* infection.

953 **(b)** Three representative lungs of *M. tuberculosis*-infected mice treated with

954 palmitoleic acid, butyrate or water. Red circles mark the TB pathology or damage

955 on the lungs of *M. tuberculosis*-infected mice.

956 **(c-d)** H&E staining of three representative lungs (c) and histological scores (d) of *M.*

957 *tuberculosis*-infected mice with dietary palmitoleic acid, butyrate or water at 5

weeks post infection. Top: original magnification; Middle: 2.5; Bottom: 10×. The red-boxed areas at the top are enlarged below. Yellow arrowheads mark the lesions and infiltration of inflammatory cells.

(e) Quantitative analysis of bacillus CFU in lung homogenates of *M. tuberculosis*-infected mice with dietary palmitoleic acid, butyrate or water at 5 weeks post infection.

(f) The *M. tuberculosis* was visualized in lung sections using acid-fast staining at 5 weeks post infection. Top: 100× of original magnification. The red-boxed areas at the top are enlarged below.

(g) Pooled bar graphic data show the expression of cytokines in serum derived from *M. tuberculosis*-infected mice with dietary palmitoleic acid, butyrate or water.

N = 6 mice per group. Error bars indicate SD. $P < 0.05$ (*); $P < 0.01$ (**); $P < 0.001$ (***); NS (no statistical significance). *P* values were calculated by one-way ANOVA with Tukey's multiple comparison test [(d), (e) and (g)]. At least two biological repeats were performed.

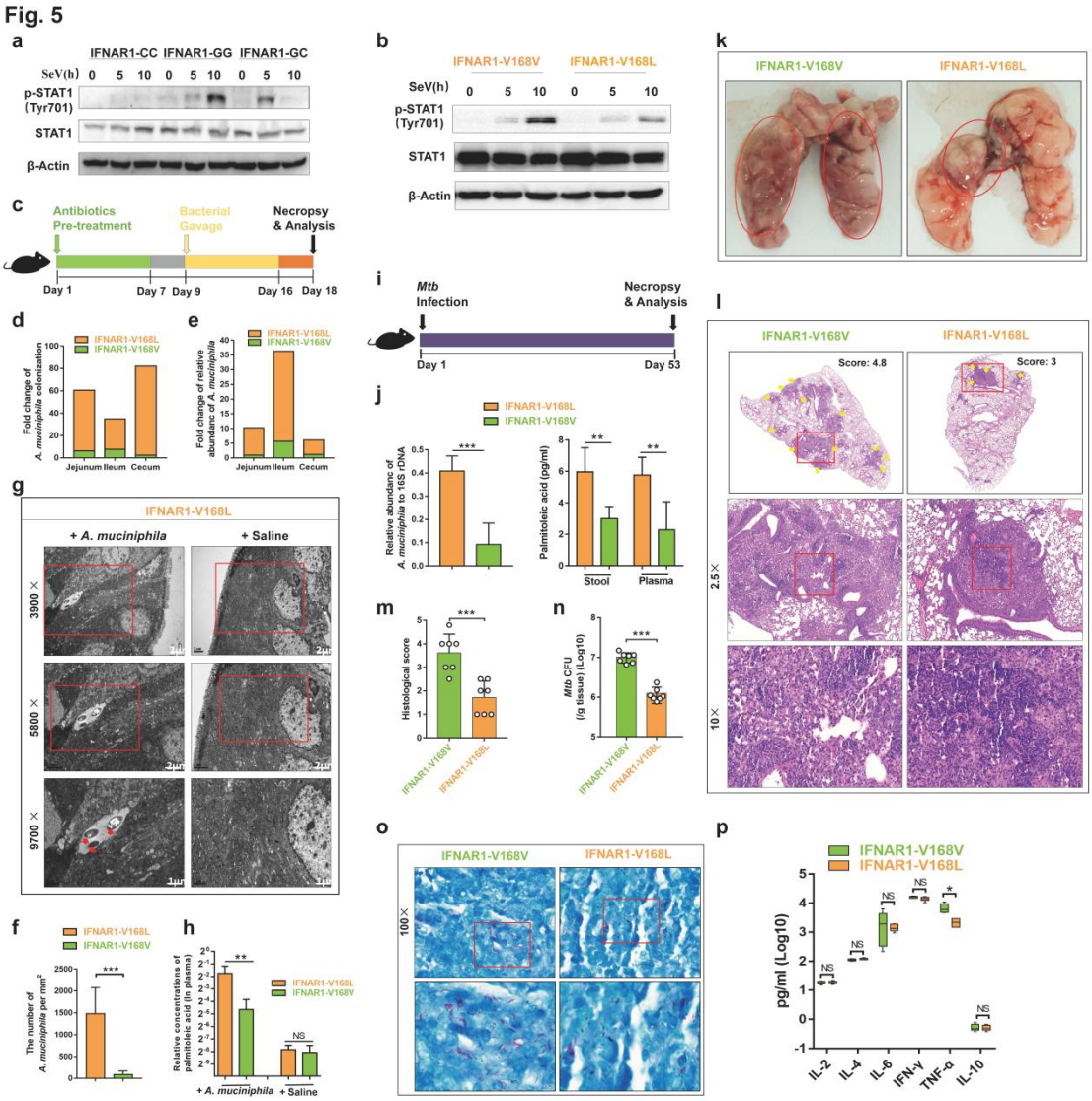

Fig. 5. *Ifnar1* rs2257167 G allele dictates stronger IFN-I signaling in both humans and mice, decreases colonization and abundance of *A. muciniphila*, and promotes higher TNF-α production and severer TB infection in transgenic mouse models.

(a) Immunoblot analysis of the levels of phosphorylated(p)- and total STAT1 in PBMCs derived from individuals carrying genotype GG, GC, CC with Sendai virus stimulation at 0, 5 and 10 hours. Data are representative of three experiments with three independent biological replicates.

983 **(b)** Immunoblot analysis of the levels of p- and total STAT1 in Bone Marrow Derived
984 Macrophage (BMDM) derived from IFNAR1-V168V and IFNAR1-V168L mice
985 at 0, 5 and 10 hours following Sendai virus stimulation. Data are representative of
986 three experiments with three independent biological replicates.
987 **(c)** Experiment design: oral administration for determining the role of IFN-I signaling
988 in *A. muciniphila* abundance.
989 **(d)** Pooled data of relative amounts of *A. muciniphila* recovered from jejunum, ileum
990 and cecum of IFNAR1-V168L (orange bar) and IFNAR1-V168V (green bar) mice,
991 respectively. Fold changes were calculated as: CFU of *A. muciniphila* mice mono-
992 colonized with *A. muciniphila* normalized to those of saline-treated mice carrying
993 the same genotype. N = 20 mice per group.
994 **(e)** Pooled data of relative expression levels of *A. muciniphila* recovered from
995 jejunum, ileum and cecum of IFNAR1-V168L (orange bar) and IFNAR1-V168V
996 (green bar) mice, respectively. Fold changes were calculated as: expression levels
997 of *A. muciniphila* of mice mono-colonized with *A. muciniphila* normalized to
998 those of same genotype mice with oral saline administration. N = 20 mice per
999 group.
1000 **(f)** FISH/Confocal microscope-based half-quantitative assessment of *A. muciniphila*
1001 on the intestinal mucosa of IFNAR1-V168L and IFNAR1-V168V mice mono-
1002 colonized with *A. muciniphila*. Twenty confocal microscopic views from each
1003 mouse line were subjected to analysis of *A. muciniphila* amounts.
1004 **(g)** Representative TEM images of intestinal samples from IFNAR1-V168L mice

gavaged with *A. muciniphila* and saline, respectively. The red-boxed areas at the upper panel are enlarged lower panel. 2 μm (Top panel), 2 μm (Middle panel) and 1 μm (Bottom panel). Red arrowheads mark the *A. muciniphila*.

(h) Palmitoleic acid concentrations in plasma derived from IFNAR1-V168L mice were higher than in plasma of IFNAR1-V168V mice when these mice were orally treated with the same amounts of *A. muciniphila*. Antibiotics-pretreated transgenic mice were gavaged with *A. muciniphila* or saline. Plasma of IFNAR1-V168L and IFNAR1-V168V mice with oral administration of *A. muciniphila* and saline were subjected to GC-TOF-MS-based metabolic analysis. N = 6 mice per group.

(i) Experimental diagram for determining the role of SNP rs2257167 during *M. tuberculosis* infection.

(j) Analysis of *A. muciniphila* abundance in stool samples using qPCR analysis, and the quantitative analyses of palmitoleic acid concentrations in plasma and fecal samples derived from IFNAR1-V168V and IFNAR1-V168L mice at 5 weeks post infection.

(k) Representative lungs derived from the *M. tuberculosis*-infected IFNAR1-V168V and IFNAR1-V168L mice, respectively. Red circles mark the hemorrhage or necrosis in the lungs of *M. tuberculosis*-infected mice.

(l-m) H&E staining of two representative lungs (L) and histological score (M) of *M. tuberculosis*-infected transgenic mice at 5 weeks post infection. Top: original magnification; Middle: 2.5× of original magnification; Bottom: 10× of original magnification. The red-boxed areas at the top are enlarged below. Yellow

arrowheads point lesions and infiltration of inflammatory cells.

(n) CFU quantification of *M. tuberculosis* in the lungs at 5 weeks post infection.

(o) The acid-fast staining-based assessment of *M. tuberculosis* inside the lung tissues. Note that more acid-fast staining-positive bacilli in lung sections derived from IFNAR1-V168V mice. Top: 100× of original magnification. The red-boxed areas at the top are enlarged below.

(p) Pooled bar graphic data show the expression of cytokines in serum derived from *M. tuberculosis*-infected IFNAR1-V168V and IFNAR1-V168L mice, respectively. Serum was collected on 35 days post *M. tuberculosis* infection for CBA-based cytokine analysis.

Error bars indicate SD. $P < 0.05$ (*); $P < 0.01$ (**); $P < 0.001$ (***). *P* value was calculated by Student's two-tailed unpaired *t*-test [(f), (h), (j), (m), (n) and (p)]. At least two biological repeats were performed.

Fig. 6

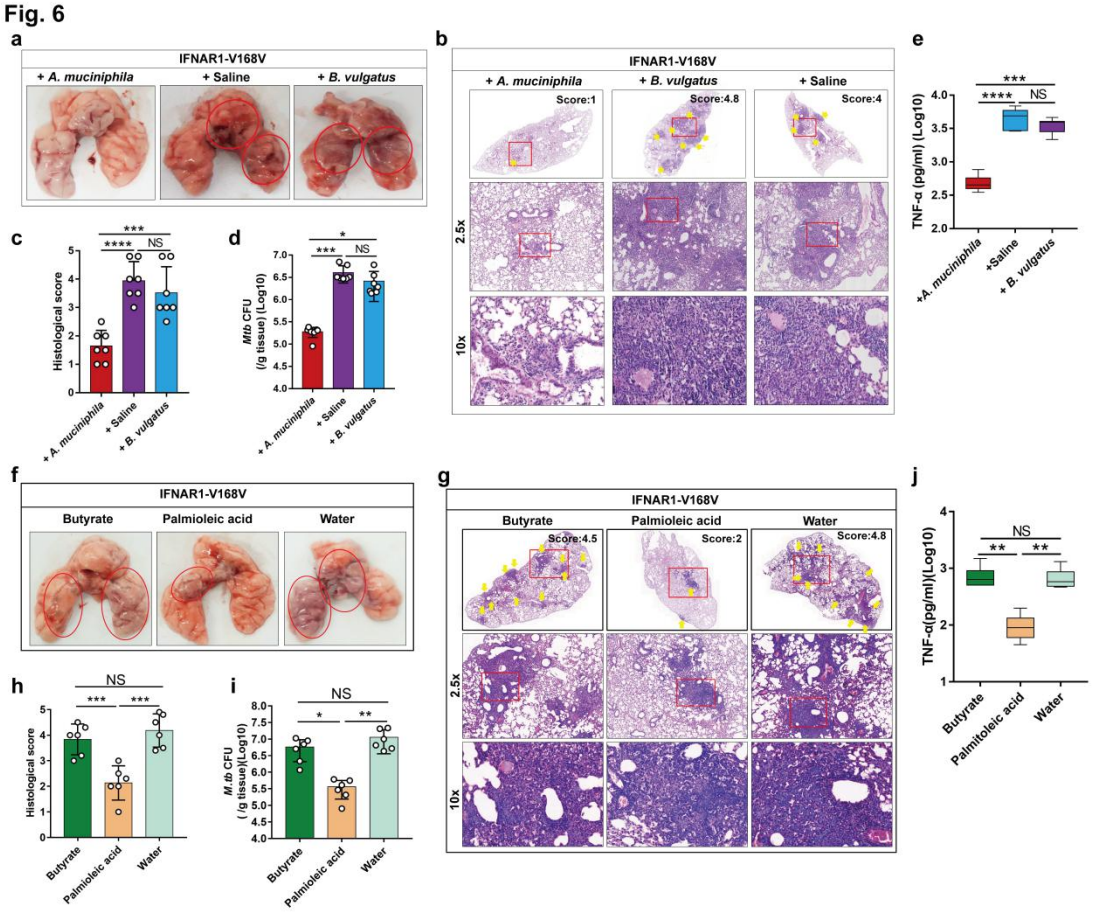

Fig. 6. Oral gavage of *A. muciniphila* or palmitoleic acid reduces TB pathology and bacillus burdens in *M. tuberculosis*-infected transgenic mice carrying human *Ifnar1* rs2257167 "G" allele (termed IFNAR1-V168V mice).

(a) Three representative lungs derived from *M. tuberculosis*-infected IFNAR1-V168V mice with oral administration of *A. muciniphila*, *B. vulgatus* and saline. Red circles mark the lung pathology of infected mice.

(b-c) H&E staining of three representative lungs (b) and histological score (c) of *M. tuberculosis*-infected IFNAR1-V168V mice at 5 weeks post infection. Top: original magnification; Middle: 2.5×; Bottom: 10×. The red-boxed areas at the top are enlarged below. Yellow arrowheads mark lesions and infiltration of inflammatory cells, compared with saline treatment. N = 7 mice per group.

(d) CFU quantification analysis of *M. tuberculosis* burdens in the lung homogenates at 5 weeks post infection. IFNAR1-V168V mice with mono-colonization of *A. muciniphila* but not *B. vulgatus* had much lower bacterial burdens, compared with saline treatment. N = 7 mice per group.

(e) Pooled bar graphic data show the expression of TNF-α in serum derived from *M. tuberculosis*-infected IFNAR1-V168V mice with oral administration of *A. muciniphila*, *B. vulgatus* and saline. Serum was collected on 35 days post *M. tuberculosis* infection for CBA-based cytokine analysis. N = 7 mice per group.

(f) Gross pathology shows that the palmitoleic acid decreases hemorrhage and necrosis in lungs of *M. tuberculosis*-infected IFNAR1-V168V mice at 5 weeks post infection. Red circles mark the TB pathology or damage on the lungs of *M. tuberculosis*-infected mice.

(g-h) H&E staining of three representative lungs (g) and histological scores (h) of *M. tuberculosis*-infected IFNAR1-V168V mice with dietary palmitoleic acid, butyrate or water at 5 weeks post infection. Top: original magnification; Middle: 2.5; Bottom: 10×. The red-boxed areas at the top are enlarged below. As marked by yellow arrowheads, mice with dietary palmitoleic acid but not butyrate showed milder lesions and less infiltration of inflammatory cells, compared with water treatment. N = 6 mice per group.

(i) Quantitative analysis of bacillus CFU in lung homogenates derived from *M. tuberculosis*-infected IFNAR1-V168V mice with dietary palmitoleic acid, butyrate or water at 5 weeks post infection. N = 6 mice per group.

(j) Pooled bar graphic data show the expression of TNF-α in serum derived from *M. tuberculosis*-infected IFNAR1-V168V mice with dietary palmitoleic acid, butyrate or water. Serum was collected on 35 days post *M. tuberculosis* infection for CBA-based cytokine analysis. N = 6 mice per group.

Error bars indicate SD. $P < 0.05$ (*); $P < 0.01$ (**); $P < 0.001$ (***); $P < 0.0001$ (****); NS (no statistical significance). *P* values were calculated by one-way ANOVA with Tukey's multiple comparison test [(c) to (e), (h) to (j)]. At least two biological repeats were performed.

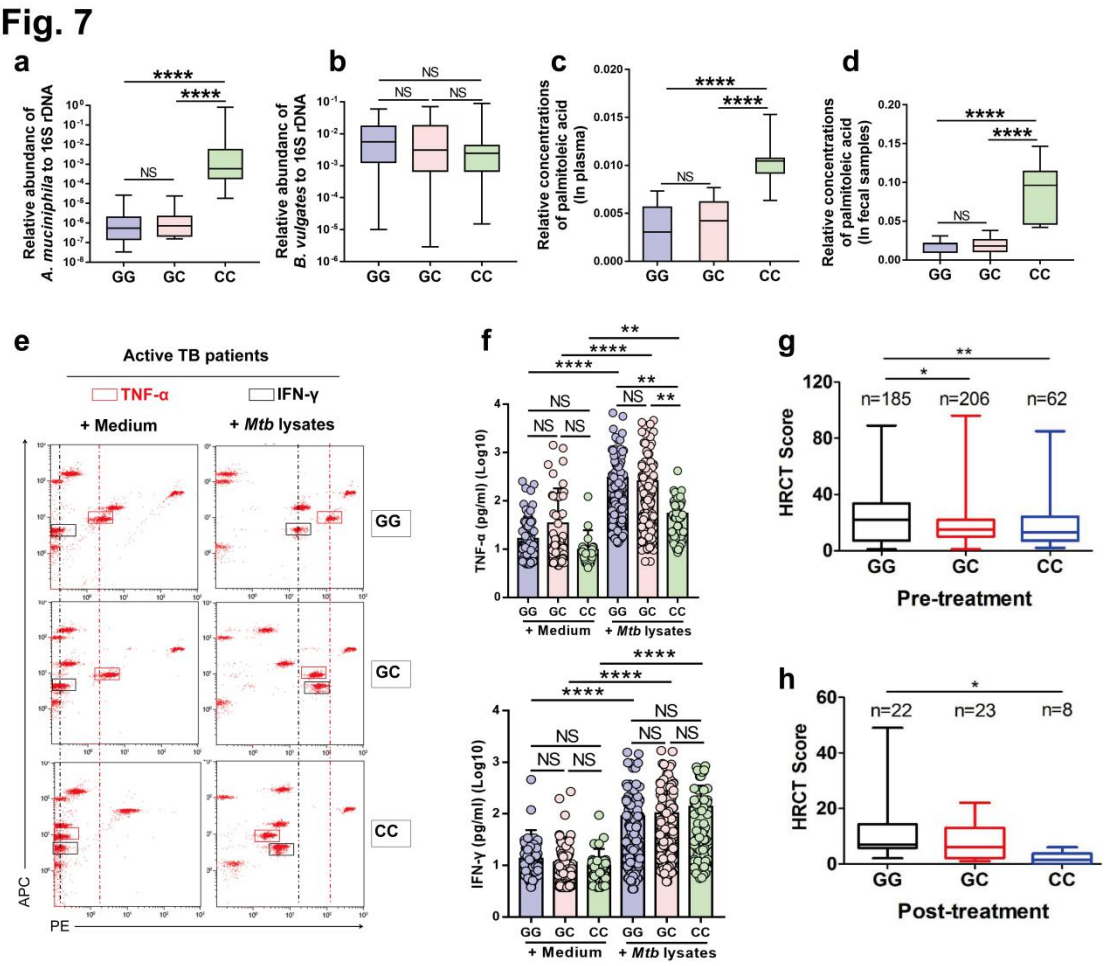

Fig. 7. *Ifnar1* rs2257167 G allele is associated with less *A. muciniphila* abundance, decreased levels of palmitoleic acid, higher TNF-α production, severer TB pathology and poorer prognosis in humans with active TB disease.

(a-b) Bar graphic data shows the qPCR-based relative abundance of *A. muciniphila* (a) and *B. vulgatus* (b) in fecal samples derived from TB patients carrying genotype GG, GC and CC. Patients were from Shenzhen cohort.

(c-d) Bar graphic data shows the Relative concentrations of palmitoleic acid in plasma (c) and fecal samples (d) derived from TB patients carrying genotype GG, GC and CC. Patients were from Shenzhen cohort.

(e) Representative CBA analysis of culture supernatants of PBMCs derived from TB

patients carrying genotype GG, GC, CC. Patients were from Shenzhen cohort. PBMCs were cultured in presence or absence of *M. tuberculosis* lysates (10 μg/ml) for 3 days, and supernatants were then subjected to CBA analysis to determine the expression of TNF-α/IFN-γ/IL-2/IL-4/IL-6/IL-10. Red and black-boxed areas mark the fluorescent clusters of TNF-α and IFN-γ, respectively, and dashed lines mark the shift of fluorescent clusters of TNF-α and IFN-γ, respectively.

(f) Pooled bar graphic data shows the expression of TNF-α (upper panel) and IFN-γ (lower panel), respectively, in culture supernatants of PBMCs derived from TB patients carrying genotype GG, GC or CC in Shenzhen cohort. Representative CBA analysis and pooled data of IL-2/IL-4/IL-6/IL-10 were shown in Supplementary Fig. 15.

(g) The HRCT scores of pulmonary TB patients carrying *Ifnar1* rs2257167 genotype GG, GC and CC before the initiation of standard 2HRZE/4HR anti-TB chemotherapy.

(h) Paired analysis of HRCT score in 2 years after anti-TB chemotherapy in pulmonary TB patients carrying *Ifnar1* rs2257167 genotype GG (n = 22), GC (n = 23), and CC (n = 8).

Each paired data set represents an individual patient. GG (n = 185), GC (n = 206) and CC (n = 62) for (A) to (G). Error bars indicate SD. $P < 0.05$ (*); $P < 0.01$ (**); $P < 0.0001$ (****); NS (no statistical significance). One-way ANOVA with Newman-Keuls multiple comparison test [(a) to (d), (f) to (h)]. At least two biological repeats were performed.

Extended Data Fig. 1

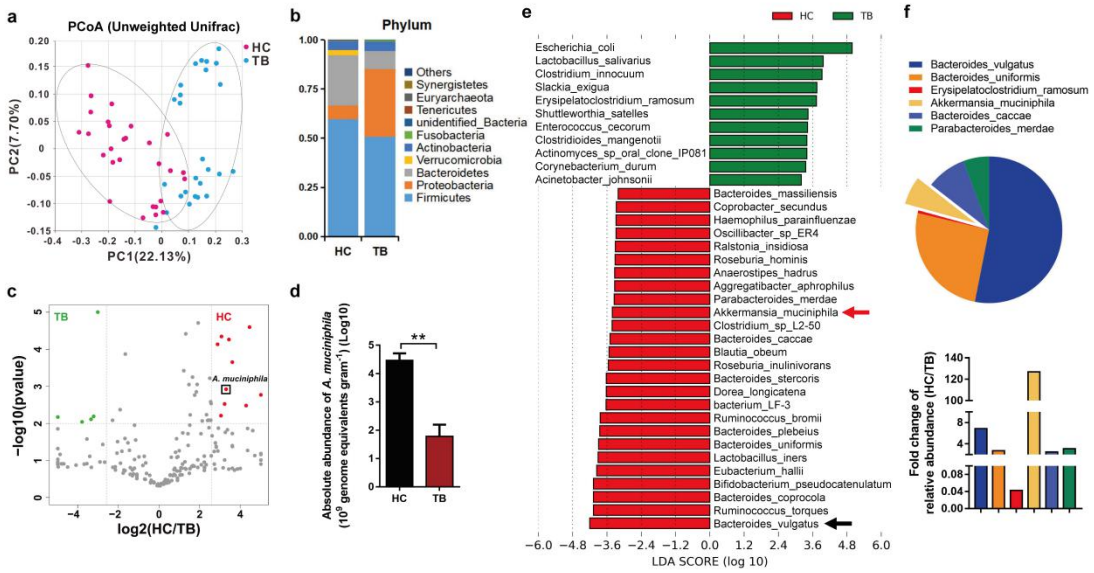

Extended Data Fig. 1. Healthy controls (HC) and active TB patients (TB) exhibit significant differences in diversity, composition, and abundance of gut bacteria at Shenzhen cohort.

(a) PCoA plot (based on Unweighted UniFrac distances). Red points indicated the microbiota enriched in HC (n = 28), blue points indicated the microbiota enriched in TB (n = 26).

(b) The relative abundance of gut bacteria at phylum level in the fecal samples from HC (n = 28) and TB (n = 26).

(c) Volcano plot of all species found in fecal samples. Red points indicated species with an adjusted $P < 0.01$ and log2 (HC/TB) > 2.5; green points indicated species with an adjusted $P < 0.01$ and log2 (HC/TB) < -2.5. *A. muciniphila*, as marked with black box, was a more abundant species enriched in HC.

(d) The absolute abundance of detected *A. muciniphila* in the fecal samples from HC (n = 28) and TB (n = 26).

(e) Histogram of the linear discriminant analysis (LDA) coupled with effect size

measurements (LEfSe) identified the species with different abundance between HC and TB. Higher abundant species in TB are shaded with green, higher abundant species in HC are shaded with red. Red arrowhead marks the *A. muciniphila,* black arrowhead marks *B. vulgatus*.

(f) Circle charts marked the relative abundance of six bacteria with differentiated relative abundance between HC and TB in Shenzhen cohort, and these differentiated six bacteria with differentiated relative abundance were also observed at both Shenzhen and Foshan cohorts. Histogram showed the fold changes of relative abundance of six bacteria, including *B. vulgatus*, *B. uniformis*, *A. muciniphila*, *B. caccae*, *P. merdae*, and *E. ramosun* between HC and TB in Shenzhen cohort (fold changes were calculated as HC/TB). Bacteria are identified by color bars above the chart.

Error bars indicate SD. $P < 0.01$ (**). *P* values were calculated by Mann–Whitney U test [(c) and (d)].

Extended Data Fig. 2

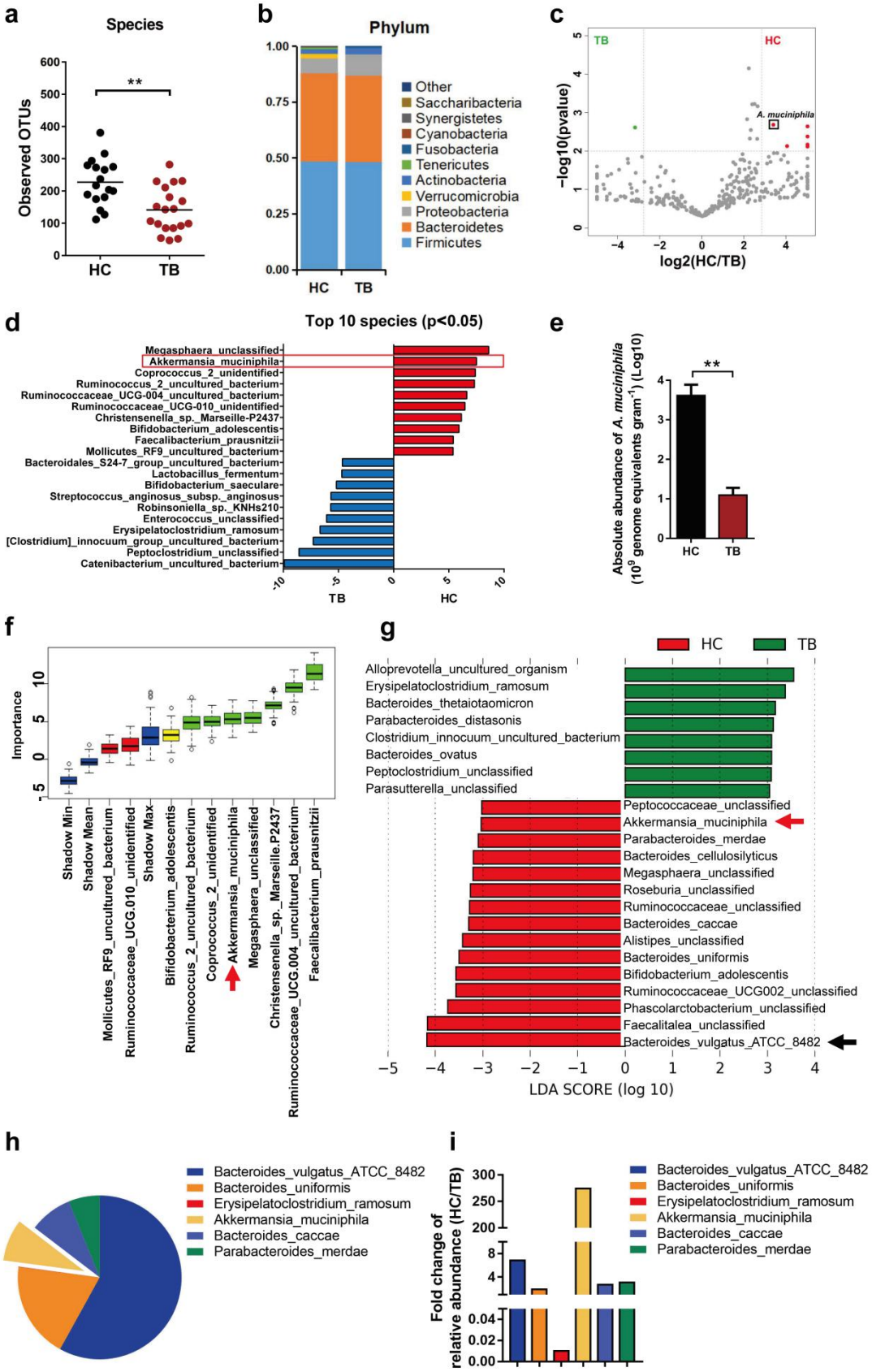

1147

Extended Data Fig. 2. HC and TB show significantly different diversity, composition and abundance of gut bacteria, and abundance of *A. muciniphila* and *B. vulgatus* are significantly higher in HC than TB at Foshan cohort.

(a) Number of observed OTUs of species in fecal microbiota from HC (n = 17) and TB (n = 19).

(b) The relative abundance of gut bacteria in phylum level in the fecal samples from HC (n = 17) and TB (n = 19).

(c) Volcano plot of all species found in fecal samples. Red points indicated species with an adjusted $P < 0.01$ and log2 (HC/TB) > 2.5; green points indicated species with an adjusted $P < 0.01$ and log2 (HC/TB) < -2.5. *A. muciniphila* pointed in black box was the species with higher abundance enriched in HC.

(d) *A. muciniphila* was belonged to top 10 bacterial species in fecal microbiota of HC. Species with enriched relative abundance in HC are adjusted $P < 0.05$ and log2 (HC/TB) > 0, species with enriched relative abundance in TB are adjusted $P < 0.05$ and log2 (HC/TB) < 0. The red-boxed area marks the *A. muciniphila*.

(e) The absolute abundance of *A. muciniphila* in the fecal microbiota from HC (n = 17) and TB (n = 19).

(f) Predictive power of top 10 species enriched in HC (i.e. the top 10 most reduced species in TB) assessed by random forest analysis. Blue boxplots correspond to minimal, average, and maximum Z-score of shadow species, which were shuffled version of real species introduced to random forest classifier and act as benchmarks to detect truly predictive species. Red boxplots represent rejected

species, yellow boxplots represent suggestive species, and green boxplots represent confirmed species. The red arrowhead marks the *A. muciniphila*.

(g) Histogram of the Linear discriminant analysis (LDA) coupled with effect size measurements (LEfSe) identified the species with different abundance in HC and TB. Higher abundant species in TB are shaded in green, higher abundant species in HC are shaded in red. Red arrowhead pointed *A. muciniphila,* black arrowhead pointed *B. vulgatus*.

(h) Circle charts showed the relative abundance of six bacteria with differentiated relative abundance between HC and TB in Foshan cohort, and these six bacteria were also observed at both Shenzhen and Foshan cohorts.

(i) Histogram showed the fold change of relative abundance of six bacteria, including *B. vulgatus*, *B. uniformis*, *A. muciniphila*, *B. caccae*, *P. merdae* and *E. ramosun* between HC and TB (calculated as HC/TB) in Foshan cohort.

Error bars indicate SD. $P < 0.01$ (**). *P* value was calculated by Mann-Whitney test [(a), (c), (d) and (e)].

Extended Data Fig. 3

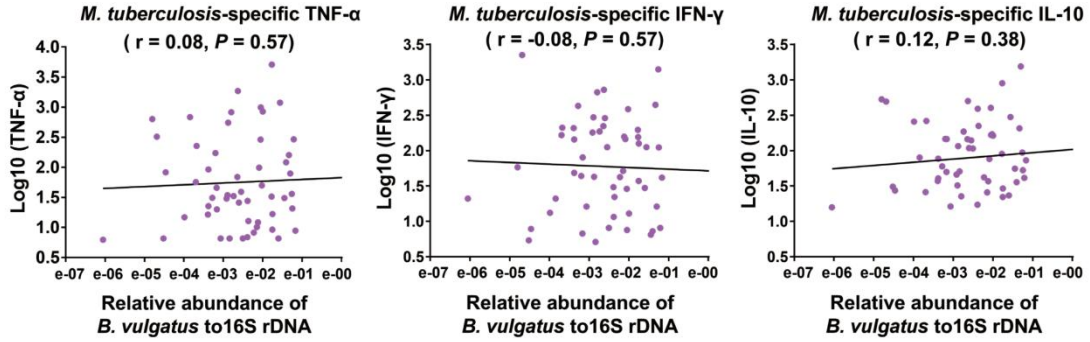

Extended Data Fig. 3. The association of *M. tuberculosis*-specific cytokines *ex vivo* produced by PBMCs and *B. vulgatus* in fecal samples of TB patients.

Spearman correlation analysis showed the association between TNF-α, IFN-γ, or IL-10 and the relative abundance of *B. vulgatus*. There were no significant correlation between *B. vulgatus* and *M. tuberculosis*-specific TNF-α, *M. tuberculosis*-specific IFN-γ or *M. tuberculosis*-specific IL-10. *P*-value was calculated by Spearman correlation.

Extended Data Fig. 4

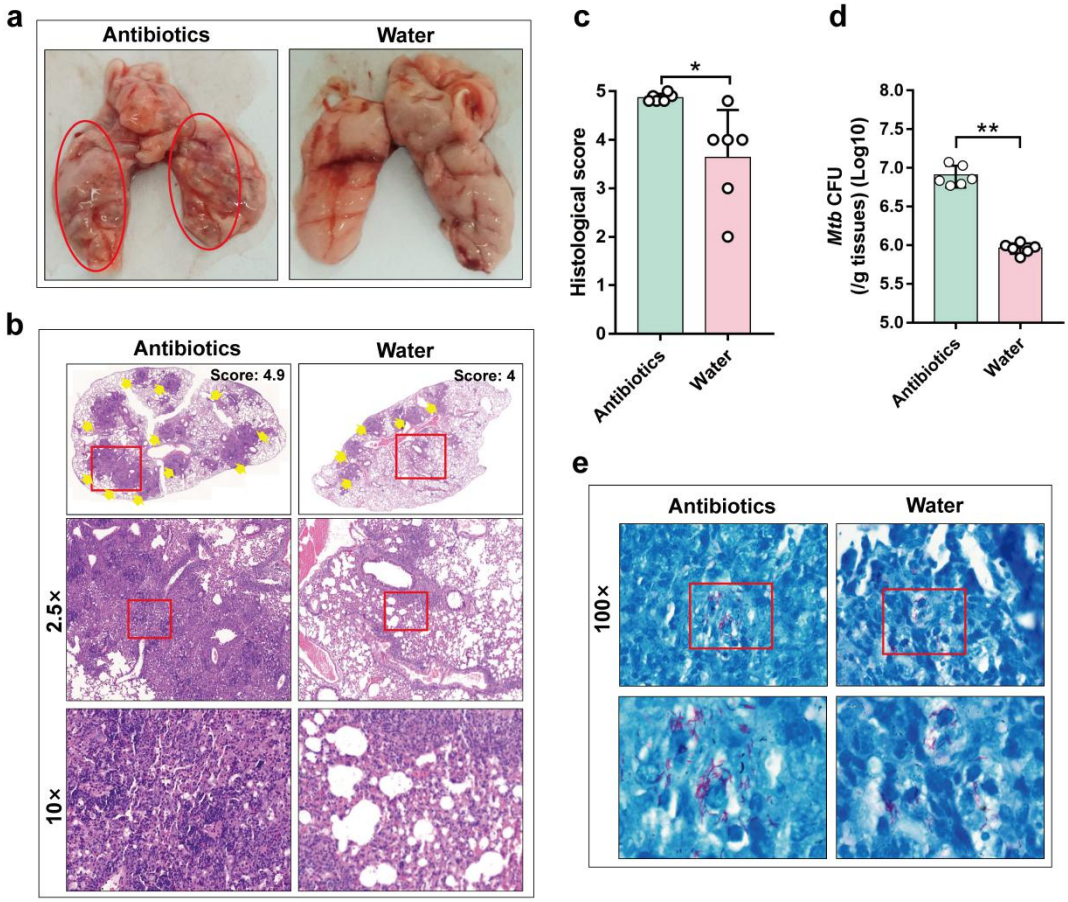

Extended Data Fig. 4. Antibiotics-treated mice show much severer pulmonary pathology and higher bacillus burdens during *M. tuberculosis* infection.

(a) Two representative lungs derived from *M. tuberculosis*-infected mice with antibiotics or water control treatment. Red circles mark the cystic changes, hemorrhage or necrosis on the lungs of infected mice.

(b-c) Hematoxylin and eosin (H&E) staining of two representative lungs (b) and the histological scores (c) of *M. tuberculosis*-infected mice with antibiotics or water control treatment at 5 weeks post infection. Top: original magnification; Middle: 2.5× of original magnification; Bottom: 10× of original magnification. The red-boxed areas at the top are enlarged below. As marked by yellow arrowheads,

antibiotics-treated mice showed much severer lesions and more infiltration of inflammatory cells than untreated mice.

(d) Quantification analysis of *M. tuberculosis* CFU in the lung homogenates of *M. tuberculosis*-infected mice at 5 weeks post infection.

(e) The acid-fast staining of *M. tuberculosis* in lung section of mice at 5 weeks post infection. Note that more acid-fast staining-positive bacilli in lung sections derived from antibiotics-treated mice. Top: 100× of original magnification. The red-boxed areas at the top are enlarged below.

N = 6 mice per group. Error bars indicate SD. $P < 0.05$ (*) and $P < 0.01$ (**). *P* values were calculated by Student's two-tailed unpaired *t*-test [(c) and (d)]. At least two biological repeats were performed.

Extended Data Fig. 5

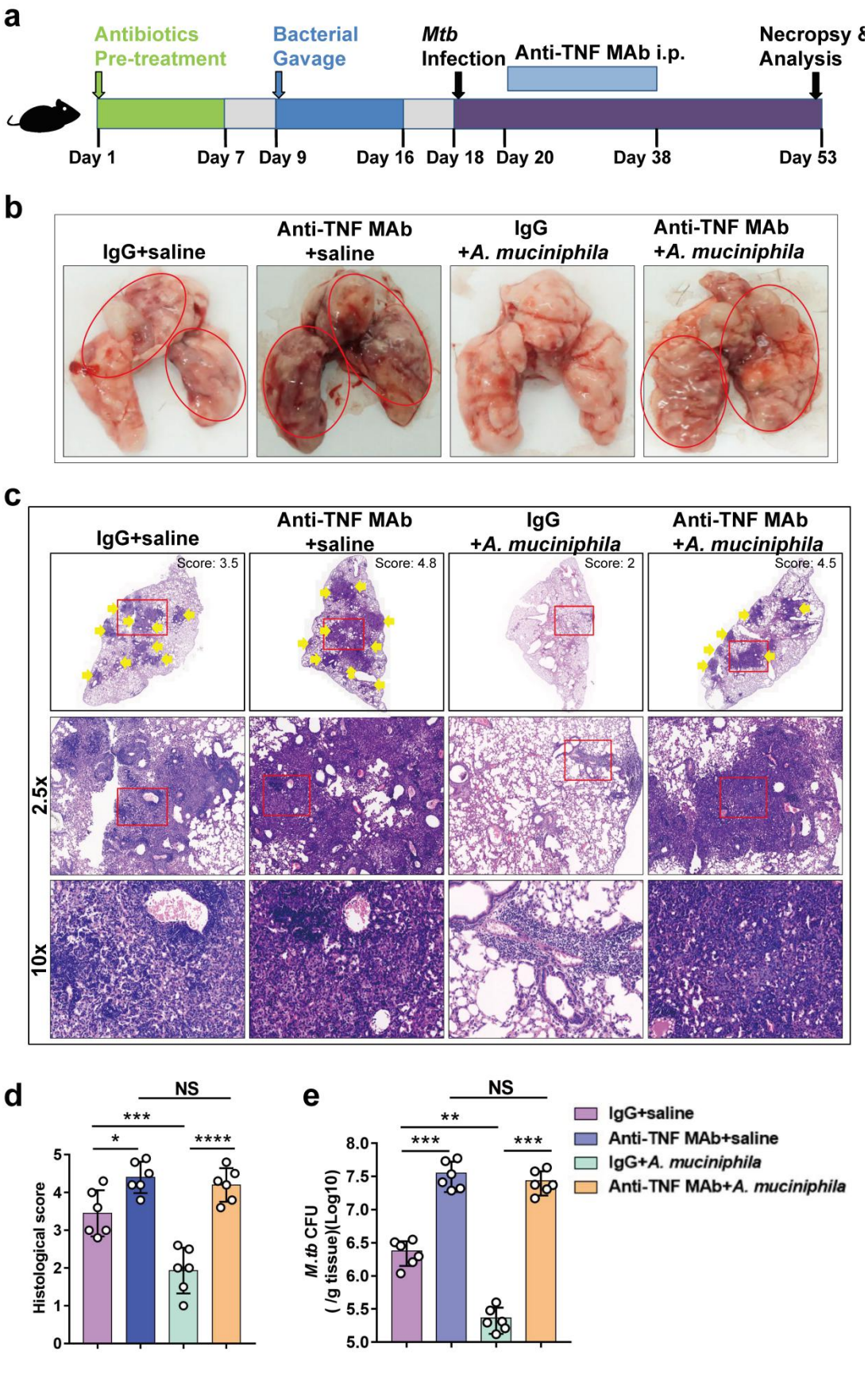

1216

Extended Data Fig. 5. *A. muciniphila*-mediated effects of reduced TB pathology and bacillus burdens were impaired in the absence of TNF-α signaling.

(a) Experimental diagram for determining whether the effect of *A. muciniphila* depends on TNF-α signaling during *M. tuberculosis* infection. Antibiotics pre-treated mice were gavaged with *A. muciniphila* (2×10^8 CFU) or saline for 3 times per week followed by aerosol *M. tuberculosis* infection. Mice were injected with 500 μg anti-TNF-α MAb or IgG antibody control at the third day after *M. tuberculosis* infection and injections were performed every third day for a total of six injections.

(b) Gross pathology shows the hemorrhage and necrosis in lungs of *M. tuberculosis*-infected mice at 5 weeks post infection. Red circles mark the severe, unresolved hemorrhage, massive disruption or caseous necrosis on the lungs of *M. tuberculosis*-infected mice.

(c-d) Hematoxylin and eosin (H&E) staining of four representative lungs (c) and the histological scores (d) of *M. tuberculosis*-infected mice at 5 weeks post infection. Top: original magnification; Middle: 2.5× of original magnification; Bottom: 10× of original magnification. The red-boxed areas at the top are enlarged below. Yellow arrowheads mark lesions and infiltration of inflammatory cells.

(e) Quantification analysis of *M. tuberculosis* CFU in the lung homogenates of *M. tuberculosis*-infected mice at 5 weeks post infection.

N = 6 mice per group. Error bars indicate SD. $P < 0.05$ (*); $P < 0.01$ (**); $P < 0.001$ (***); $P < 0.0001$ (****); NS (no statistical significance). *P* values were calculated by

1239 one-way ANOVA with Tukey's multiple comparison test [(d) and (e)]. At least two

1240 biological repeats were performed.

1241

Extended Data Fig. 6

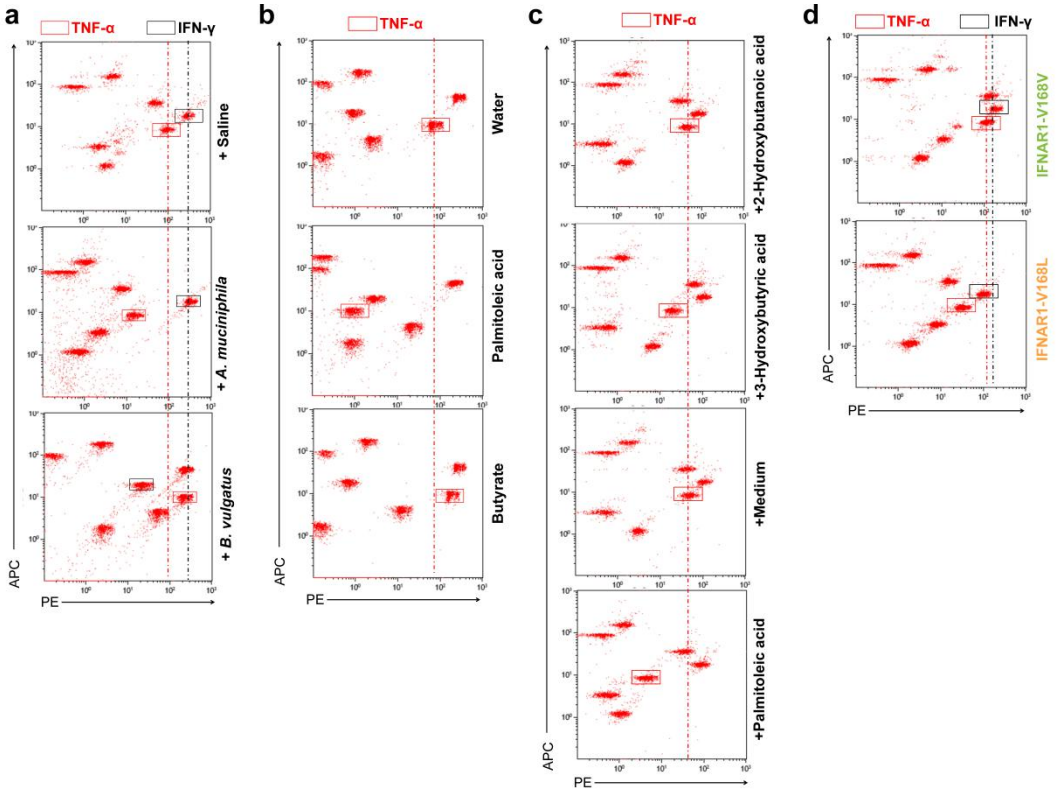

Extended Data Fig. 6. CBA analysis of cytokine productions in serum derived from *M. tuberculosis*-infected mouse models.

(a) Representative CBA analysis of serum derived from *M. tuberculosis*-infected mice with oral administration of *A. muciniphila*, *B. vulgatus* and saline. Red and black-boxed areas mark the fluorescent clusters of TNF-α and IFN-γ, respectively, and dashed lines mark the shift of fluorescent clusters of TNF-α and IFN-γ, respectively. Pooled data were shown in Fig. 2i.

(b) Representative CBA analysis of serum derived from *M. tuberculosis*-infected mice treated with palmitoleic acid, butyrate and water. Red and black-boxed areas mark the fluorescent clusters of TNF-α, and dashed lines mark the shift of fluorescent clusters of TNF-α. Pooled data were shown in Fig. 4g.

(c) Representative CBA analysis of culture supernatants of CD3+ T cells. CD3+ T

cells isolated from spleens of mice were cultured with *M. tuberculosis* lysates (10 μg/ml) only or with 2-Hydroxybutanoic acid, 3-Hydroxybutyric acid or palmitoleic acid for 3 days. Red-boxed areas mark the fluorescent clusters of TNF-α, dashed line mark the shift of fluorescent clusters of TNF-α. Pooled data were shown in Supplementary Fig. 3c.

(d) Representative CBA analysis of serum derived from *M. tuberculosis*-infectedIFNAR1-V168L and IFNAR1-V168V mice, respectively. Red and black-boxed areas mark the fluorescent clusters of TNF-α and IFN-γ, respectively, and dashed lines mark the shift of fluorescent clusters of TNF-α and IFN-γ, respectively. Pooled data were shown in Fig. 5p.

Extended Data Fig. 7

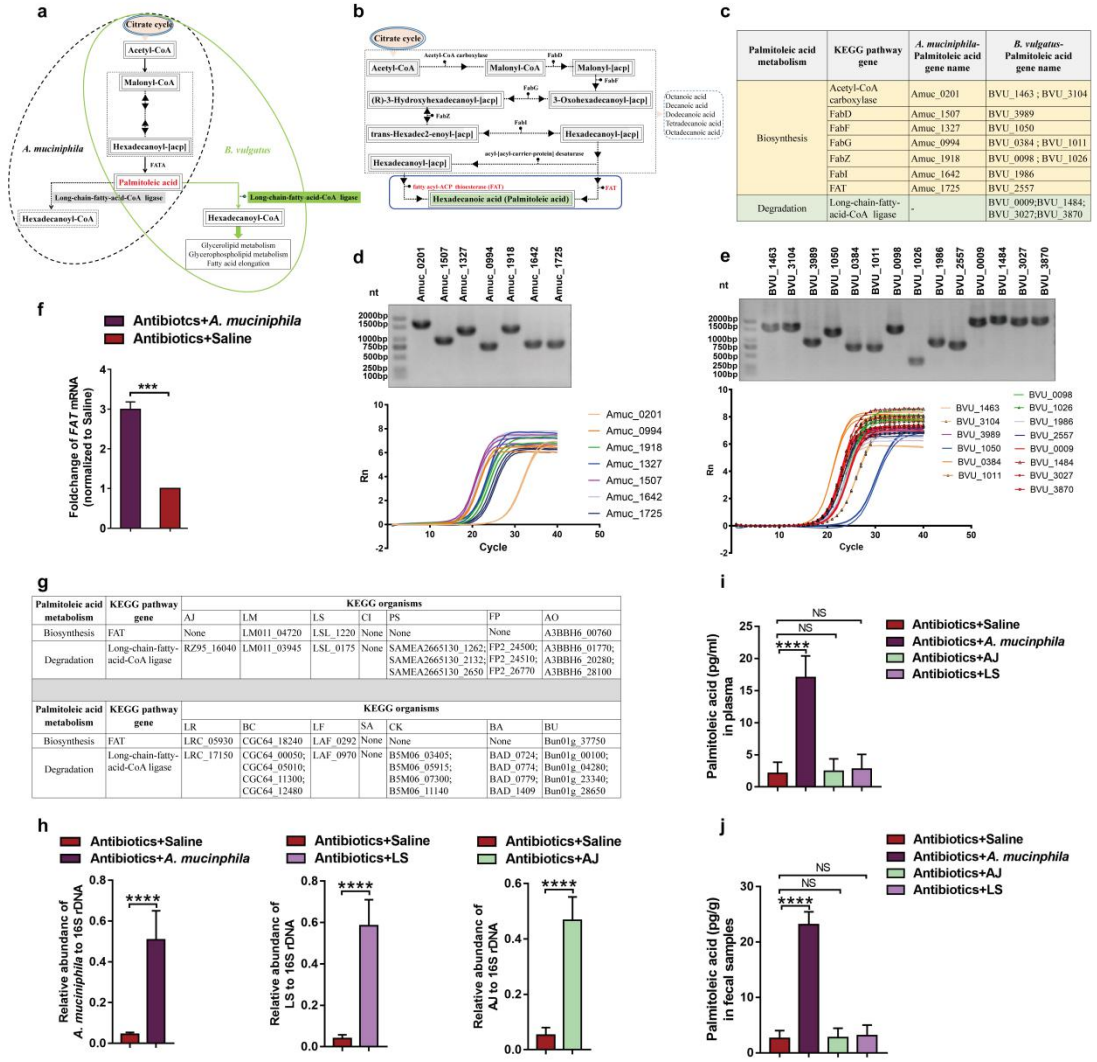

Extended Data Fig. 7. *A. muciniphila* played a dominant role in contributing to increased levels of palmitoleic acid in mice.

(a) Comparative KEGG pathway analyses of palmitoleic acid synthesis and degradation between *A. muciniphila* (marked with oval black dashed line) and *B. vulgatus* (marked with green solid line). The green box mark the presence of long-chain-fatty-acid-CoA ligase for degrading/processing palmitoleic acid in *B. vulgatus*, and the gray box point the lack of presence (or at least lower level) of long-chain-fatty-acid-CoA ligase in *A. muciniphila*. The solid green arrow mark the downstream metabolic pathways for degrading/processing palmitoleic acid in

B. vulgatus, and the black dashed arrow point that no (or at least less) long-chain-fatty-acid-CoA ligase to degrade/process palmitoleic acid in *A. muciniphila*.

(b) Schematic diagram for palmitoleic acid biosynthesis pathway in *A. muciniphila*.

(c) Genes involved in palmitoleic acid biosynthesis pathway in *A. muciniphila* and *B. vulgatus*, respectively.

(d-e) The existences of genes involved in palmitoleic acid biosynthesis pathway in *A. muciniphila* and *B. vulgatus* were confirmed from the bacterial genome DNA and bacterial mRNA.

(f) The qPCR-based analysis of fatty acyl-ACP thioesterase (*FAT*) mRNA expression in fecal samples from *M. tuberculosis*-infected mice with *A. muciniphila* and saline treatment.

(g) Genes involved in palmitoleic acid metabolism pathway in gut bacteria, which showed significantly different abundance between HC and TB. These bacteria include *Acinetobacter johnsonii* (AJ), *Lactobacillus mucosae* (LM), *Lactobacillus salivarius* (LS), *Clostridium innocuum* (CI), *Plesiomonas shigelloides* (PS), *Comamonas kerstersii* (CK), *Alistipes onderdonkii* (AO), *Lactobacillus ruminis* (LR), *Streptococcus anginosus* (SA), *Lactobacillus fermentum* (LF), *Faecalibacterium prausnitzii* (FP), *Bifidobacterium adolescentis* (BA), *Bacteroides uniformis* (BU) and *Bacteroides caccae* (BC).

(h) The qPCR-based quantitative analyses of *A. muciniphila, A. johnsonii* (AJ) and *L. salivarius* (LS) abundance in stool samples from antibiotics-treated mice with oral administration of *A. muciniphila*, AJ, LS or saline at the third day after

bacteria gavage.

(i-j) The quantitative analyses of palmitoleic acid concentrations in plasma (I) and fecal samples (J) derived from antibiotics-pretreated mice with oral administration of *A. muciniphila*, AJ, LS or saline at the third day after bacteria gavage.

N = 6 mice per group. Error bars indicate SD. $P < 0.0001$ (****). *P* values were calculated by Student's two-tailed unpaired *t*-test [(f), (h)] and one-way ANOVA with Tukey's multiple comparison test [(i) and (j)]. At least two biological repeats were performed.

Extended Data Fig. 8

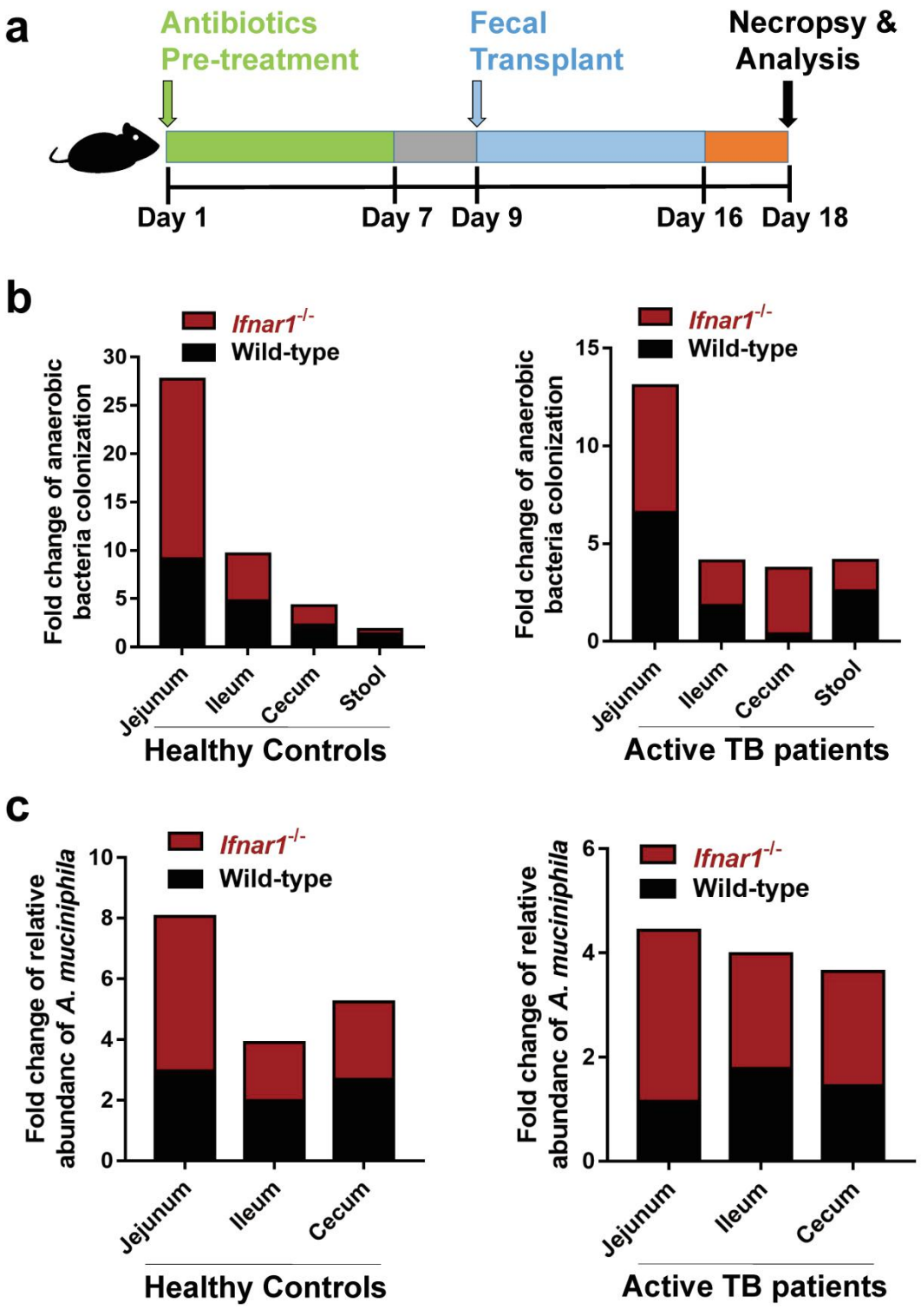

Extended Data Fig. 8. Knock-out of an IFN-I receptor (*Ifnar1*) increases the intestinal colonization and abundance of bulk anaerobic bacteria and *A. muciniphila*.

(a) Experiment design: Fecal microbiota transplantation (FMT) of fecal samples derived from TB and HC was performed following 7 days of antibiotics in *Ifnar1*$^{-/-}$ mice and wild-type mice. Eighteen days later, the anaerobic bacteria as well as *A. muciniphila* in jejunum, ileum, cecum and fecal samples were analyzed.

(b) Pooled data of relative amounts of anaerobic bacteria recovered from jejunum, ileum or cecum of *Ifnar1*$^{-/-}$ mice (red bar) and wild-type mice (black bar), respectively. Mice were administrated with fecal samples of HC (Left panel) or TB (Right panel) as described in (a), and then tissues of jejunum, ileum or cecum and fecal samples of mice were subjected to anaerobic culture, followed by quantitative analysis of anaerobic bacteria CFU. Fold changes were calculated as CFU of anaerobic bacteria recovered from jejunum, ileum or cecum and fecal samples of mice administrated with fecal samples of HC or TB normalized to those of saline-treated *Ifnar1*$^{-/-}$ mice and wild-type mice. N = 6 mice per group.

(c) Pooled data of relative gene expression levels of *A. muciniphila* recovered from jejunum, ileum, or cecum of *Ifnar1*$^{-/-}$ mice (red bar) and wild-type mice (black bar), respectively. Mice were administrated with fecal samples of HC (Left panel) or TB (Right panel) as described in (a), and then tissues of jejunum, ileum, or cecum were subjected to qPCR analysis of DNA extracted from jejunum, ileum, and cecum of mice. Fold changes were calculated as gene expression levels of *A. muciniphila* recovered from jejunum, ileum, or cecum of mice administrated with fecal samples of HC or TB normalized to those of same genotype mice with oral saline administration. N = 6 mice per group.

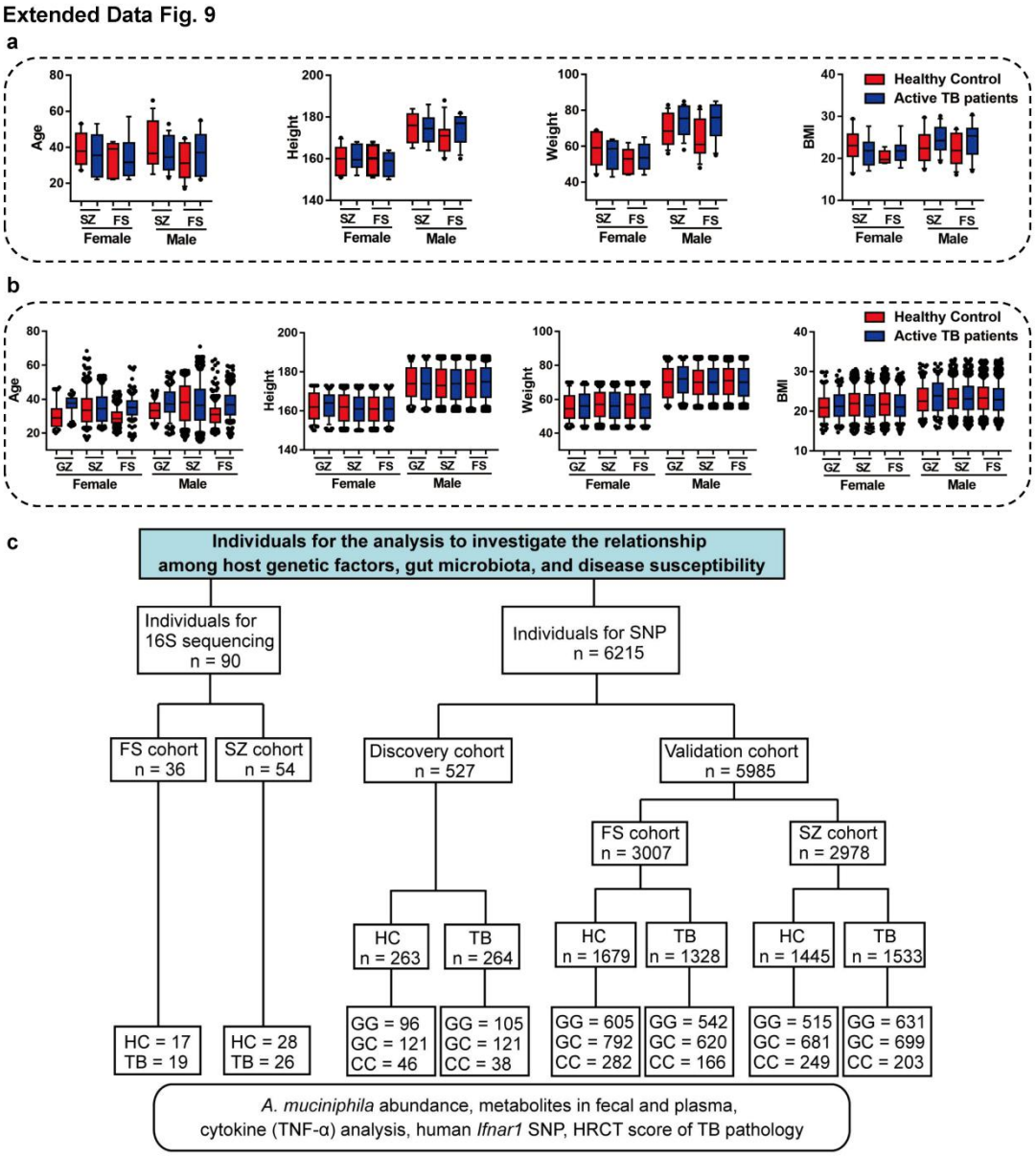

Extended Data Fig. 9. Boxplot and flow chart illustration of characteristics of Shenzhen, Foshan and Guangzhou cohorts.

(a) Boxplot illustrating the distribution of age, height, weight, and body mass index (BMI) of individuals for analyses of 16S rDNA in Shenzhen (HC = 28, TB = 26) and Foshan (HC = 17, TB = 19) cohorts. SZ: Shenzhen cohort. FS: Foshan cohort.

(b) Boxplot illustrating the distribution of age, height, weight, and body mass index (BMI) of individuals for SNP analyses in Guangzhou (HC = 263, TB = 264),

Shenzhen (HC = 1445, TB = 1533) and Foshan (HC = 1679, TB = 1328) cohorts. GZ: Guangzhou cohort. SZ: Shenzhen cohort. FS: Foshan cohort.

(c) Flow chart for each cohort. Flow chart to illustrate sample collection and analyses that were undertaken with them.

Extended Data Fig. 10

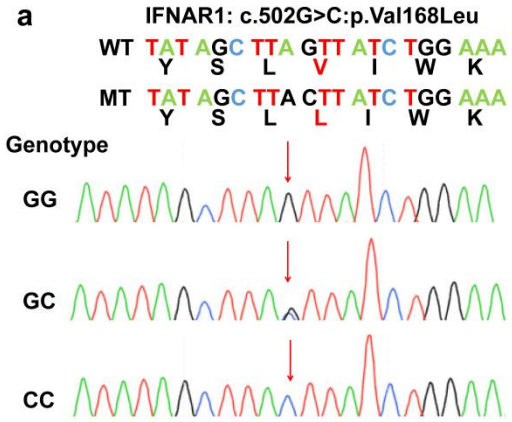

b

SNP ID	Location	Allele change	Amino acid change
rs2257167	*Ifnar1* Exon 4	G>C	V168L

c

168

WT: GLSFTYSL**V**IWKNSSG

V168L: GLSFTYSL**L**IWKNSSG

Extended Data Fig. 10. Identified rs2257167 variant in *Ifnar1* gene leads to a V168L variant.

(a) DNA sequencing data of three men with the different genotype of rs2257167 in *Ifnar1* gene. WT, wild-type; MT, mutant.

(b) SNP locus rs2257167 in human *Ifnar1* gene.

(c) Comparison of the wild-type and mutated element in human IFNAR1 protein.

Extended Data Fig. 11

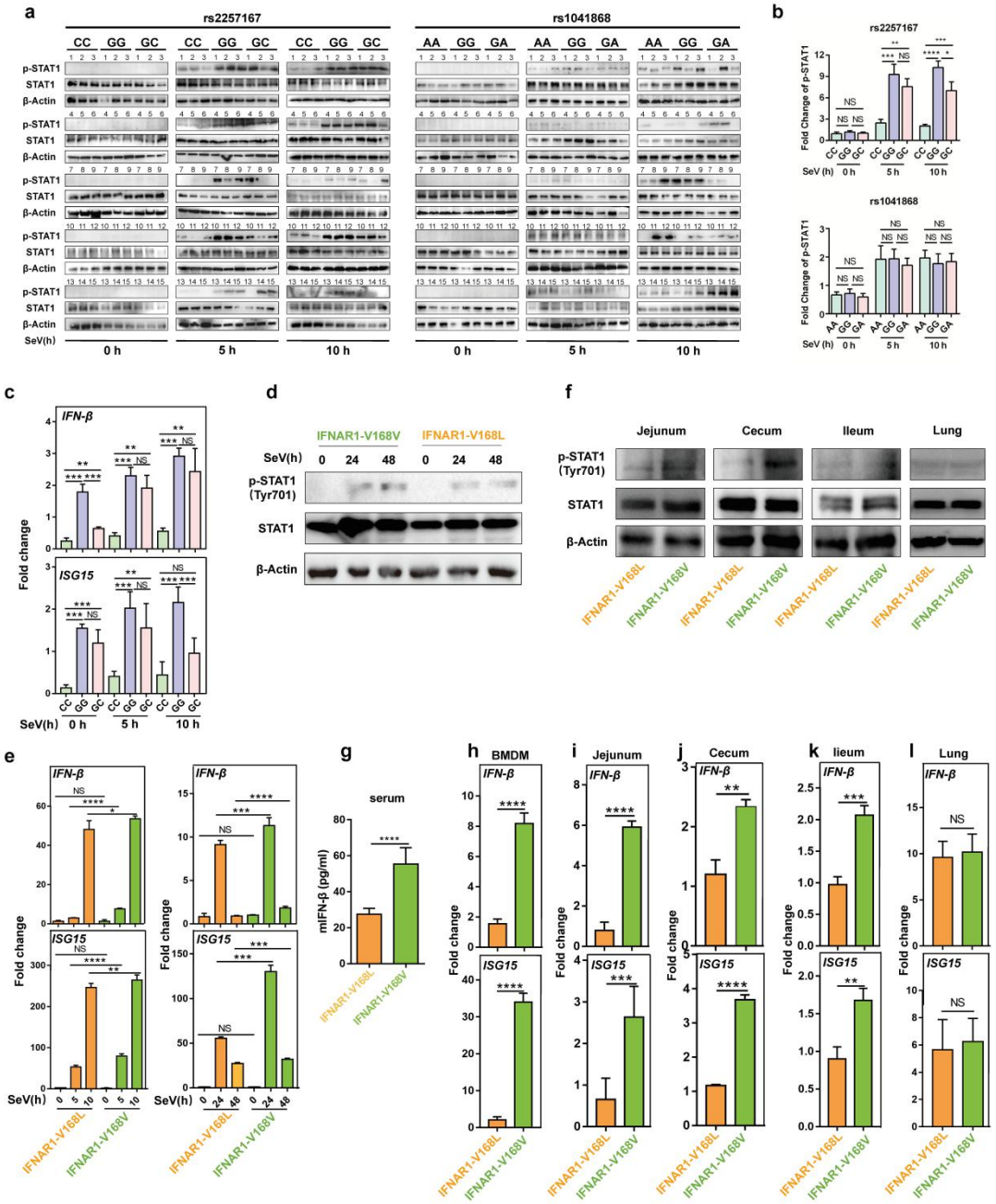

Extended Data Fig. 11. Rs2257167 G allele in *Ifnar1* gene enhances IFN-I signaling in both humans and mice.

(a) Immunoblot analysis of the levels of phosphorylated(p)- and total STAT1 in PBMCs. Fifteen individuals of each genotype were examined (individual numbers for rs2257167, GG = 15, GC = 15, CC = 15; individual numbers for rs1041868,

GG = 15, GA = 15, AA = 15). Patient number is shown above in each of blot lane.

(b) Quantitative immunoblot analysis of expression of p-STAT1. ImageJ was used for quantitative analysis of immunoblot.

(c) The qRT-PCR-based mRNA expression of *IFN-β* and *ISG15* in PBMCs derived from individuals carrying genotype GG, GC, CC at 0, 5 and 10 hours after stimulation with Sendai virus. Data are representative of three experiments with three independent biological replicates.

(d) Immunoblot analysis of the expression levels of p- and total STAT1 in BMDM derived from IFNAR1-V168V and IFNAR1-V168L mice at 0, 24 and 48 hours following Sendai virus stimulation. Data are representative of three experiments with three independent biological replicates.

(e) The qRT-PCR-based analysis of mRNA expression of *IFN-β* and *ISG15* in BMDM derived from IFNAR1-V168V and IFNAR1-V168L mice at 0, 5, 10, 24 and 48 hours following Sendai virus stimulation. N = 6 mice per group.

(f) Immunoblot analysis of the expression levels of p- and total STAT1 in jejunum, ileum,cecum and lung derived from IFNAR1-V168V and IFNAR1-V168L mice at 7 days following *M. tuberculosis* infection. Data are representative of three experiments with three independent biological replicates.

(g) ELISA analysis of IFN-β concentrations in serum derived from IFNAR1-V168V and IFNAR1-V168L mice at 7th day following *M. tuberculosis* infection. N = 6 mice per group.

(h-l) The mRNA expression of *IFN-β* and *ISG15* in tissues including BMDM (h),

jejunum (i), cecum (j),ileum (k) and lung (l) derived from IFNAR1-V168V and IFNAR1-V168L mice, respectively, at 7th day following *M. tuberculosis* infection. N = 6 mice per group.

Error bars indicate SD. $P < 0.01$ (**); $P < 0.001$ (***); $P < 0.0001$ (****); NS (no statistical significance). *P* values were calculated by one-way ANOVA with Tukey's multiple comparison test [(b), (c)], Student's two-tailed unpaired *t*-test [(e), (g) to (l)]. At least two biological repeats were performed.

Extended Data Fig. 12

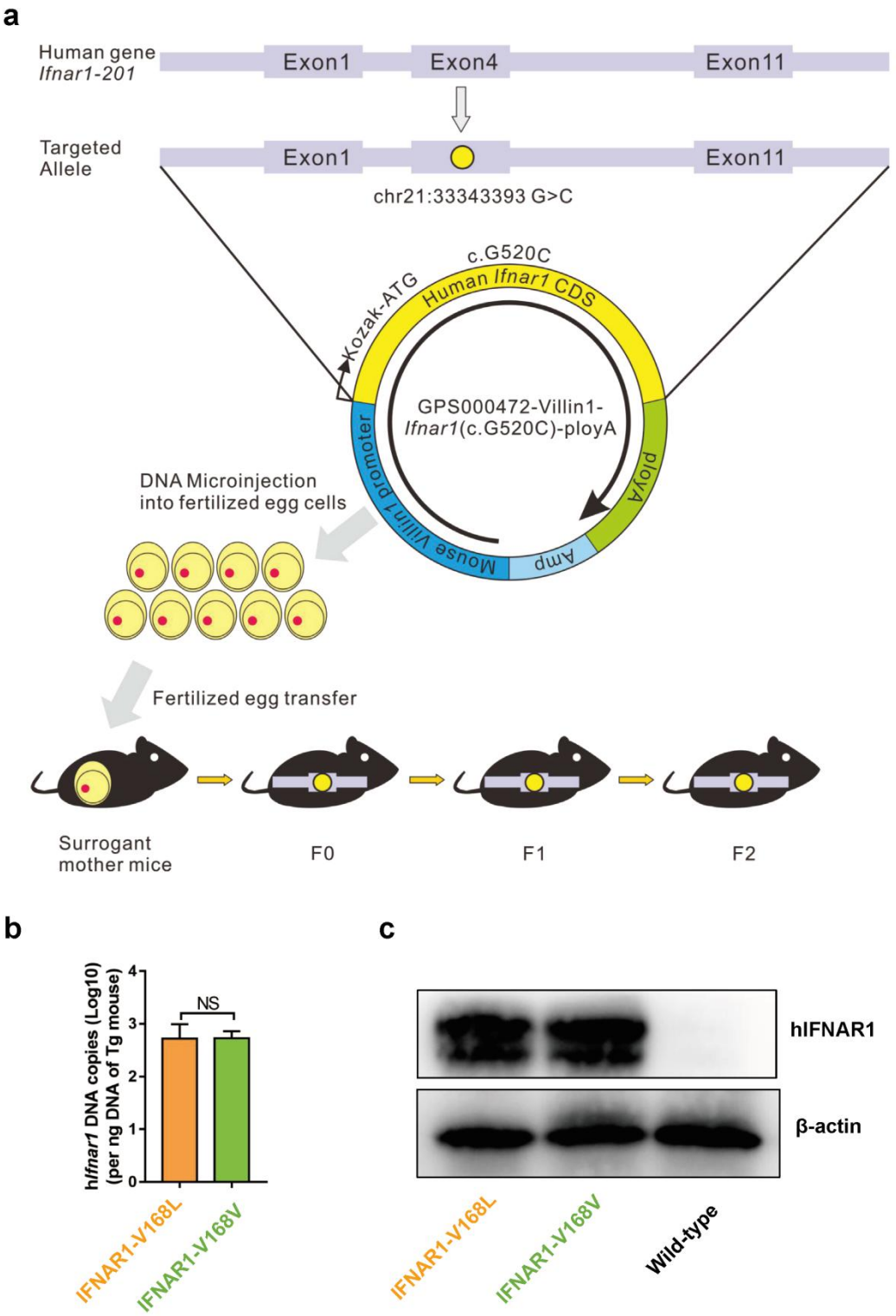

Extended Data Fig. 12. Construction strategy of transgenic mice with the human *Ifnar1* rs2257167 G allele or C allele.

(a) *Ifnar1*-201(ENST00000270139.7) was selected for construction of transgenic

mice. The 520th base of the fourth exon of the human *Ifnar1* gene was changed from G to C, The resulting human *Ifnar1* was ligated to the mouse epithelium promoter, *villin1* as regulatory element. The transgenic fragment was obtained: mouse- Kozak-villin1-human *Ifnar1* (c.G520C) CDS. The DNA fragments were randomly integrated into the mouse genome by microinjection technology, and the born mice were genetically identified by PCR to obtain F0 generation mice with the target DNA. *Ifnar1*-201(ENST00000270139.7) has 11 coding exons, transcript length of 6,139 bp and translation length of 557 residues. Kozak sequence (GCCGCCACC) was added before the ATG, which allowed the ribosome to recognize the initiation codons.

(b) Absolute quantitation analysis of h*Ifnar1* copies in transgenic mice. N = 6 mice per group.

(c) Representative western blot showed that there was no significant difference in expression of hIFNAR1 in intestines between IFNAR1-V168L and IFNAR1-V168V transgenic mice. N = 6 mice per group.

NS (no statistical significance). *P* value was calculated by Student's two-tailed unpaired *t*-test.

Extended Data Fig. 13

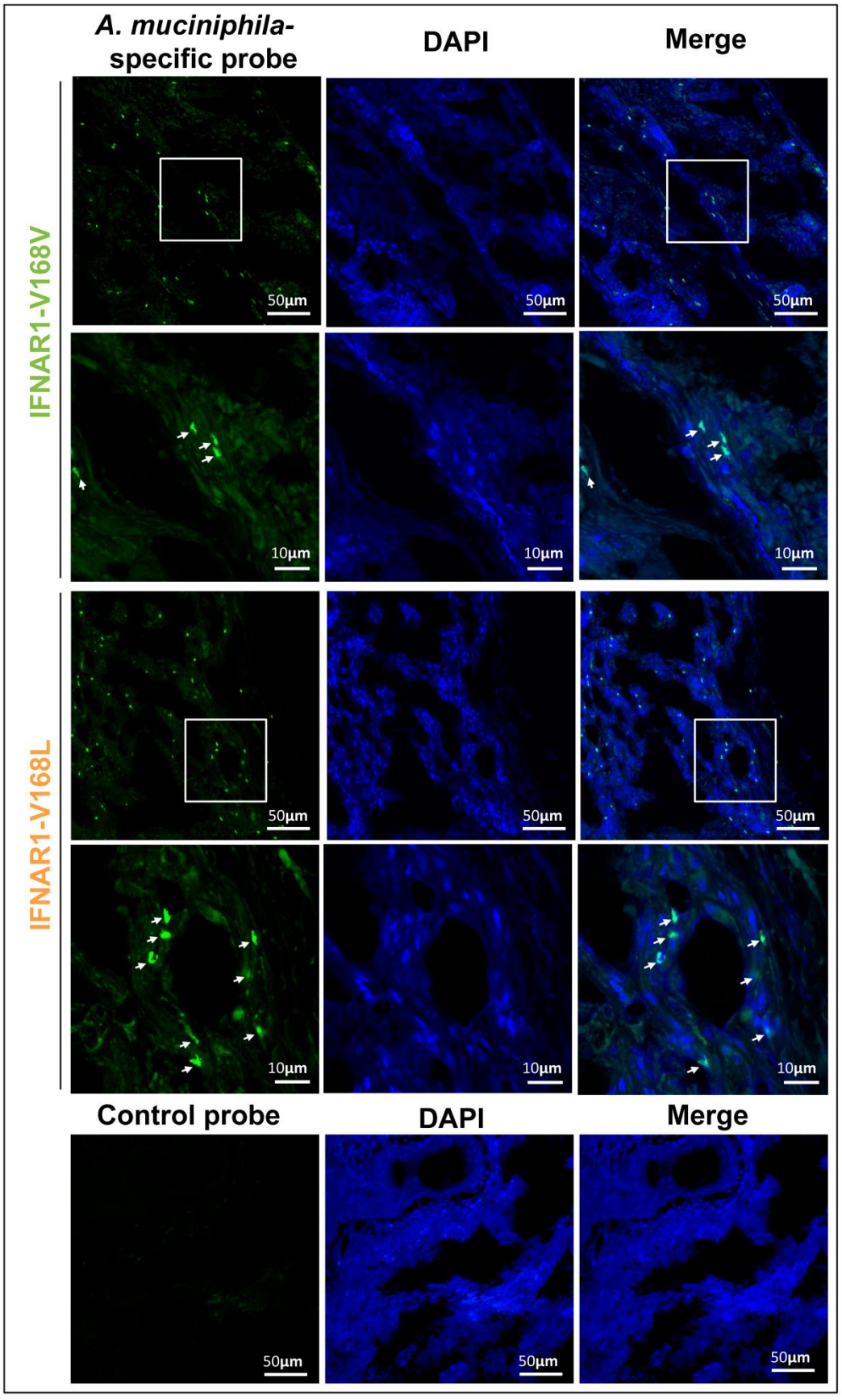

Extended Data Fig. 13. Confocal microscopic imaging shows that IFNAR1-

V168V mice contain less *A. muciniphila* on intestinal mucosa than IFNAR1-V168L mice.

Representative fluorescent *in situ* hybridization (FISH)/confocal microscopic imaging analysis of *A. muciniphila* (green) on the intestinal mucosa by using an *A. muciniphila*-specific probe. DAPI (4′, 6-diamidino-2-phenylindole) was used for nuclear staining (blue). The white-boxed areas at the upper panel images are enlarged in the lower panel. The upper images were obtained at 20× magnification, the lower images were obtained at 60× magnification. Scale bars, 50 μm (Top) and 10 μm (Bottom). The white arrowheads mark the *A. muciniphila*.

Extended Data Fig. 14

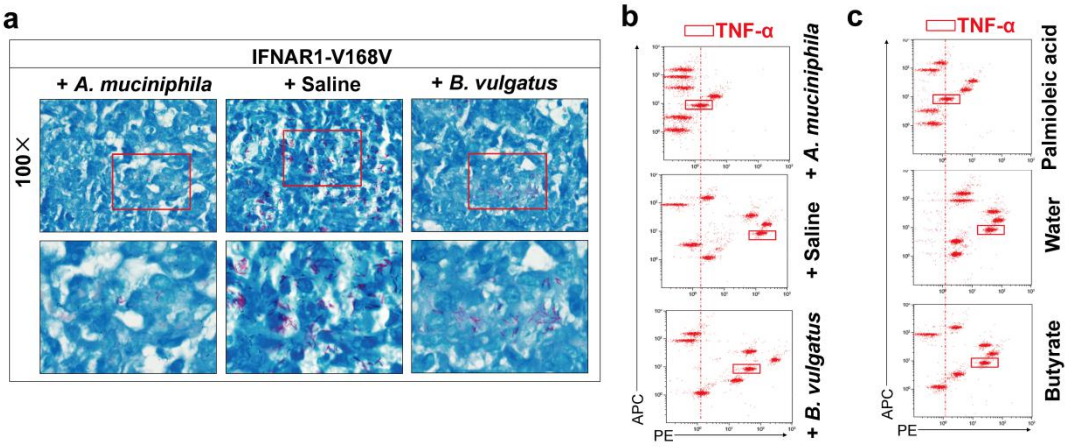

Extended Data Fig. 14. Oral gavage of *A. muciniphila* or palmitoleic acid reduces bacillus burdens and TNF-α production in *M. tuberculosis*-infected IFNAR1-V168V mice.

(a) The acid-fast staining to visualize *M. tuberculosis* in lung sections at 5 weeks post infection. Note that less acid-fast staining-positive bacilli in lung sections derived from *A. muciniphila*-treated IFNAR1-V168V mice. Top: 100× of original magnification. The red-boxed areas at the top are enlarged below.

(b) Representative CBA analysis of serum derived from *M. tuberculosis*-infected IFNAR1-V168V mice with oral administration of *A. muciniphila*, *B. vulgatus* and saline. Red-boxed areas mark the fluorescent clusters of TNF-α and dashed lines mark the shift of fluorescent clusters of TNF-α.

(c) Representative CBA analysis of serum derived from *M. tuberculosis*-infected IFNAR1-V168V mice with dietary palmitoleic acid, butyrate or water. Red-box mark the fluorescent clusters of TNF-α and dashed lines mark the shift of fluorescent clusters of TNF-α.

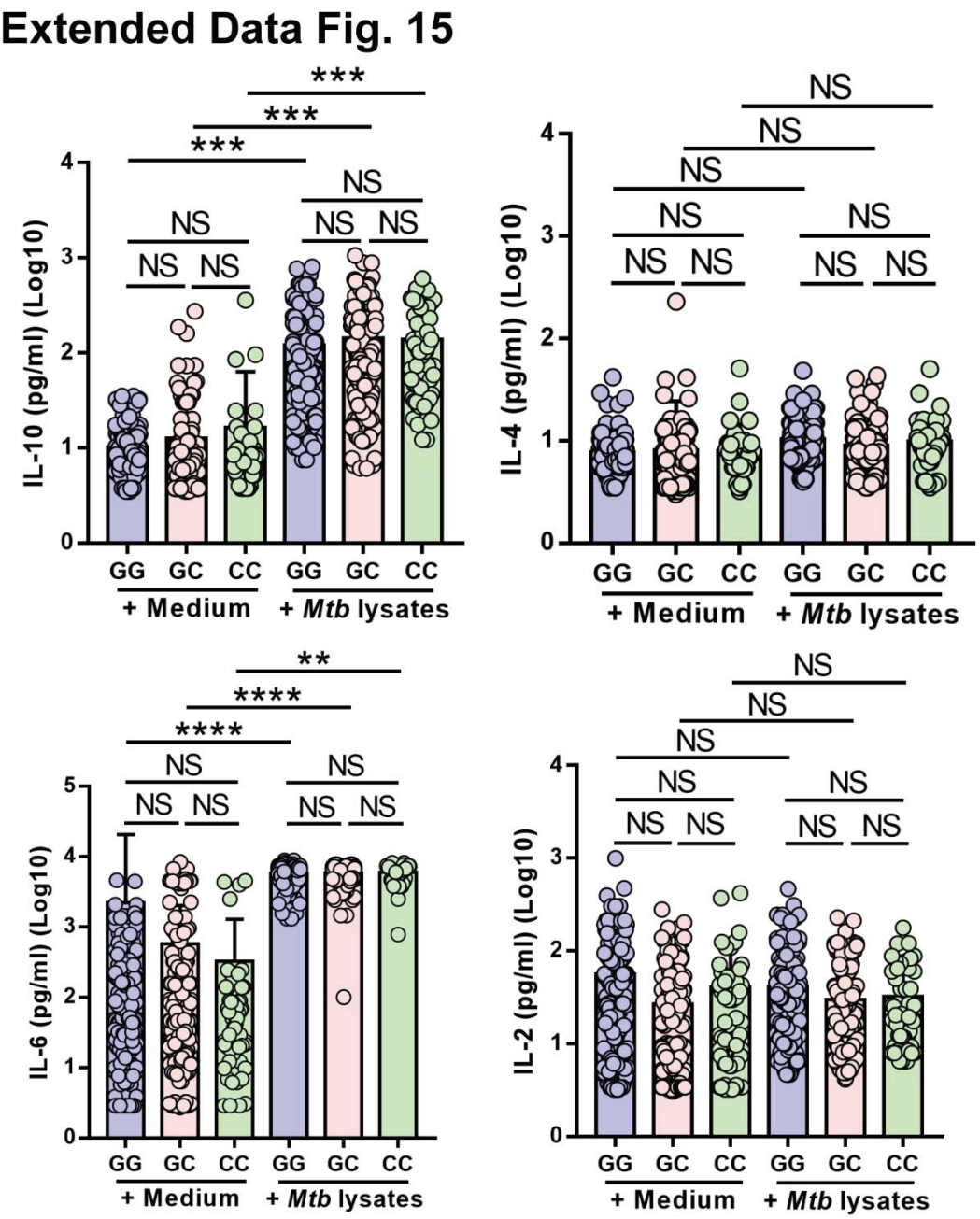

Extended Data Fig. 15. Pooled bar graphic data shows the expression of IL-10, IL-6, IL-2, and IL-4 in culture supernatants of PBMCs derived from TB patients carrying genotype GG, GC, CC.

PBMCs derived from TB patients carrying genotype GG (n = 185), GC (n = 206) or CC (n = 62) were *ex vivo* stimulated with *M. tuberculosis* lysates and analyzed as in Fig. 7.

1443 Error bars indicate SD. $P < 0.01$ (**); $P < 0.001$ (***); $P < 0.0001$ (****); NS (no
1444 statistical significance). P values were calculated by one-way ANOVA with
1445 Newman-Keuls multiple comparison test.
1446

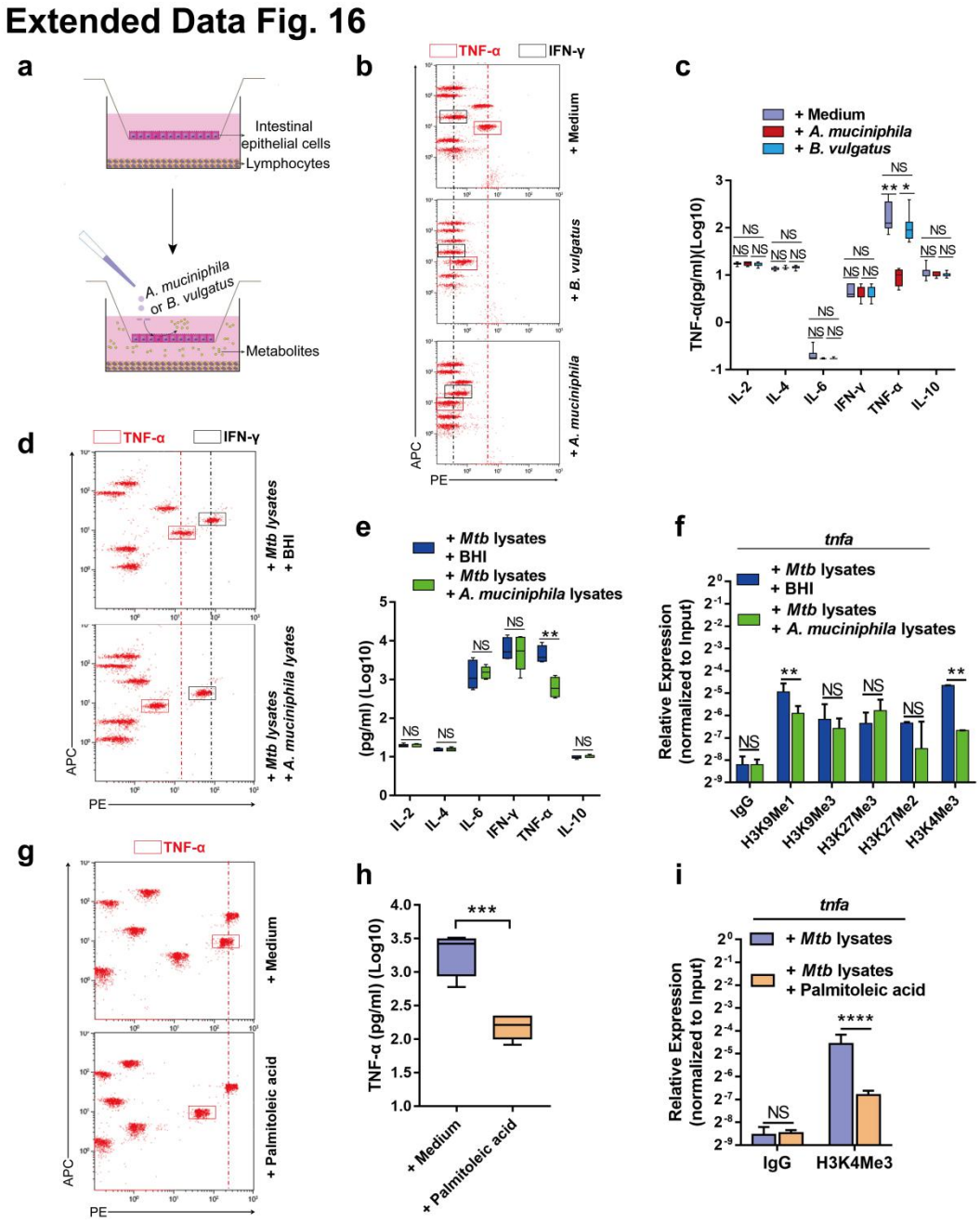

Extended Data Fig. 16. Intestine-colonized *A. muciniphila* and an *A. muciniphila*-derived metabolite palmitoleic acid, inhibit *M. tuberculosis*-specific TNF-α expression *via* an epigenetic mechanism.

(a) The experimental diagram of transwell assay to mimic the effects of epithelium-colonized gut bacteria on cytokine production. intestinal epithelial cells (2×10^5) were seeded into the upper chamber, CD3+ T cells isolated from autologous

spleens (2×10^5) were seeded to the lower chamber, and *A. muciniphila* (1×10^5 CFU) or *B. vulgatus* (1×10^5 CFU) were added to the upper chamber. After 12 hours incubation, culture supernatants in the lower chamber were detected for the expression of cytokines.

(b) Representative CBA analysis of culture supernatants of CD3+ T cells in the lower chamber for transwell assay. Red and black-boxed areas mark the fluorescent clusters of TNF-α and IFN-γ, respectively, and dashed line mark the shift of fluorescent clusters of TNF-α and IFN-γ, respectively.

(c) Pooled bar graphic data show the expression of TNF-α/IFN-γ/IL-2/IL-4/IL-6/IL-10 in culture supernatants of CD3+ T cells in the lower chamber. CD3+ T cells were cultured with medium only or with *A. muciniphila* (1×10^5 CFU) (+ *A. muciniphila*) and *B. vulgatus* (1×10^5 CFU) (+ *B. vulgatus*) for 12 hours. N = 7 mice per group.

(d) Representative CBA analysis of culture supernatants of CD3+ T cells of *M. tuberculosis*-infected mice. CD3+ T cells were co-cultured with *A. muciniphila* lysates (10 μg/ml) or BHI in presence of *M. tuberculosis* lysates (10 μg/ml). Red and black-boxed areas mark the fluorescent clusters of TNF-α and IFN-γ, respectively, and dashed line mark the shift of fluorescent clusters of TNF-α and IFN-γ, respectively.

(e) Pooled bar graphic data show the *in vitro* expression of TNF-α/IFN-γ/IL-2/IL-4/IL-6/IL-10 in culture supernatants of CD3+ T cells. T cells were co-cultured with *A. muciniphila* lysates (10 μg/ml) or BHI in presence of *M. tuberculosis*

lysates (10 μg/ml) for 3 days. N = 7 mice per group.

(f) CHIP-qPCR analysis of IgG, H3K4Me3, H3K9Me1, H3K9Me3, H3K27Me2 and H3K27Me3, and control antibodies at the promoter of *tnfα*. CD3+ T cells were randomly selected for co-culturing with *A. muciniphila* lysates (10 μg/ml) or BHI in presence of *M. tuberculosis* lysates (10 μg/ml) for 3 days.

(g) Representative CBA analysis of culture supernatants of CD3+ T cells. CD3+ T cells derived from spleen of mice were cultured with *M. tuberculosis* lysates (10 μg/ml) only or with *A. muciniphila*-derived metabolite, palmitoleic acid for 3 days. Red-boxed areas mark the fluorescent clusters of TNF-α, dashed line mark the shift of fluorescent clusters of TNF-α.

(h) Pooled bar graphic data show the expression of TNF-α in culture supernatants of CD3+ T cells of wild-type mice. CD3+ T lymphocytes isolated from spleens were cultured with palmitoleic acid (10 μM) plus *M. tuberculosis* lysates (10 μg/ml) or with *M. tuberculosis* lysates (10 μg/ml) only. N = 7 mice per group.

(i) CHIP-qPCR analysis of H3K4Me3 and IgG control at *tnfα* promoter. CD3+T cells from mouse spleens were cultured with *M. tuberculosis* lysates (10 μg/ml) only or with palmitoleic acid (10 μM) plus *M. tuberculosis* lysates (10 μg/ml).

Error bars indicate SD. $P < 0.01$ (**); $P < 0.001$ (***); $P < 0.0001$ (****); NS (no statistical significance). *P* values were calculated by one-way ANOVA with Tukey's multiple comparison test (c) and Student's two-tailed unpaired *t*-test [(e), (f), (h) and (i)]. At least two biological repeats were performed.

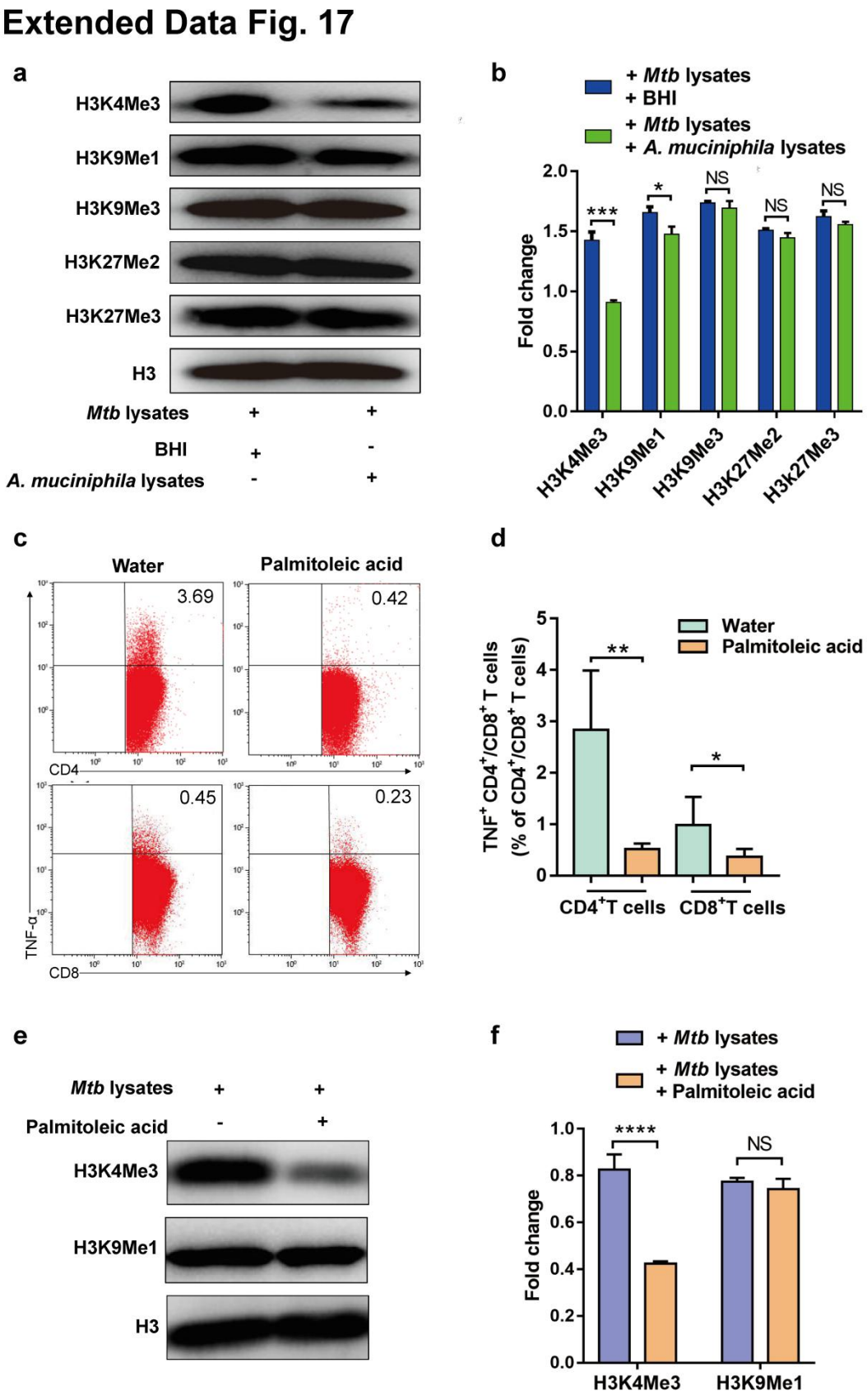

1497

1498 **Extended Data Fig. 17. *A. muciniphila* uses its metabolite, palmitoleic acid, to**

reduce H3K4Me3 expression.

(a) Immunoblot analysis of H3K4Me3, H3K9Me1, H3K9Me3, H3K27Me2 and H3K27Me3 in CD3+ T cells co-cultured with *A. muciniphila* lysates (10 μg/ml) or BHI in presence of *M. tuberculosis* lysates (10 μg/ml) for 3 days.

(b) Quantitative immunoblot analysis of expression of H3K4Me3, H3K9Me1, H3K9Me3, H3K27Me2 and H3K27Me3. ImageJ was used for quantitative analysis of immunoblot.

(c-d) Representative flow cytometric dot plots and pooled bar graphic data show the expression of TNF-α on CD4+ (CD8+) T cells in spleens derived from *M. tuberculosis*-infected mice with dietary treatments of palmitoleic acid, butyrate or water at 5 weeks post infection. N = 6 mice per group.

(e) Immunoblot analysis of H3K4Me3 and H3K9Me of CD3+ T cells cultured with *M. tuberculosis* lysates (10 μg/ml) only or with *A. muciniphila*-derived metabolite, palmitoleic acid.

(f) Quantitative immunoblot analysis of H3K4Me3 and H3K9Me1 by imageJ.

Error bars indicate SD. $P < 0.05$ (*); $P < 0.01$ (**); $P < 0.001$ (***); $P < 0.0001$ (****); NS (no statistical significance). *P* values were calculated by Student's two-tailed unpaired *t*-test [(b), (d) and (f)]. At least two biological repeats were performed.

Supplementary information

Cohort	Groups	Sample size	Sex	Number	Age	Height	Weight	BMI
Shenzhen cohort	Healthy controls (HC)	28	Female	10 (35.7%)	37.90 (23.46 -52.34)	159.40 (152.33 – 166.47)	58.35 (49.61 – 67.09	23.11 (18.95 – 27.27
			Male	18 (64.3%)	41.56 (28.47 – 54.65)	176.00 (170.48 – 181.52)	66.45 (58.41 – 74.49)	21.56 (18.24 – 24.88)
	TB patients (TB)	26	Female	8 (30.8%)	35.88 (23.80 – 47.96)	160.38 (154.53 – 166.23)	55.88 (47.85 -63.91)	21.78 (18.34 – 25.22)
			Male	18 (69.2%)	36.33 (26.55 – 46.11)	174.39 (167.22 – 181.56)	73.94 (65.36 – 82.52)	24.41 (21.03 -27.79)
Foshan cohort	Healthy controls (HC)	17	Female	5 (29.4%)	33.60 (23.36 -43.84)	159.40 (152.03 – 166.77)	51.60 (44.23 – 58.97)	20.23 (18.63 – 21.83)
			Male	12 (70.6%)	31.43 (21.60 – 41.26)	170.50 (162.72 – 178.28)	64.08 (53.48 – 74.68)	22.09 (18.47 – 25.71)
	TB patients (TB)	19	Female	8 (42.1%)	33.88 (21.85 -45.91)	157.63 (152.05 – 163.21)	54.25 (46.64 -61.86)	21.84 (18.83 -24.85)
			Male	11 (57.9%)	36.82 (24.86 – 48.78)	174.73 (167.73 – 181.73)	73.82 (63.46 – 84.18)	24.33 (20.15 -28.51)
Combined cohort	Healthy controls (HC)	45	Female	15 (33.3%)	36.47 (23.49 – 49.45)	159.40 (152.49 – 166.31)	56.10 (47.41 – 64.79)	22.15 (18.43 – 25.87)
			Male	30 (66.7%)	37.51 (24.76 – 50.26)	173.27 (165.8 – 180.74)	67.08 (57.51 – 76.65)	22.46 (18.76 – 26.16)
	TB patients (TB)	45	Female	16 (35.6%)	34.88 (23.19 – 46.57)	159.00 (153.30 – 164.70)	55.06 (47.46 – 62.66)	21.81 (18.69 – 24.93)
			Male	29 (64.4%)	36.52 (26.07 – 46.97)	174.52 (167.54 – 181.50)	73.90 (64.79 – 83.01)	24.38 (20.75 – 28.01)

Supplementary Table 1. Demographic characteristics of active TB patients (TB) and healthy controls (HC) for gut bacterial analyses of 16S rDNA.

Cohort	Groups	Sample size	Sex	Number	Age	Height	Weight	BMI
Guangzhou cohort	Healthy controls (HC)	263	Female	86 (32.7%)	32.98 (20.78 – 45.18)	162.22 (155.05 – 169.39)	55.76 (47.70 – 63.82)	21.31 (17.68 – 24.94)
			Male	177 (67.3%)	33.81 (22.50 – 45.12)	174.16 (164.88 – 182.44)	69.46 (60.23 – 78.69)	23.05 (19.27 – 26.83)
	TB patients (TB)	264	Female	101 (38.3%)	36.40 (24.68 – 48.12)	162.79 (156.06 – 169.52)	56.51 (48.29 – 64.73)	21.43 (17.83 – 25.03)
			Male	163 (61.7%)	37.71 (19.91 -55.51)	174.15 (165.30 – 183.00)	71.05 (62.07 – 80.03)	23.63 (19.67 – 27.59)
Shenzhen cohort	Healthy controls (HC)	1445	Female	563 (39.0%)	34.26 (17.58 – 49.56)	161.55 (154.40 – 168.70)	56.76 (48.91 – 64.61)	21.90 (18.16 – 25.64)
			Male	882 (61.0%)	37.18 (17.00 – 56.75)	173.82 (165.31 – 182.33)	70.08 (61.10 – 79.06)	23.35 (19.64 – 27.06)
	TB patients (TB)	1533	Female	553 (36.1%)	35.18 (21.38 – 49.18)	161.19 (154.22 – 168.16)	56.14 (47.95 – 64.33)	21.72 (18.07 – 25.39)
			Male	980 (63.9%)	37.23 (22.93 – 52.69)	173.96 (164.55 – 182.37)	70.28 (61.29 – 79.27)	23.40 (19.54 – 27.26)
Foshan cohort	Healthy controls (HC)	1679	Female	574 (34.2%)	29.06 (19.90 – 45.35)	161.16 (154.18 – 168.14)	56.57 (48.51 – 64.63)	21.91 (18.21 – 25.61)
			Male	1105 (65.8%)	31.10 (20.10 – 46.70)	173.98 (165.50 – 182.46)	70.41 (61.55 – 79.27)	23.42 (19.71 – 27.13)
	TB patients (TB)	1328	Female	437 (32.9%)	35.11 (21.21 – 49.01)	161.29 (154.48 – 168.10)	55.76 (47.71 – 63.81)	21.55 (17.94 – 25.16)
			Male	891 (67.1%)	37.95 (23.18 – 49.08)	174.44 (166.24 – 182.64)	69.98 (60.85 – 79.11)	23.16 (19.35 – 26.97)
Combined cohort	Healthy controls (HC)	3387	Female	1223 (36.1%)	31.73 (19.00 – 47.45)	161.41 (154.34 – 168.48)	56.60 (48.64 – 64.56)	21.86 (18.14 – 25.58)
			Male	2164 (63.2%)	33.80 (19.20 – 51.78)	173.93 (165.45 – 182.41)	70.2 (61.26 – 79.14)	23.36 (19.64 – 27.08)
	TB patients (TB)	3125	Female	1091 (34.91%)	35.26 (21.32 – 49.08)	161.38 (154.49 – 168.27)	56.02 (47.89 – 64.15)	21.63 (17.99 – 25.25)
			Male	2034 (65.09%)	37.58 (23.04 – 51.16)	174.18 (165.83 – 182.53)	70.21 (61.16 – 79.26)	23.32 (19.47 – 27.17)

Supplementary Table 2. Demographic characteristics of active TB patients (TB) and healthy controls (HC) for SNP analyses.

Chromosome 21 position	SNP ID	Genotype	HC	TB	Additive	
			NO (%)	NO (%)	*P*	OR (95%CI)
chr21:33343393	rs2257167	GG	96 (36.50)	105 (39.77)	0.28	1.32 (0.80 - 2.23)
		GC	121 (46.01)	121 (45.83)	0.45	1.21 (0.75 - 1.99)
		CC	46 (17.49)	38 (14.39)	Ref.	Ref.
chr21:33355024	rs1041868	GG	108 (41.06)	112 (42.42)	0.59	1.16 (0.68 - 1.96)
		GA	116 (44.11)	117 (44.32)	0.66	1.12 (0.67 - 1.90)
		AA	39 (14.83)	35 (13.26)	Ref.	Ref.
chr21:33326436	rs4408796	CC	142 (54.00)	143 (54.17)	0.89	0.95 (0.48 - 1.89)
		CG	103 (39.16)	102 (38.63)	0.86	0.94 (0.47 - 1.89)
		GG	18 (6.84)	19 (7.20)	Ref.	Ref.
chr21:33331291	rs13050445	CC	130 (49.43)	132 (50.00)	0.96	1.02 (0.54 - 1.90)
		CT	110 (41.83)	109 (41.29)	0.98	0.99 (0.52 – 1.87)
		TT	23 (8.74)	23 (8.71)	Ref.	Ref.
chr21:33331895	rs2252930	CC	256 (97.34)	257 (97.35)	-	-
		CG	7 (2.66)	7 (2.65)	-	-
		GG	0 (0.00)	0 (0.00)	Ref.	Ref.
chr21:33332014	rs2252931	GG	102 (38.78)	105 (39.77)	0.83	1.06 (0.60 - 1.90)
		GA	131 (49.81)	130 (49.24)	0.93	1.03 (0.58 - 1.81)
		AA	30 (11.41)	29 (10.98)	Ref.	Ref.
chr21:33340113	rs2253923	AA	123 (46.77)	122 (46.21)	0.98	0.99 (0.52 - 1.89)
		AT	118 (44.87)	120 (45.45)	0.96	1.02 (0.53 - 1.94)
		TT	22 (8.36)	22 (8.33)	Ref.	Ref.
chr21:33351188	rs2243599	TT	126 (47.90)	127 (48.11)	0.92	0.97 (0.54 - 1.74)
		TG	110 (41.83)	109 (41.29)	0.88	0.96 (0.53 - 1.73)
		GG	27 (10.27)	28 (10.60)	Ref.	Ref.
chr21:33353924	rs2254180	TT	145 (55.13)	144 (54.55)	0.98	0.99 (0.49 - 2.02)
		TC	101 (38.40)	103 (39.01)	0.96	1.02 (0.49 – 2.11)
		CC	17 (6.46)	17 (6.44)	Ref.	Ref.
chr21:33355181	rs2254315	CC	251 (95.44)	253 (95.83)	-	-
		CT	12 (4.56)	11 (4.17)	-	-
		TT	0 (0.00)	0 (0.00)	Ref.	Ref.

• Discovery cohort (Guangzhou), Chromosome 21 *IFNAR1* locus (GRCh38.p12, 33324395 - 33359864).

• *P-value* (*P*) was calculated comparing active TB patients (TB) group to healthy controls (HC) group in allele distribution.

Supplementary Table 3. Association of *Ifnar1* SNPs and TB susceptibility in a discovery cohort.

SNP ID	Cohort		Genotype	HC NO (%)	TB NO (%)	Multiplicative P	Multiplicative OR (95% CI)	Additive P	Additive OR (95% CI)	Dominant P	Dominant OR (95% CI)	Recessive P	Recessive OR (95% CI)
rs2257167	Validation	Shenzhen cohort	GG	515 (35.64)	631 (41.16)	0.0002	1.22 (1.10-1.36)	0.0003	1.50 (1.21-1.87)	0.0024	1.36 (1.12-1.67)	0.002	1.26 (1.09-1.47)
			GC	681 (47.13)	699 (45.60)			0.03	1.26 (1.02-1.56)				
			CC	249 (17.23)	203 (13.24)			Ref.	Ref.				
		Foshan cohort	GG	605 (36.03)	542 (40.81)	0.0003	1.21 (1.09-1.35)	0.0002	1.52 (1.22-1.90)	0.001	1.41 (1.15-1.74)	0.007	1.22 (1.06-1.42)
			GC	792 (47.17)	620 (46.69)			0.01	1.33 (1.07-1.66)				
			CC	282 (16.80)	166 (12.50)			Ref.	Ref.				
	Combined cohort		GG	1120 (35.85)	1173 (41.00)	0.000	1.22 (1.13-1.31)	0.000	1.51 (1.29-1.76)	0.000	1.38 (1.20-1.60)	0.000	1.24 (1.12-1.38)
			GC	1473 (47.15)	1319 (46.10)			0.001	1.29 (1.11-1.51)				
			CC	531 (17.00)	369 (12.90)			Ref.	Ref.				
rs1041868	Validation	Shenzhen cohort	GG	521 (36.05)	560 (36.53)	0.47	1.04 (0.94-1.15)	0.38	1.10 (0.44-1.37)	0.31	1.11 (0.91-1.35)	0.79	1.02 (0.88-1.19)
			GA	682 (47.20)	737 (48.08)			0.33	1.11 (0.90-1.36)				
			AA	242 (16.75)	236 (15.39)			Ref.	Ref.				
		Foshan cohort	GG	563 (33.53)	461 (34.71)	0.89	1.01 (0.91-1.12)	0.89	0.98 (0.80-1.22)	0.54	0.94 (0.78-1.14)	0.50	1.05 (0.91-1.23)
			GA	837 (49.85)	635 (47.82)			0.37	0.91 (0.75-1.12)				
			AA	279 (16.62)	232 (17.47)			Ref.	Ref.				
	Combined cohort		GG	1084 (34.70)	1021 (35.69)	0.47	1.03 (0.96-1.11)	0.54	1.05 (0.45-1.24)	0.74	1.02 (0.89-1.17)	0.42	1.04 (0.94-1.16)
			GA	1519 (48.62)	1372 (47.96)			0.94	1.01 (0.87-1.31)				
			AA	521 (16.68)	468 (16.35)			Ref.	Ref.				

• *P-value* (*P*) was calculated comparing active TB patients (TB) group to healthy controls (HC) group in allele distribution

• 0.000 means $P < 0.0001$

•OR odds radio, numbers in parentheses following OR are 95% confidence intervals

Supplementary Table 4. The association of *Ifnar1* SNP rs2257167 or rs1041868 and TB susceptibility in Shenzhen and Foshan cohorts.

Primers	Sequence	
A. muciniphila	For: 5′-CAGCACGTGAAGGTGGGGAC-3′	Rev:5′-CCTTGCGGTTGGCTTCAGAT-3′
B. vulgatus	For: 5′-CGGGCTTAAATTGCAGATGA-3′	Rev:5′-CATGCAGCACCTTCACAGAT-3′
	Probe: FAM-CCAACCTGCCGACAACACTGGGATA-TAM	
16S rDNA	For: 5′-CGGTGAATACGTTCCCGG-3′	Rev:5′-TACGGCTACCTTGTTACGACTT-3′
	Probe: FAM-CTTGTACACACCGCCCGTC-MGB	
h*IFN-β*	For: 5′-CCTACAAAGAAGCAGCAA-3′	Rev:5′-TCCTCAGGGATGTCAAAG-3′
h*ISG15*	For: 5′-CGCAGATCACCCAGAAGATCG-3′	Rev:5′-TTCGTCGCATTTGTCCACCA-3′
GAPDH	For: 5′-CGGAGTCAACGGATTTGGTC-3′	Rev:5′-GACAAGCTTCCCGTTCTCAG-3′
m*IFN-β*	For: 5′-AGATCAACCTCACCTACAGG-3′	Rev:5′-TCAGAAACACTGTCTGCTGG-3′
m*ISG15*	For: 5′-TCCATGACGGTGTCAGAACT-3′	Rev:5′-GACCCAGACTGGAAAGGGTA-3′
mGAPDH	For: 5′-GAAGGGCTCATGACCACAGT-3′	Rev:5′-GGATGCAGGGATGATGTTCT-3′
FAT	For: 5′-GCGAATGGCCTGATGAAACC-3′	Rev:5′-CCACCGTTTCTTTGCATGGG-3′
Amuc0201	For: 5′-ATGGCTATTGATCCCAAATT-3′	Rev:5′-TTAGAGCGGAATGTTGCCGT-3′
Amuc1507	For: 5′-ATGGACGCAGTATTATTGTTTT-3′	Rev:5′-TTATTTGTTCAGCTCCGCAA-3′
Amuc1327	For: 5′-ATGACCGACCGCAGAATTGT-3′	Rev:5′-TCAGGCGAATCGTTTCACGA-3′
Amuc0994	For: 5′-ATGCAAAAGTTAGCAGGTAAAA-3′	Rev:5′-CTACATCGTCATGCCTCCGT-3′
Amuc1918	For: 5′-ATGGCATGTGGAAACCAAAG-3′	Rev:5′-TCAAGCATCCTGAAGGCCGA-3′
Amuc1642	For: 5′-ATGTCAAGTAAATTACTCGAAGG-3′	Rev:5′-TTACATTCCCATGATCTGATAAC-3′
Amuc1725	For: 5′-ATGGAACATGCCAGCAACAA-3′	Rev:5′-TTATGCGATTTCAGCGGTTT-3′
BVU1463	For: 5′-ATGATACAAAAGGTTCTAATTGC-3′	Rev:5′-TCAGATTCTCAACACTCCTTTC-3′
BVU3104	For: 5′-ATGATAAAGAAAGTATTGATTGCA-3′	Rev:5′-TCAGATTCTCAATACTCCTTTCTG-3′
BVU3989	For: 5′-ATGAAAGCATTTGTATTCCCC-3′	Rev:5′-TCAAGCAATACCGTGTGCGT-3′
BVU1050	For: 5′-ATGGAATTAAAAAGAGTAGTAGTAA-3′	Rev:5′-TTATTCAGCATATTTTTTTACG-3′
BVU0384	For: 5′-ATGGGATTATTAACAGGAAAGAC-3′	Rev:5′-TTACATGTTCATACCGCCGT-3′
BVU1011	For: 5′-ATGAAATACGCACTAGTAACAGG-3′	Rev:5′-TTATGTATAGATTCCTCCATTGATG-3′
BVU0098	For: 5′-ATGTTGAAACAGAAGACATTAAAAG-3′	Rev:5′-TTATTTATTTTTTACTATTTGTGCC-3′
BVU1026	For: 5′-ATGCTGCTGGAGAACTTTTATA-3′	Rev:5′-TCATTGATACTTACTTGCCATC-3′
BVU1986	For: 5′-ATGAGTTACAATTTGTTGAAAGG-3′	Rev:5′-TTATCCGTAAATGATGTTTCC-3′
BVU2557	For: 5′-ATGATGAGTGAGAATAAAGTAGGAA-3′	Rev:5′-CTAAATAAATATCACCTTACTGCG-3′
BVU0009	For: 5′-ATGATAAAAGAAAACTTTATCAAGC-3′	Rev:5′-TTATTCTTCGGTAATACTGTTATAT-3′
BVU1484	For: 5′-ATGAGTAGTTCTTTCTTATCTGTCC-3′	Rev:5′-TTATTCTTCGTACATCTTTTCTATT-3′
BVU3027	For: 5′-ATGGAACTAGAACAGAGTTTTATTG-3′	Rev:5′-TTATTCTTTTATATCTTGGTACAAG-3′
BVU3870	For: 5′-ATGGAGCAGAGTTTTATTGC-3′	Rev:5′-TTATTTTACTTCCTGATATAAGAAA-3′

Supplementary Table 5. Primers used in this study.

Supplementary Files

This is a list of supplementary files associated with this preprint. Click to download.

- STROBEchecklistcohort.pdf
- nreditorialpolicychecklist.pdf
- nrreportingsummary.pdf
- AblankversionoftheInformedConsentofGuangzhouShenzhenandFoshancohorts.pdf
- TheethicalboardapprovalsofGuangzhouShenzhenandFoshancohorts.pdf